8-2013

Multifunctional Polymeric Micro- and Nanocomposite Fibers for Radiation Detection

Stephen Andrew Young
syoung13@utk.edu

To the Graduate Council:

I am submitting herewith a dissertation written by Stephen Andrew Young entitled "Multifunctional Polymeric Micro- and Nanocomposite Fibers for Radiation Detection." I have examined the final electronic copy of this dissertation for form and content and recommend that it be accepted in partial fulfillment of the requirements for the degree of Doctor of Philosophy, with a major in Engineering Science.

Dayakar Penumadu, Major Professor

We have read this dissertation and recommend its acceptance:

Roberto S. Benson, Kevin M. Kit, Charles L. Melcher, Laurence F. Miller

Accepted for the Council:
Dixie L. Thompson

Vice Provost and Dean of the Graduate School

(Original signatures are on file with official student records.)

Multifunctional Polymeric Micro- and Nanocomposite Fibers for Radiation Detection

A Dissertation Presented for the
Doctor of Philosophy
Degree
The University of Tennessee, Knoxville

Stephen Andrew Young
August 2013

DEDICATION

This dissertation is dedicated to the Universe, my parents, Dr. John H. Young, Jr. and Sonja F. Young, and by brothers, John H. Young III, and Paul K. Young, the rest of my family and friends for their unwavering love and support throughout my course of study.

ACKNOWLEDGEMENTS

My sincere appreciation goes to my advisor and mentor, Dr. Dayakar Penumadu, for his guidance and support throughout my course of study. I am grateful to have been under his tutelage. Special thanks go to Dr. Roberto S. Benson, Dr. Kevin M. Kit, Dr. Charles L. Melcher, and Dr. Laurence F. Miller for their time and dedication as committee members and for providing invaluable insight to this dissertation. I would like to thank Dr. Indraneel Sen for his research guidance, friendship, and support of my research. Special thanks to Mr. Kenneth G. Thomas for his significant help with fabrication of parts for my experiments. I would also like to thank Dr. Akawut Siriruk, Mr. Robin Woracek, Mr. Jeffrey Bunn, Mr. Matthew E. Kant, Mr. Aashish Sharma, Mr. Stephen Puplampu, Mr. Nathan Meek, and Dr. Felix Kim for their camaraderie and sharing their expertise in sample preparation, mechanical testing, and image analysis. Special thanks to Dr. Rohit Uppal for his great help, friendship, and support of my research. Special thanks to Dr. David P. Harper for his sharing his expertise with melt-spinning and characterization of fibers. Thanks to my colleagues, specifically, Mr. Matthew J. Urffer, Mr. Andrew N. Mabe, Dr. John D. Auxier II, Mr. Alexander D. Green, Mrs. Merry Koschan, Dr. George K. Schweitzer, Dr. Mariya Zhuravleva, Dr. Martin R. Williamson and Mr. Dan Henn for sharing their expertise regarding chemistry, radiation detection, and scintillation materials. Thanks to Mr. Jonathan Turnmire for sharing his expertise regarding electrical engineering. I would like to thank Ms. Hua Wei for sharing her expertise with

optical characterization of scintillation materials. Special thanks to Dr. John R. Dunlap and Mr. Gregory L. Jones for sharing their expertise of microscopy related characterization. Special thanks to Mr. James T. Pippin, Dr. Ronald B. McFadden, Ms. Celeste Brooks, and Dr. Arnold Lumsdaine for believing in me and giving me a chance to pursue academic research. Thanks to Mrs. Samantha Allen, Mrs. Betty Chittum, Ms. Lindsi Whitaker, Mrs. Annette Costar, Ms. Sharon Hale, Mrs. Jocelyn Miller, Mr. Larry Roberts, Mrs. Lisa Smith, and Mr. Travis Griffin for their academic support.

ABSTRACT

Due to the shortage of ^{3}He (helium-3), there is a great demand to develop alternative technologies for thermal neutron detection. The Department of Homeland security is interested in applications with polymeric scintillation detectors that can directly discriminate between neutron and gamma radiation using manufacturing techniques that are both inexpensive and which can be effectively implemented to produce large-area detectors. The ^{6}Li (lithium-6) isotope has a significant thermal neutron cross-section and produces high-energy charged particles upon thermal neutron absorption. This research focuses on the development of small-diameter fibers (micro-/nanoscale) loaded with ^{6}Li for thermal neutron detection by electrospinning and melt-spinning methods. Electrospun polymer nanofibers are attractive due to their unique volume-to-surface area as well as their chemical, electrical, and optical properties. The fibers are characterized by polymeric properties, including microstructure evaluation, response to thermal neutrons, and alpha, beta, and gamma radiation using suitable radiation facilities. ^{6}Li-loaded polyethylene naphthalate (PEN) oriented microfibers were fabricated by melt-spinning and tested for thermal neutron detection. Additionally, (PEN)-based microfibers were integrated with carbon fiber/vinyl ester-reinforced backing to form a composite laminate with the dual function of serving as a scintillator and a structural composite material. Laminate scintillators were evaluated to study the mechanical properties and the effect of scintillation performance. Important

microstructural information using a digital optical microscope and mechanical behavior, including the modulus, are both reported.

TABLE OF CONTENTS

LIST OF TABLES

LIST OF FIGURES

INTRODUCTION

Great attention and resources have been directed toward developing effective neutron detection-based technologies for nuclear and homeland security applications. ^{3}He, commonly used in gas proportional counters for thermal detection, is in short supply. The imminent shortage of ^{3}He has prompted research for suitable replacement technologies for thermal neutron detection to develop an effective detector with good neutron to gamma discrimination that can be economically fabricated on a large scale and installed in public places [1-3]. Additionally, there is a great need to implement suitable neutron-based inspection of cargo and marine-based containers to detect nuclear threats [4]. Kouzes has extensively summarized replacement technologies in detail [1]. There is growing interest in the development of ^{6}Li-loaded plastic scintillators for thermal neutron detection and investigating their effects [5]. Organic materials as solid plastic scintillators have unique advantages, offering ease of fabrication, fast response time, and high light yield [6]. Furthermore, small-diameter plastic scintillator fibers have been successfully used as tracking devices [7].

The goal of this research study is to evaluate and attain highly ordered alignment of polymeric small-diameter fibers (micro-/nanoscale) for thermal neutron detection. The attraction of nanofibers is due to growing interest in the use of subwavelength-diameter luminescent fiber optic waveguides in nanotechnologies. For example, polymethyl methacrylate (PMMA) based microfibers and nanofibers have been electrospun and successfully

demonstrated as waveguides [8]. Electrospinning is a novel and low-cost method to fabricate nanofibers [9, 10]. Despite these unique properties, there are only a few reports related to ^{6}Li-loaded micro and nanofiber plastic scintillators for thermal neutron detection.

This research study focuses on the scintillation mechanism and the evaluation of small-diameter fibers for thermal neutron detection. The first chapter investigates ^{6}Li-loaded electrospun polymeric nanofibers for thermal neutron detection using a novel electrospinning technique. The second chapter studies oriented melt-spun ^{6}LiF loaded polyethylene naphthalene (PEN) microfibers as neutron detectors. The third chapter explores the use of PEN-based microfibers integrated with carbon-fiber vinyl ester (CFVE) backing as a dual functional composite laminate as a structural material and scintillation detector.

REFERENCES

[1] Kouzes, R. T., 2009, "The ^{3}He Supply Problem," Pacific Northwest National Laboratory Technical Report, PNNL-18388.

[2] Sen, I., Penumadu, D., Williamson, M., Miller, L. F., Green, A. D., and Mabe, A. N., 2011, "Thermal Neutron Scintillator Detectors Based on Poly(2-Vinylnapthalene) Composite Films," IEEE Trans. Nucl. Sci., **59**(3), pp. 1386-1393.

[3] Sen, I., Urffer, M., Penumadu, D., Young, S. A., Miller, L. F., and Mabe, A. N., 2012, "Polyester Composite Thermal Scintillation Films," IEEE Trans. Nucl. Sci., **59**(4), pp. 1781-1786.

[4] Gozani, T., and Strellis, D., 2007, "Advances in Neutron Based Bulk Explosive Detection," Nuclear Instruments and Methods in Physics Research Section B: Beam Interactions with Materials and Atoms, **261**(1-2), pp. 311-315.

[5] Breukers, R. D., Bartle, C. M., and Edgar, A., 2013, "Transparent Lithium Loaded Plastic Scintillators for Thermal Neutron Detection," Nuclear Instruments and Methods in Physics Research A, **701**, pp. 58-61.

[6] Knoll, G. F., 2000, *Radiation Detection and Measurement, 3rd ed*. John Wiley and Sons, Hoboken, NJ, pp. 227-522.

[7] Blumenfeld, H., Bourdinaud, M., Rebourgeard, P., and Thevenin, J. C., 1989, "Production and Test of Coherent Bundles of Plastic Scintillating

Microfibers,"Nuclear Instruments and Methods in Physics Research A, **364**, pp. 619-621.

[8] Li, L., Yang, X., and Yuan, L., 2012, "One-dimensional Optical Materials of Microfibers by Electrospinning," Materials Letters, 1, pp. 292-295.

[9] Doshi, J., and Reneker, D. H., 1995, "Electrospinning Process and Applications of Electrospun Fibers," Journal of Electrostatics, **35**, pp. 151-160.

[10] Andrady, A. L., 2008, *Science and Technology of Polymer Nanofibers*, John Wiley and Sons, Inc., Hoboken, NJ, pp. 81-311.

1 CHAPTER I
LITERATURE REVIEW

1.1 Plastic Scintillators

Neutron-based detectors are of great importance in the fields of nuclear, neutron imaging, and homeland security applications [1 - 3]. Neutrons, due to their uncharged nature, can deeply penetrate a detector medium without directly ionizing. Their detection, such as the detection of thermal neutrons, with energy of 0.025 eV, proceeds as neutron-induced reactions create secondary ionizing particles of sufficient energy [1, 4, 5]. Organic scintillators are attractive for thermal neutron detection due to their ability to discriminate between neutrons and gamma. Liquid organic scintillators are very efficient as neutron counters; however, the organic solvents used for these detectors are highly flammable and pose a hazard [5]. Pure organic scintillator crystals such as anthracene and stilbene are widely used as nuclear scintillator detectors due to their scintillation efficiency. However, these monocrystals lack mechanical integrity, they are difficult to obtain in large volumes, and their scintillation efficiency depends upon the incident radiation angle [6-8]. In these respects, solid organic plastics are good alternatives for the development of effective thermal neutron detectors, as they are mechanically robust and non-volatile [5].

Organic materials can be machined into complex geometries, including thin film and thin fibers, can be produced in large volume, and can have high luminescence efficiency [9, 10]. For example, polystyrene (PS) and polyvinyltoulene (PVT) are two commonly used aryl-vinyl polymers for scintillation detection due to their ease of fabrication and low cost. Such

polymers have a low fluorescence yield; however, they can be blended with wavelength-shifting fluors to improve the light yield to be detected on a standard photomultiplier tube (PMT) [3]. Additionally, poly(methyl methacrylate) (PMMA), a non-aromatic polymer, has been used for scintillation. For example, Inagaki et al. studied a copolymer consisting of PMMA and styrene. Due to the low fluorescence yield of these polymers, wavelength shifters were added to improve the light output. The primary wavelength shifters were naphthalene-based, with secondary fluors to be detectable on PMT [11].

Polyethylene naphthalene (PEN) has been reported to have high scintillation properties and strong absorption in the blue region without the need for wavelength-shifting fluors [12]. One advantage of PEN is that its naphthalene units are located on the backbone of the polyester compared to pendant groups for PS and PVT. These photophysical phenomena are due to the intramolecular energy transfer along the naphthalene units, where the molecules are excited to higher energy levels before the excimeric emission of photon [13-15]. An effective thermal neutron polymeric scintillator is highly transparent, having a neutron absorber element with a high thermal neutron cross-section and a suitable wavelength-shifting fluor embedded in the polymer matrix. Neutron capture nuclei gadolinium -157 (^{157}Gd), boron-10 (^{10}B) and lithium-6 (^{6}Li) have been used for the development of efficient neutron detectors [16]. Bell et al. studied Gd-based plastic scintillators, where Gd has a very large thermal neutron cross-section, that discriminated between neutron and gamma radiation [17].

Ovechkina et al. studied styrene-based plastic scintillators loaded with gadolinium (Gd) compound for neutron detection. The plastic scintillators, a few millimeters thick, were observed to be transparent up to a concentration of 0.3%. However, when irradiated with neutrons, an increase in Gd concentration beyond 0.5% decreased the light output [18].

For thin detectors, the options can be narrowed to ^{6}Li and ^{10}B due to their high Q-value and short charged particle ranges suitable for thin films and thin fibers [19]. Plastic scintillators loaded with boron have been developed and are commercially available [20]. However, ^{6}Li nuclei are most attractive, as, in addition to having a comparatively higher Q value than ^{10}B (4.78 MeV for ^{6}Li compared to 2.78 MeV for ^{10}B), gamma emissions are not associated with their reaction products [1, 21]. The neutron capture of ^{6}Li is written as

$$^{6}_{3}Li + ^{1}_{0}n \rightarrow ^{3}_{1}H + ^{4}_{2}He + 4.78MeV \qquad \text{(Eq. 1.1)}$$

where, upon absorption of a thermal neutron, a "^{6}Li nucleus undergoes fission producing secondary electrons α particle (2.05 MeV) and triton particle (2.73 MeV)" [1, 22]. Despite these advantages, there are a few reports of ^{6}Li-loaded polymers as promising candidates for thermal neutron detection [21].

Katagiri et al. investigated ^{6}Li-loaded plastic scintillators using a commercial PVT-based plastic scintillator, BC-414 (Bicron). The ^{6}LiF and BC-414 were mixed into toluene, and the toluene was evaporated off. This plastic scintillator was found to

exhibit neutron/gamma discrimination, measured using pulse height discrimination [23].

Im et al. fabricated a transparent poly(ethylene oxide) (PEO) based scintillator loaded with lithium chloride and organic fluor. An increase in the neutron count rate was observed in relation with an increase in ^{6}Li content [24].

Breukers et al. fabricated polystyrene-based film scintillators loaded with lithium methacrylate (LiME) and organic fluors to create highly transparent films. An increase in luminescence with an increased concentration of LiME was observed when the plastic scintillator was placed in a thermal neutron beam [21].

Additionally, in an independent study, Mabe et al. developed a transparent copolymer poly(styrene-co-lithium maleate (PS-co-PLiMAn) film loaded with ^{6}Li for thermal neutron detection [25]. The film had desirable neutron efficiencies and low sensitivity to gamma, making it suitable for thermal neutron detection.

Mabe et al. also studied polystyrene-based thin films loaded with ^{6}LiF and wavelength-shifting fluor to detect thermal neutrons [26].

Sen et al. studied poly(2-vinyl naphthalene) (P2VN) thin films loaded with ^{6}Li salicylate (^{6}Li Sal) [22]. Although it obtained a higher light yield compared to neat PS and PVT films, the P2VN-based scintillator did not have mechanical integrity and was non-transparent due to phase separation between the polymer and ^{6}LiSal. Sen et al. also investigated PEN-based films loaded with ^{6}LiF and organic fluor [27]. ^{6}LiF is attractive due to its high atomic mass density of ^{6}Li and thermal

stability. The film exhibited high neutron to gamma discrimination, but the film was opaque due to micron-sized ^{6}LiF crystal scattering light.

Plastic Fiber Scintillators. Plastic scintillators can also be formed into fibers with various cross-sections, including cylindrical, and have been used as charged-particle tracking devices [28-33]. Plastic scintillator microfibers have been demonstrated to be effective scintillators [34]. The basic idea is that a drawn polymer scintillator core is cladded with another polymer with a lower refractive index to guide the light along the fiber. PS is the most common material used as a core for scintillation due to its high refractive index (refractive index = 1.58) and because it is easy to draw into fiber [1, 31]. The benefits of organic plastic scintillation are due to their low Z constituents (hydrogen, carbon, and oxygen), higher light yield, and faster response time compared to glass fibers [1, 34, 35]. Saclay fabricated PS-based scintillating fibers with a core diameter of 0.5 mm to 1.5 mm cladded with polyvinyl acetate with a thickness of 7 to 22 microns. PS fiber was doped with organic fluors to improve yield [28-30]. There is growing interest in small-diameter fibers (micro-/nanoscale) due to its 1-D structure as a waveguide, where light is emitted isotropically and guided along the long axis of the fiber by total internal reflection, exhibiting interesting optical properties such as optical confinement [9,36]. McIntosh et al. proposed that a cylindrical geometry is 1 to 1.9 times more efficient than planar geometry for luminescent solar concentrators (LSC), having similar properties to scintillating

fibers when luminescence occurs close to the surface for the same volume and area [37]. This result, based on equations derived for scintillating fibers, has triggered additional studies on the optimal characteristics for cylindrical geometry compared to planar geometry [38-41]. A thin and continuous fiber geometry affords a high surface area to diameter ratio where luminescence emission occurs close to the surface, while the cylindrical geometry has a larger optical concentration potential than planar geometry. Furthermore, fibers are lightweight and flexible, and manufacturing processes can be optimized to produce on a large scale [39]. However, small-diameter (<500 microns) fibers have remained challenged due to poor light yield and inefficient energy migration along the fiber [28]. Plastic scintillators have two predominate types of energy migration mechanisms, radiative and nonradiative [42, 43]. As illustrated in Figure 1.1, light absorbed by polymer monomer units are excited to higher energy levels, where the excitations transfer their energy to acceptor units (fluor). When the energy is efficiently transported to the acceptor fluor, the fluorescence can be significantly amplified. This light-harvesting concept can be applied to thermal neutron scintillator nanofibers. Following neutron capture event, the energy travels through the polymer matrix where the excitation energy is transported along the monomer units to the acceptor (fluor), where it readily emits light [9, 22]. The light is then confined and guided down the long axis of the fiber by total internal reflection until the light is emitted on the fiber ends. It must be noted that the efficiency of the light-harvesting effect depends strongly upon the distance

between the fluorophores [9]. Despite these unique properties, there is a dearth of scientific literature concerning development of neutron capture elements loaded plastic scintillating fibers for thermal neutron detection. Axemann et al. studied ^{6}Li-loaded plastic scintillator fibers [44]. Grazioso et al. studied the potential use of boron-loaded plastic fibers of various diameters through modeling and experimentally observed detection of thermal neutron. The cylindrical fibers were composed of a polystyrene core with PMMA cladded loaded with 1% wt boron [45].

1.2 Fabrication of Fibers

The production of fiber scintillators consisting of a core and cladding have traditionally been manufactured using fiber drawing techniques. An example schematic of the typical fiber-drawing process is illustrated in Figure 1.2. A preform consisting of a polished core surrounded by a cladding is suspended at one end and placed into an oven until the preform softens and is drawn into fibers that are collected onto a drum. There are typically two drawing stages. The first draw produces large-diameter, single-aligned fibers, and the second draw reduces the fiber diameter; then, a fiber bundle can be obtained [28, 46]. For example, Blumenfeld et al. studied polystyrene fibers doped with wavelength-shift fluors cladded with PMMA [34]. The fibers were drawn and then compacted into a hexagonal bundle geometry during secondary drawing to form a bundle of “perfectly aligned fibers” for optimal scintillation performance. However, some

degradation was observed for PS due to high temperature exposure during secondary drawing [34].

Electrospinning. Electrospinning is a low-cost method where the polymer solution is pumped through a metal syringe needle over a distance under an electric field onto a grounded collector [47, 48]. Electrospinning has demonstrated the ease of fabrication of nanofibers that have tunable properties and bright and uniform photoluminescence [49]. The extrinsic properties are important parameters that directly influence the formation of fibers during the electrospinning process. The quantitative relationship between extrinsic properties and fiber diameter is variable due to the complexity of the electrospinning process, and although noted with caution some trends have been observed. For example, an increase in applied voltage has been reported to yield smaller-diameter fibers [47, 48, 50]. Kidoaki et al. reported that an increase in the feed rate tended to yield larger-diameter fibers with reduced bead morphology [51]. Smaller-diameter fibers have been observed when the gap distance between the needle tip and the target was increased, but, by adjusting other parameters, the fiber diameter can actually be increased [48, 51-53].

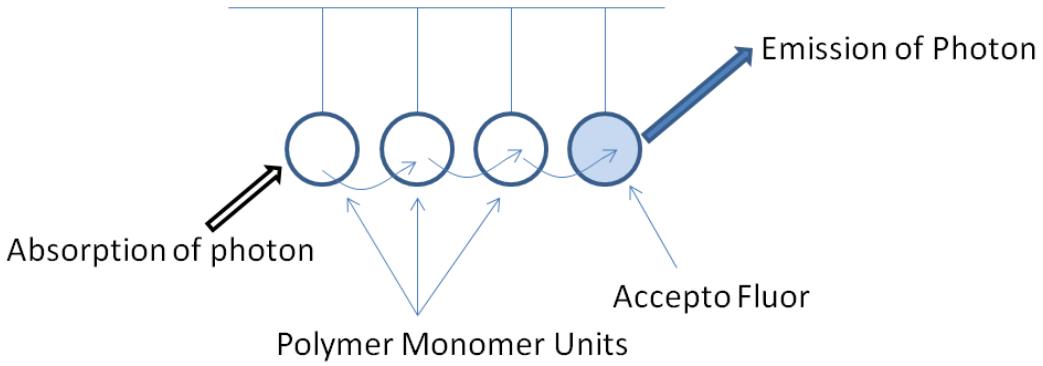

Figure 1.1: Schematic of energy transfer between a polymer monomer unit and a fluor: light-harvesting effect [9].

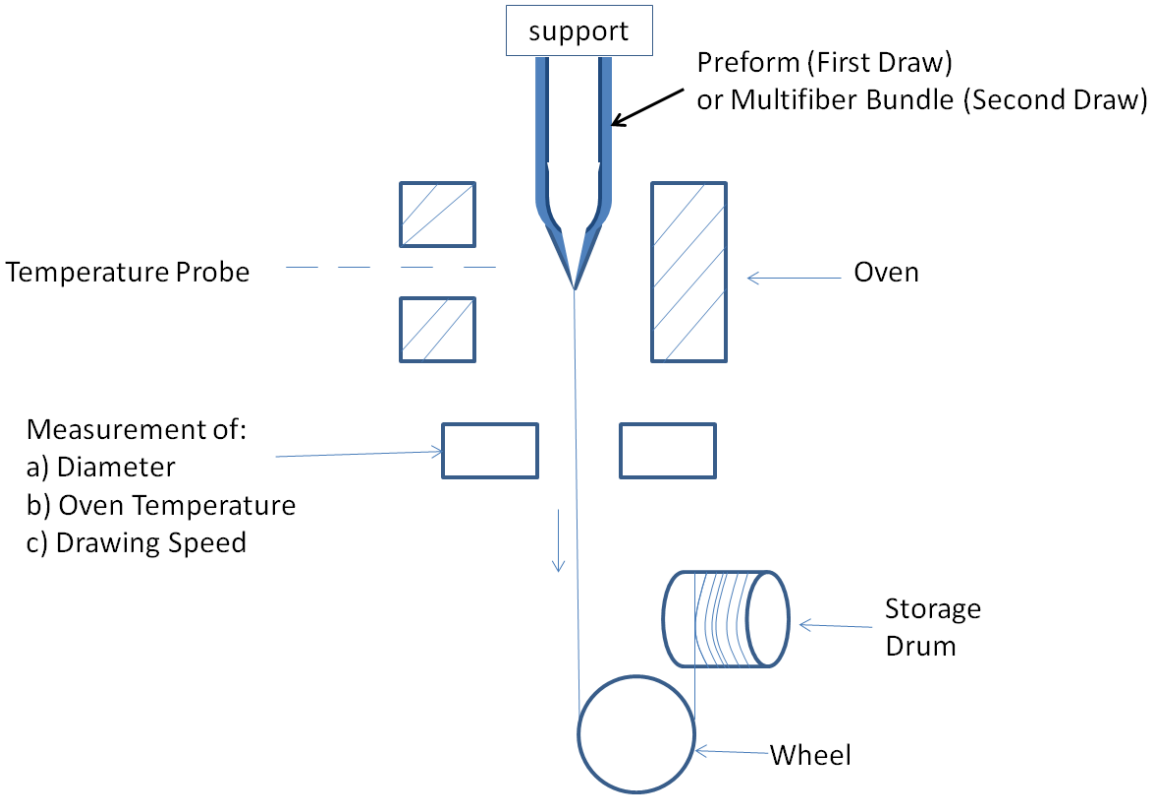

Figure 1.2: Schematic of fiber drawing setup [28].

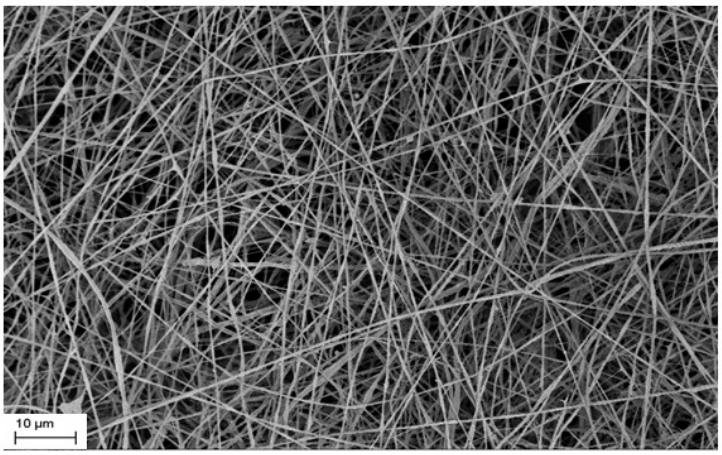

Figure 1.3: Example scanning electron micrograph (SEM) of electrospun random nanofiber mat.

Additionally, the collector geometry can change the morphology of the fiber. For example, the commonly used stationary metal target collector at a fixed distance from the syringe needle tip yields a random mat, as shown in Figure 1.3 [48]. A rotating target collector (Figure 1.4(a)) can yield oriented fibers, as shown in Figure 1.4(b).

The intrinsic properties of the polymer solution play a very important role in the formation of the fiber in the electrospinning process. The polymer concentration is a determining factor in the spinnability of the polymer solution, where sufficient chain entanglement is needed to fabricate continuous fibers. Although used with caution due to the complexity of the electrospinning process, generally, an "increase in polymer concentration increases the average fiber diameter" [48, 54, 55]. However, the quantitative relationship between the polymer concentration and the diameter appears to be variable [48]. Using Simha's schematic representation of concentration regime, the transition of dilute solution to a critical polymer chain entanglement can be visualized as shown below in Figure 1.5 [48, 56].

In dilute solutions, there is no chain overlap (Figure 1.5(a)) and little interaction among the polymer chains. However, by increasing the concentration, the interaction between the polymer chains is increased (Figure 1.5(b), Figure 1.5(c)). When the critical concentration is reached, the polymer chains begin to overlap and the interaction energy is increased (Figure 1.5(c)).

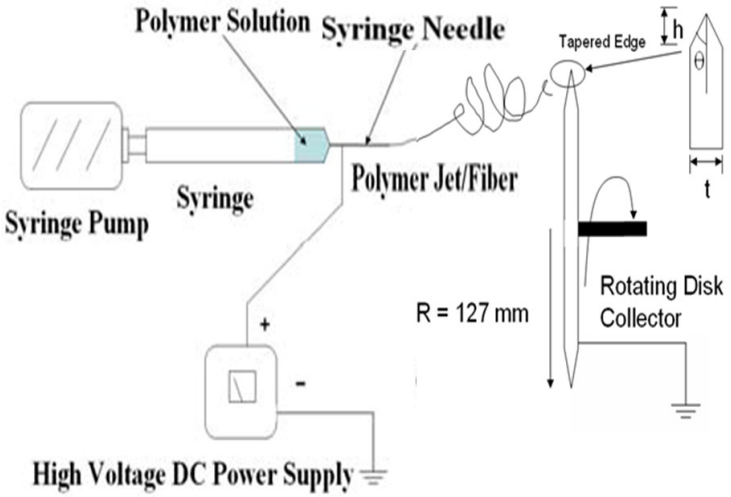

(a)

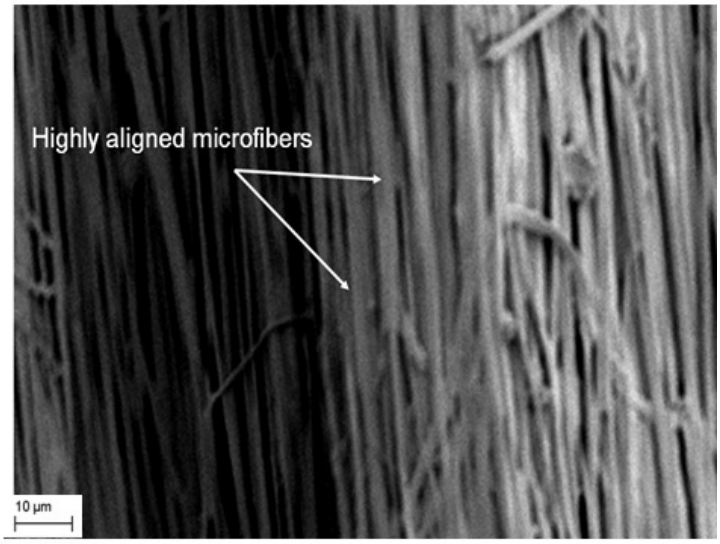

(b)

Figure 1.4: (a) Schematic diagram of electrospinning setup with rotating target and (b) example SEM micrograph of electrospun aligned fiber mat.

As the normalized concentration, x/x', is increased, the entanglement regime will have polymer chains that are sufficiently entangled, resulting in a viscous polymer solution. Additionally, as x/x' is increased, a "gradual change from (a) electrospraying of particles, (b) beaded fibers to (c) smooth continuous fibers will be deposited on collector (assuming molecular weight of polymer is sufficiently high for electrospinning)" [48].

The viscosity of the polymer solution is one of the most important variables in the electrospinning process and is considered the variable that determines the fiber morphology [56-58]. The intrinsic viscosity is inversely related to the chain overlap concentration, as shown in Eq. 1.2.

$$x' \sim [\eta]^{-1} \qquad \text{(Eq. 1.2)}$$

The intrinsic viscosity is strongly related to the average molecular weight, M_v, using the Mark-Houwink-Sakurada equation:

$$[\eta] = K M_v^a \qquad \text{(Eq. 1.3)}$$

where "*K* is characteristic of a specified polymer and solvent and *a* relates to the shape of the polymer coil in the solvent" [58, 59].

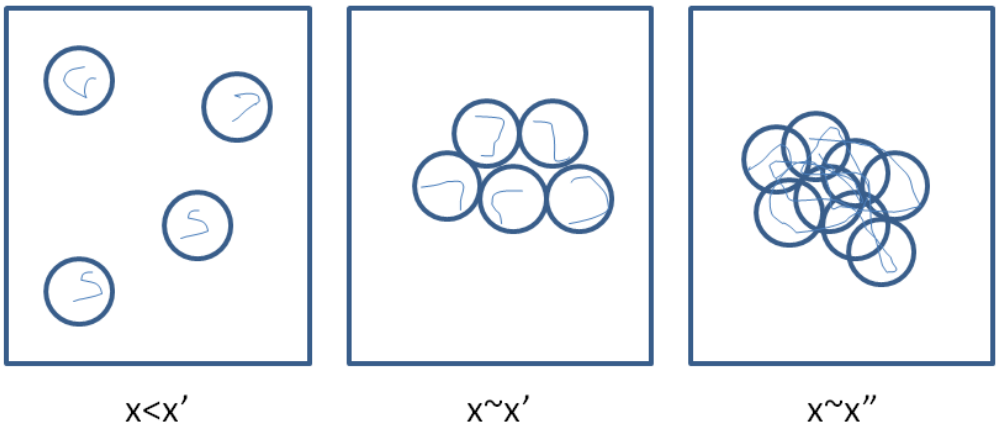

Figure 1.5: Schematic representation of a polymer solution in different concentration regimes where x is the polymer concentration, x' is the critical concentration of the polymer solution, and x'' is the entanglement regime were chains begin to overlap [48, 56]

Furthermore, the viscosity of the solution is strongly related to the configuration of the polymer chains in solution. In a “thermodynamically good solvent,” the polymer chains will uncurl or extend and have a high interaction energy, leading to an increase in the intrinsic viscosity of the solution.

On the other hand, in a “thermodynamically bad solvent,” the polymer chains will curl, having low interaction energy and leading to a decrease in the intrinsic viscosity in polymer solution [58]. In addition, the flexibility of the polymer chain is important for the intrinsic viscosity of the solution. If the polymer chains are too rigid, the intrinsic viscosity of the solution is lower [58, 60]. The intrinsic viscosity is related to the temperature in terms of the Flory-Huggins Θ temperature [61]. The Θ temperature is where in a polymer-solvent system, the polymer has “unperturbed dimensions” will not be able to tell whether it is in contact with another segment or a solvent molecule [62]. If the polymer-solvent is initially below the Θ temperature, the viscosity will increase when heated to just above Θ temperature.

The molecular weight of the polymer is very influential in the electrospinning process. The molecular weight is the sum of the individual monomers, represents the length of the polymer chain [58, 59], and directly influences the viscosity of the solutions in the sense that the higher the molecular weight is, the more resistant the polymer is to dissolving in solvent. Conversely, the lower the molecular weight is, the less resistant the polymer is to dissolving in solvent [58]. The threshold value to achieve sufficient polymer chain entanglement is the

critical molecular weight or entanglement weight, M_c [48]. Additionally, the critical concentration, x', is directly proportional to the molecular weight. The higher the molecular weight, the longer the polymer chain will be and, thus, the lower the concentration required to electrospin will be [48]. Hence, for the polymer jet formation during the electrospinning process, the polymer chains will be sufficiently entangled to form continuous fibers. Conversely, a lower molecular weight will lower the viscosity of the solution and yield smaller polymer chains that may not have sufficient entanglement to spin continuous fibers, where a polymer jet would be discontinuous [58].

The electrical conductivity of the solution plays an essential role in the electrospinning process in terms of the transfer of electric charge and stretching of the polymer solution, where an increase in conductivity in the solution leads to more charges that can be carried [58]. Due to repulsive and bending instabilities of the polymer during electrospinning, bead formation may occur in the resulting fiber if the polymer is not fully stretched due to a lack of adequate surface charge density [48].

Using the second law of thermodynamics,

$$\Delta G = \Delta H - T\Delta S \qquad \text{(Eq. 1.4)}$$

where ΔG is the change in free energy, ΔH is the change in enthalpy, T is the temperature, and ΔS is the change in entropy. The polymer-solvent system is soluble if $\Delta G<0$, where both T and ΔS are increased and the polymer solution is

in a single phase (homogenous solution). However, for two-phase systems, additional criteria must be considered to determine ΔG [48]. For polymer-solvent systems, solubility parameters are essential to electrospinning in determining which solvents will dissolve the polymer. Solubility parameters are related to the energy of vaporization, which is "a measure of cohesive energy density, c, holding the liquids together" [63]. The interaction of polymer chains with solvent is based on Hildebrand. The cohesive energy density relates to the energy required to separate the liquid molecules by overcoming the molecules together. The cohesive energy density is given by the following expression:

$$c = \frac{\Delta H - RT}{V} \qquad \text{(Eq. 1.5)}$$

where ΔH is the change in enthalpy, R is the gas constant, T is the temperature and V is the molar volume [48].

The Hildebrand solubility parameter is defined as

$$\delta = \sqrt{c}\,\frac{cal}{cm^2}^{1/2} \qquad \text{(Eq. 1.6)}$$

for predicting solubility in terms of the cohesive energy density. The basic idea is that a polymer and solvent with approximately the same values are soluble.

However, there are limitations to this parameter because it takes into account only dispersion forces [48]. Hansen further developed this concept to include polar and hydrogen components, which are useful in electrospinning due to the frequent use of mixed solvents to dissolve a polymer [64, 65].

$$(\delta)^2 = (\delta_D)^2 + (\delta_P)^2 + (\delta_H)^2 \qquad \text{(Eq. 1.7)}$$

where D, P, and H correspond to the dispersive, polar and hydrogen components to determine total Hansen solubility parameter.

Melt-spinning. Melt-spinning is a process where a polymer melt is extruded through a spinneret positioned vertically, where the filament is cooled and collected onto a take-up winder [66]. Extrusion generally consists of three zones, namely “feed, compression and metering” zones [59]. A neat resin or composite mixture is fed into the hopper, where it is transported to the compression zone by a rotating screw [67]. In the compression zone, the polymer is melted at a sufficiently high temperature, and the polymer melt is subjected to shearing between the screw and the inner wall of the extruder and forced out through the spinneret [59]. The formed fibers are then subjected to a high degree of stretching such that an increase in the take-up speed can increase the crystallinity and mechanical properties of the fiber [66]. For example, PEN melt-spun fibers have shown increased crystallinity and mechanical properties with

increased take-up speed [68]. Additionally, intrinsic values have been reported for PEN [69].

Carbon Fiber/Vinyl Ester. Carbon fiber composites are well known for their high stiffness, high strength, low weight and resistance to environmental degradation [70]. Carbon fiber with vinyl ester resin (CFVE) is an attractive composite for aerospace and marine applications due to its mechanical properties and the relatively low cost of fabrication using the vacuum-assisted resin transfer molding (VARTM) technique. Shivakumar investigated the mechanical properties of the carbon fiber composite and found CFVE modulus and strength exceed that of marine steel [71].

1.3 References

[1] Knoll, G. F., 2000, *Radiation Detection and Measurement, 3rd ed*. John Wiley and Sons, Hoboken, NJ, pp. 224-522.

[2] Kouzes, R. T., 2009, "The ^{3}He Supply Problem," Pacific Northwest National Laboratory Technical Report, PNNL-18388.

[3] Kulkarni, P. V., et al., 1997, "Plastic Scintillating Materials in Nuclear Medical Imaging," Polymer-Plastics Technology and Engineering, **36(1)**, pp. 1-51.

[4] Squires G. L., 1978, *Introduction to the Theory of Thermal Neutron Scattering,* Dover Publications, Mineola, NY, p. 1.

[5] Pawelczak, I. A., 2011, "NSTAR –A Capture Gated Plastic Neutron Detector," Nuclear Instruments and Methods in Physics Research A, **629**, pp. 230-238.

[6] Horrocks, D. L. and Peng, C. T., 1971, *Organic Scintillators and Liquid Scintillation Counting,* Academic Press, Inc., New York, NY, p. 471.

[7] Oliver, D. B. and Knoll, G. F.,1968, "Anisotropy of Scintillation Response of Anthracene to Neutron Generated Recoil Protons and Carbon Ions," IEEE Trans. Nucl. Sci., **NS-15(3)**, pp. 122-126.

[8] Hamel, M., Simic, V., and Normand, S., 2008, "Fluorescent 1,8-Naphthalimides-Containing Polymers as Plastic Scintillators. An Attempt for Neutron-Gamma Discrimination," Reactive and Functional Polymers, **68**, pp. 1671-1681.

[9] Fery-Forgues, S., and Fournier-Noël, C., 2010, "Organic Fluorescent Nanofibers and Sub-Micrometer Rods, Nanofibers," Kumar, A. (Ed.), ISBN:

978-953-7619-86-2, InTech, DOI: 10.5772/8164. Available from: <http://www.intechopen.com/books/nanofibers/organic-fluorescent-nanofibers-and-sub-micrometer-rods> (accessed 07.25.2013).

[10] Tsoulfanidis, N. and Landsberger S., 2011, *Measurement and Detection of Radiation,* Taylor and Francis Group, Boca Raton, FL, p. 178.

[11] Inagaki, T., and Takashima, R., 1982, "New Types of Plastic Scintillators," Nuclear Instruments and Methods in Physics Research, **201(2-3)**, pp. 511-517.

[12] Nakamura, H., et al., 2011, "Evidence of Deep-Blue Photon Emission at High Efficiency by Common Plastic", EPL (Europhysics Letters), 95(2), pp. 22001 –p1 – 22001-p3.

[13] Cheung, P. S. R., Roberts C. W., and Wagener, K. B., 1979, "Synthesis, Photodegradation, and Energy Transfer in a Series of Poly(ethylene Terephthalate-co-2,6-Naphthalenedicarboxylate) Copolymers," Journal of Applied Polymer Science, **24**, pp. 1809-1830.

[14] Ouchi, I., Nakai, I., Ono, M., and Kimura, S., 2007, "Features of Fluorescence Spectra of Polyethylene 2,6-Naphthalate Films," Journal of Applied Polymer Science, **105**, pp. 114-121.

[15] Moser, S. W., Harder, W. F., Hurlbut, C. R., and Kusner, M. R., 1993, "Principles and Practice of Plastic Scintillator Design," Radiat. Phys. Chem., **41(1/2)**, pp. 31-36.

[16] Brudanin, V. B., et al.., H., 2001, “Elemented-Loaded Organic Scintillators for Neutron and Neutrino Physics,” Particles and Nuclei, Letters, 109(6), pp. 69-77.

[17] Bell, Z. W., H., Brown, G. M., Ho, C. H., and Sloop, Jr., F. V., 2003, “Organic Scintillators for Neutron Detection,” X-ray and Gamma-ray Detector and Applications 7-9 July 2002 Proceedings of SPIE, **4784**, pp. 150-163.

[18] Ovechkina, L., Riley, K., Miller, S., Bell, Z., and Nagarkar, V., 2009, “Gadolinium Loaded Plastic Scintillators for High Efficiency Neutron Detection,” Physics Procedia, **2**, pp. 161-170.

[19] Fisher, B. M., et al., 2011, “Fast Neutron Detection with 6Li-loaded Liquid Scintillator,” Nuclear Instruments and Methods in Physics Research A, **646**, pp. 126-134.

[20] EljenTechnology,EJ254,2013,<http://www.eljentechnology.com/index.php/products/loaded-scintillators/78-ej-254> (accessed 07.02.2013).

[21] Breukers, R. D., Bartle, C. M., and Edgar, A., 2013, “Transparent Lithium Loaded Plastic Scintillators for Thermal Neutron Detection,” Nuclear Instruments and Methods in Physics Research A, **701**, pp. 58-61.

[22] Sen, I., Penumadu, D., Williamson, M., Miller, L. F., Green, A. D., and Mabe, A. N., 2011, “Thermal Neutron Scintillator Detectors Based on Poly(2-Vinylnapthalene) Composite Films,” IEEE Trans. Nucl. Sci., **59**(3), pp. 1386-1393.

[23] Katagiri, M., Sakasai, K., Matsubayashi, M., and Kojima, T., 2004, "Neutron/γ-ray Discrimination Characteristics of Novel Neutron Scintillators," Nuclear Instruments and Methods in Physics Research A, **529**, pp. 317-320.

[24] Im, H. J., Saengkerdsub, S., Stephan, A. C., M., Pawal, M. D., Holcomb, D. E., and Dai, S., 2004, "Transparent Solid-State Lithiated Neutron Scintillators Based on Self-Assembly of Polystyrene-block-Poly(ethylene Oxide) Copolymer Architectures," Adv. Mater., **16**(19), pp. 1757-1761.

[25] Mabe, A. N., Auxier II, J. D., Urffer, M. J., Penumadu, D., Schweitzer, G. K., and Miller, L. F., 2013, "Transparent Lithiated Polymer Films For Thermal Neutron Detection," Nuclear Instruments and Methods in Physics Research A, **772**, pp. 29-33.

[26] Mabe, A. N., Auxier II, J. D., Urffer, M. J., Young, S. A., Penumadu, D., Schweitzer, G. K., and Miller, L. F., 2013, "Thin Film Polymer Composite Scintillators for Thermal Neutron Detection," Journal of Composites, **2013**, Article ID 539060, pp. 1-8.

[27] Sen, I., Urffer, M., Penumadu, D., Young S. A., Miller, L. F., and Mabe, A. N., 2012, "Polyester Composite Thermal Scintillation Films," IEEE Trans. Nucl. Sci., **59**(4), pp. 1781-1786.

[28] Kirkby, J., 1987, "Today and Tomorrow for Scintillating Fibres (SCIFI) Detectors," European Organization For Nuclear Research, CERN-EP/87-60.

[29] Allemand, L. R., Calvet J., Cavan, J. C. and Thevenin, J. C., 1984, "Optical Scintillating Fibres for Particle Detectors," IEEE Trans. Nucl. Sci., **225**, pp. 522-524.

[30] Blumenfeld, H., Bourdinaud M., and Thevenin, J. C., 1986, "Scintillating Plastic Fibres for Calorimetry and Tracking Devices," IEEE Trans. Nucl. Sci., **33(1)**, pp. 54-56.

[31] Rebourgeard, Ph., et al., 1999, "Fabrication and Measurements of Plastic Scintillating Fibers," Nuclear Instruments and Methods in Physics Research A, **427**, pp. 543-567.

[32] Ruchti, R. C., 1996, "The Use of Scintillating Fibers for Charged-Particle Tracking," Nucl. Part. Sci., **46**, pp. 281-319.

[33] White, T. O., 1988, "Scintillating Fibres," Nuclear Instruments and Methods in Physics Research, **A273**, pp. 820-825.

[34] Blumenfeld, H., Bourdinaud, M., Rebourgeard, P., and Thevenin, J. C., 1989, "Production and Test of Coherent Bundles of Plastic Scintillating Microfibers," Nuclear Instruments and Methods in Physics Research A, **364**, pp. 619-621.

[35] Blumenfeld, H., Bourdinaud, M., and Thevenin, J. C., 1984, Nucleophot CERN, **85-10**, p. 246.

[36] Li, L., Yang, X., and Yuan, L., 2012, "One-dimensional Optical Materials of Microfibers by Electrospinning," Materials Letters, **1**, pp. 292-295.

[37] McIntosh, K., Yamada, N., and Richards, B. S., 2007, “Theoretical Comparison of Cylindrical and Square-Planar Luminescent Solar Concentrators,” Appl. Phys. B, **88(2)**, pp. 285-290.

[38] Leutz, H., 1995, “Scintillating Fibres,” Nuclear Instruments and Methods in Physics Research A, **364**, pp. 422-448.

[39] Edelenbosch, O. Y., Fisher, M., Patrignani, L., van Sark, W. G. J. H. M., and Chatten, A. J., “Luminescent Solar Concentrators with Fiber Geometry,” Optical Express, **21(S3)**, pp.A 503-A514.

[40] Colantuono, G., Buckley, A., and Erdelyi R., 2013, “Ray-Optics Modelling of Rectangular and Cylindrical 2-Layer Solar Concentrators,” J. Lightwave Technol., **31(7)**, pp. 1033-1044.

[41] Inman, R. H., Scherbatyuk, G., Medvedko, D., Gopinathan, A., and Ghosh, S., 2011, “Cylindrical Luminescent Solar Concentrators with Near-Infrared Quantum Dots,” Opt. Express., **19(24)**, pp. 24308-24313.

[42] Birks, J. B., 1964, *Theory and Practice of Scintillating Counting,* Pergamon Press, Oxford.

[43] Rebourgeard, P., Blumenfeld, H., and Bourdinaud, M., 1989, “A Simple Method for Measuring the Performance of Plastic Scintillating Materials,” IEEE Transactions on Nuclear Science, **36(1)**, pp. 150-157.

[44] Convert, P., and Forsyth, J. B., 1983, *Positon-Sensitive Detection of Thermal Neutrons,* Academic Press, New York, NY, pp. 91-94.

[45] Grazioso, R. F., et al., 1999, “Feasibility of Using Boron-Loaded Plastic Fibers for Neutron Detection,” Nuclear Instruments and Methods in Physics Research A, **422**, pp. 59-63.

[46] Daly, J. C., 1984, *Fiber Optics,* CRC Press, Boca Raton, FL, p. 31.

[47] Doshi, J., and Reneker, D. H., 1995, “Electrospinning Process and Applications of Electrospun Fibers,” Journal of Electrostatics, **35**, pp. 151-160.

[48] Andrady, A. L., 2008, *Science and Technology of Polymer Nanofibers*, John Wiley and Sons, Inc., Hoboken, NJ, pp. 81-311.

[49] Camposeo, A., Di Benedetto, F., Stabile, R., Neves, A. A. R., Cingolani, R., and Pisignano, D., 2009, “Laser Emission from Electrospun Polymer Nanofibers,” Small, **5**(5), pp. 562-566.

[50] Jalili, R., Hosseini, S. A., and Morshed, M., 2005, “The Effects of Operating Parameters on the Morphology of Electrospun Polyacilonitrile Nanofibers,” Iranian Polymer Journal, 14(12), pp. 1074-1081.

[51] Kidoaki, S., Kwon, K., and Matsuda, T., 2006, “Structural Features and Mechanical Properties of In-Situ-Bonded Meshes of Segmented Polyurethane Electrospun from Mixed Solvents,” Journal of Biomedical Materials Research Part B: Applied Biomaterials, **76B(1)**, pp. 219-229.

[52] Baker, S C., et al., 2006, “Characterisation of Electrospun Polystyrene Scaffolds for Three-Dimensional in Vitro Biological Studies,” Biomaterials, **27(16)**, pp. 3136-3146.

[53] Lee, J. S., et al., 2004, “Role of Molecular Weight of Atactic Poly(vinyl alchohol) (PVA) in the Structure and Properties of PVA Nanofabric Prepared by Electrospinning,” Journal of Applied Polymer Science, 93, pp. 1638-1646.

[54] Subbiah, T., Bhat, G. S., Tock, R. W., Parameswaran, S., and Ramkumar, S. S., 2005, “Electrospinning of Nanofibers,” Journal of Applied Polymer Science, **96(2)**, pp. 557-569.

[55] Deitzel, J. M., Kleinmeyer, J., Harris, D., and Tan, N. C. B., 2001, “The Effect of Processing Variables on the Morphology of Electrospun Nanofibers and Textiles,” Polymer, **42(1)**, pp. 261-272.

[56] Simha, R. and Zakin, J. L., 1962, “Solution Viscosities of Linear Flexible High Polymers,” Colloid Science, **17(3)**, pp. 270-287.

[57] Jun, Z., Hou, H.Q., Schaper, A., Wendorff, J. H. and Greiner, A., 2003, “Poly-L-lactide Nanofibers by Electrospinning-Influence of Solution Viscosity and Electrical conductivity on Fiber Diameter and Fiber Morphology,” e-Polymers, **009[2003]**, pp. 1-9.

[58] Ramakrishna, S., 2005, *An Introduction to Electrospinning and Nanofiber*, World Scientific Publishing Company, Hackensack, NJ, pp. 22-189.

[59] Fried, J.R., 2003, *Polymer Science and Technolgy*,2nd Ed., Prentice Hall, Upper Saddle River, NJ, pp. 87-277.

[60] Alfrey, T., Bartovics, A., and Mark, H., 1942, “The Effect of Temperature and Solvent Type on the Intrinsic Viscosity of Polymer Solution,” Journal of the American Chemical Society, **64**, pp. 1557-1560.

[61] Flory, P.J. and Krigbaum, W.R., 1950, “Statistical Mechanics of Dilute Polymer Solutions,” J. Chem. Phys., **18**, pp. 1086-1094.

[62] Holmberg, K., 2003, *Surfactants and Polymers in Aqueous Solutions*, John Wiley and Sons, West Sussex, England p. 203.

[63] Hansen, C. M., 2000, *Hansen Solubility Parameters: A User’s Handbook,* CRC Press, Boca Raton, FL, p. 2

[64] Hansen C. M., 1967, “The Three Dimensional Solubility Parameter – Key to Paint Component Affinities. Part I: Solvents, Plasticizers, Polymers, and Resins,” Journal of Paint Technology, **39(511)**, pp. 104-117.

[65] Hansen C. M. and Skaarup, K., 1967, “The Three Dimensional Solubility Parameter – Key to Paint Component Affinities. Part III: Independent Calculation of the Parameter Components,” Journal of Paint Technology, **39(511)**, pp. 511-514.

[66] Lawrence, C. A., 2003, *Fundamentals of Spun Yarn Technology,* CRC Press, Boca Raton, FL., p. 48.

[67] Pla-Dalmau, A., Bross, A. D., and Rykalin, V. V., 2003, “Extruding Plastic Scintillator at Fermilab,” Nuclear Science Symposium Conference Record, 2003 IEEE, 19-25 Oct. 2003, **1**, pp. 102-104.

[68] Cakmak. M., and Kim, J. C., 1997, “Structure Development in High-Speed Spinning of Polyethylene Naphthalate (PEN) Fibers,” Journal of Applied Polymer Science, **64(4)**, pp. 729-747.

[69] Teonex®, "Polyethylene Naphthalate Resin," Teijin Chemicals, Ltd. Catalog

[70] Chung, D.D. L., 1994, *Carbon Fiber Composites*, Butterworth-Heinemann, Newton, MA, pp. ix.

[71] Shivakumar, K. N., "Carbon/Vinyl Ester Compostes for Enhanced Performance in Marine Applications," J. Reinf Plast Comp, **25(10)**, pp. 1101-1116.

2 CHAPTER II
INVESTIGATION OF LITHIUM-6 ENRICHED PARTICLE DISPERSION IN FLUORESCENT ELECTROSPUN NANOFIBERS BE USED AS THERMAL NEUTRON SCINTILLATORS

A slightly revised version of this chapter was originally published in *Journal of Engineering Materials and Technology* by Stephen A. Young, Indraneel Sen, and Dayakar Penumadu:

Stephen A. Young, Indraneel Sen and Dayakar Penumadu. "Investigation of Lithium-6 Enriched Particle Dispersion in Fluorescent Electrospun Nanofibers to be Used as Thermal Neutron Scintillators," *Journal of Engineering Materials and Technology*, 134(1) (2012): pp. 010908-1-010908-7

My main contributions to this manuscript included (a) development of research topic into experimental work, (b) performing literature review, (c) conducting electrospinning experiments, (d) characterization, analysis, and interpretation of the experimental results, and (e) writing majority of the manuscript.

2.1 Abstract

Electrospun polymer nanofibers are attractive due to their unique volume-to-surface area, chemical, electrical, and optical properties. Department of Homeland security has interest in applications with polymeric scintillation detectors that directly discriminate between neutron and gamma radiations using manufacturing techniques that are inexpensive and which can be effectively implemented to produce large area detectors. Lithium-6 (^{6}Li) isotope has a significant thermal neutron cross-section and produces high energy charged particles upon thermal neutron absorption. In this research, ^{6}Li loaded polymer composite was successfully spun onto a stationary stainless steel target creating

a thermal neutron scintillator made of randomly oriented fibers. Fiber mats thus obtained were characterized using scanning electron microscopy (SEM) and energy dispersive x-ray spectroscopy (EDS) for morphology, and fluorospectroscopy for optical properties. Additionally, the fiber mats were characterized for polymeric properties including microstructure evaluation and response to thermal neutrons, alpha, beta, and gamma radiation using suitable radiation facilities. Fiber matrix was made out of an aryl vinyl polymer and a wavelength shifting fluor with efficient resonant energy transfer characteristics. The mats produced had scintillation fibers having diameters from 200 nm to 3.2 microns.

Index Terms— detectors, lithium compounds, nanoparticles, electrospinning, amplified spontaneous emission

2.2 Background

There is a growing demand in thermal neutron scintillation research due to the need for neutron detectors for the department of homeland security applications [1]. ^{6}Li has a relativity large thermal neutron cross section of 940 barns and works as an efficient scintillation converter for detecting thermal neutrons [2]. Efficient thermal neutron detectors can be synthesized by uniformly dispersing particles enriched with ^{6}Li based compounds within a scintillating polymer matrix [3]. Polymer composites and blends are the materials of choice for modern

technological applications, due to their unique surface-chemistry and their mechanical and optical properties that are not attainable in pure polymers. The microstructure of polymeric composite materials can significantly influence the mechanical properties and quantum efficiency. When a polymer composite consisting of hydrophilic salt and hydrophobic polymer components is cast into a film by evaporation techniques from a homogeneous solution, phase separations generally occur within the polymer matrix. The size of the phase separated domains depends on several parameters including the kinetics of solvent evaporation, relative solubility of the components in the common solvent or mixture of solvents, and relative concentration of the components of the composite [4]. If the separated phase dimensions are in micron sizes, the optical properties of the composite film or disk thus obtained is significantly compromised due to scattering and absorption, as shown in Figure 2.1. Thus, for a scintillation device the dimension of phase separations plays an important role in deciding the quantum efficiency. In many such cases, in order to obtain high optical transparency, the concentration of the precipitating secondary phase needs to be lowered/sacrificed in order to achieve non-scattering nanometer size domains. Nanometer size phases of the secondary hydrophilic component can be obtained by making electrospun submicron fibers of the polymer composite in a pre-processing step [5-6]. Spherical and coaxial phase separations have been reported in electrospinning literature [7-9]. It is imperative that a separate phase domain within a nanofiber will be of nanometer dimension.

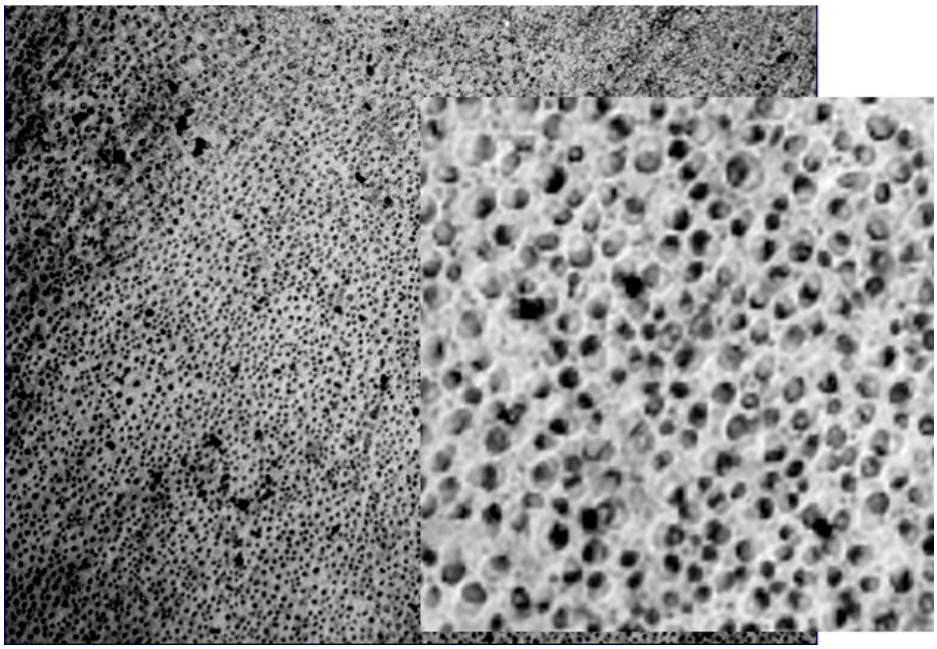

Figure 2.1 : Optical micrograph showing 4.2 μm equivalent diameter of ^{6}Li-Salicylate (^{6}LiSal) domains separated within poly(2-vinylnaphthalene) (P2VN) matrix [5].

Our hypothesis is that the nanometer size domains can be substantially retained in a composite film made by suitable post-processing of the electrospun nanofibers. A second possibility is a neat homogeneous mixed system without any nanophase separation. Such a homogeneous system can be obtained in principle since the phase stability of electrospun fibers is driven by a competition between the solvent evaporation kinetics and thermodynamics of phase separation [10,11]. A representative scanning electron microscope (SEM) micrograph of polystyrene (PS)/poly(2-vinylnaphthalene) (P2VN) polymer blend with ^{6}LiSal (^{6}Li-Salicylate) sample is shown in Figure 2.2(a).

The benefits of nanophases are well known due to their ultra-fine dimensions, and they are well-dispersed in polymer matrix, which yields unique properties that are different from those corresponding bulk materials because of encapsulated quantum confinement effects and their large surface to volume ratio [12-15]. The nanoparticles surface interaction with matrix has a critical role to yield these properties [16]. Electrospinning is a novel processing technique which is a low-cost method yielding nonwoven fibers and fiber mats for a variety of applications [6,10,17-20]. Electrospinning is vastly influenced by spinning conditions including solution concentration, applied voltage, feed rate, distance between needle tip and collector, volatility of solvents, and solubility parameters.

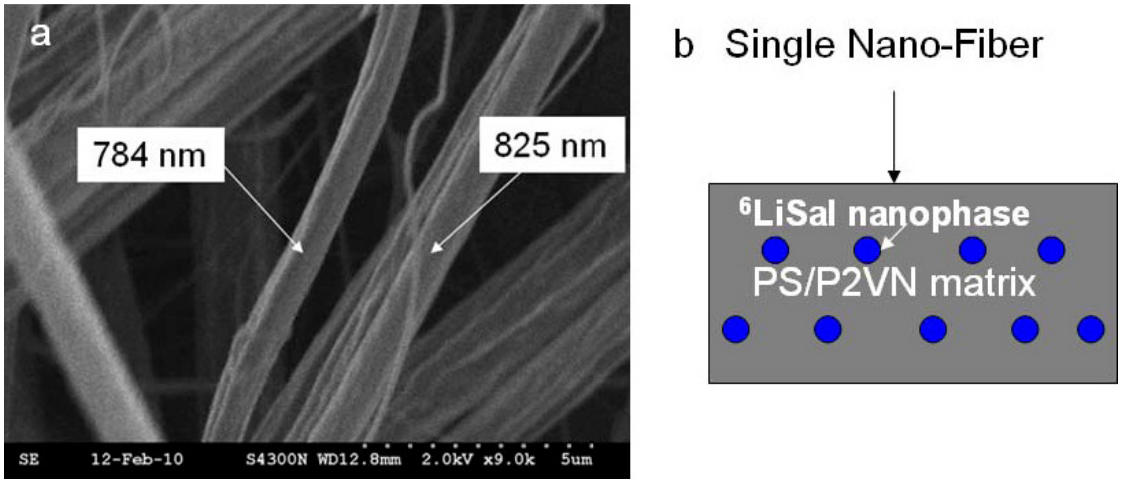

Figure 2.2: (a) Scanning electron microscope (SEM) micrograph of electrospun nanofibers and (b) illustration of nanophases uniformly dispersed within the nanofiber.

It is well known for the process of electrospinning polymer fibers that solvent evaporation is one of the most critical steps to produce dry fibers where the morphology of the nanofiber is directly influenced by interactions between the polymer and solvent [6,21]. Although extensive studies have been performed in this area, it is still not well understood given the complex electrohydrodynamic interactions during the formation of the fibers [22,23]. For instance, control of the competitive rates between phase separation and solvent evaporation requires a complicated organic solvent system [24]. This kinetically driven process induces phase separation, where the rapid solvent evaporation is on a time scale in the millisecond range [25]. Formation of metastable phases within electrospun fibers is possible due to deformation of jet and fast solidification, where the process tends to align polymer chains and subsequently rapid solidification can freeze the alignment of the molecules [26,27]. This rapid solidification produces nanofibers with occurrence of nucleation and crystallization of nanoparticles/nanophases inside the nanofibers restricting crystal growth within the fibers [28].

The uniqueness of aryl vinyl polymers (AVP) is the ease of forming them into flexible structures such as films, fibers, fabric etc. that emit visible light at high quantum efficiency when the pendant aromatic rings are excited by various means. Among these polymers, P2VN has advantageous features of higher quantum yield than PS and efficient energy transport within its matrix [5,29]. PS has been shown to be an attractive polymer due to its ease of synthesizing and solubility in various solvents that are well suited for electrospinning [6]. ^{6}Li either

in molecular inclusions or in the form of nanoparticles can be blended in a matrix of AVP and additives to form an effective neutron scintillation detector. The essential steps in the development of nanoscience and nanotechnology includes material preparation, property characterization, and device fabrication, with the latter two yielding the most challenging tasks [12,30]. The motivations in development of scintillation neutron detectors based on electrospun fabric are to obtain a thin, low density composite material made out of low (Z) atomic number components, and high ^{6}Li concentration that would directly discriminate between neutron and γ radiations due to its low γ interaction. An additional requirement is an easily and economically fabricated product, available as a large surface area fabric or sheet in different shapes with ease of implementation in public places.

Luminescent nanofibers with fiber diameter dimensions 500 nm and below provide unique properties and can act as an active component to generate or transmit light from one point to another [31,32]. Amplified spontaneous emission (ASE) is a luminescence process that occurs when spontaneous emitted photons are amplified as they travel through a gain medium [32]. This process is achieved typically by fabricating a waveguide array of the gain medium [32-35]. ASE has been observed for polymeric nanofibers showing a spectral narrowing following excitation of a single nanofiber [36,37].

Our group has electrospun poly[(p-phenylenevinylene)-alt-(m-phenylenevinylene) PPV (polymer 7a) [38] copolymer (15 wt. %) blend in PS nanofibers onto a substrate, as shown in Figure 2.3(b).

The shape of the spectrum of light emitted from the PPV/PS blend nanofiber changes drastically when the intensity of the exciting light pulse is λ scanned ($\lambda = 365$ nm) over a single nanofiber using a laser confocal microscope with maximum emission peak at wavelength, 489 nm, as reported in Figure 2.3(a). The results shown in Figure 2.3 strongly suggest that such fibers may act in ASE mode, which serves as motivation for their use as scintillation materials [34].

In this study, we tackle a particular problem of micron size separated phases of highly polar and hydrophilic lithium salt aggregates within a hydrophobic polymer matrix (Figure 2.1). The particular polymer composite material is used to fabricate highly discriminative thermal neutron scintillation detectors. Using electrospinning as a precursor step, we investigate a novel method where optical transparency can be enhanced, compared to an otherwise optically translucent composite film of the same composition. Some of the ^{6}Li compounds that we considered for thermal neutron absorption are presented in Table 2.1. These lithium compounds were selected due to their unique properties, which include nonhygroscopic and nonpyrophoric properties. Figure 2.4 shows a typical electrospun ^{6}Li based PS nanofiber mat and its exposure to UV radiation.

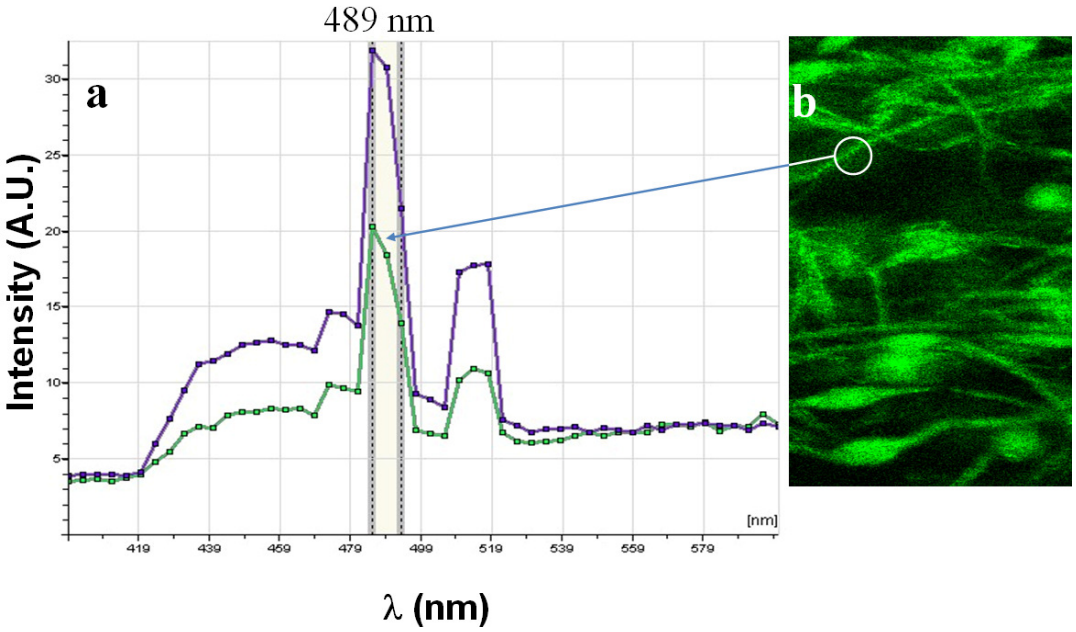

Figure 2.3: Our group has electrospun poly[(p-phenylenevinylene)-alt-(m-phenylenevinylene) PPV (polymer 7a) [38] copolymer (15 wt. %) blend in PS nanofibers onto a substrate, as shown in Figure 2.3(b). The shape of the spectrum of light emitted from the PPV/PS blend nanofiber changes drastically when the intensity of the exciting light pulse is λ scanned (λ = 365 nm) over a single nanofiber using a laser confocal microscope with maximum emission peak at wavelength, 489 nm, as reported in Figure 2.3(a). The results shown in Figure 2.3 strongly suggest that such fibers may act in ASE mode, which serves as motivation for their use as scintillation materials [33, 34].

Table 2.1: Different ^{6}Li Based Compounds that were Considered

Compound	Mass % ^{6}Li	Density	Thermal Stability	Hygroscopic
$LiClO_4$	5.64	2.42	Yes	Slightly
LiF	23.82	2.64	Yes	No
LiSal	4.15	1.45	No	Slightly

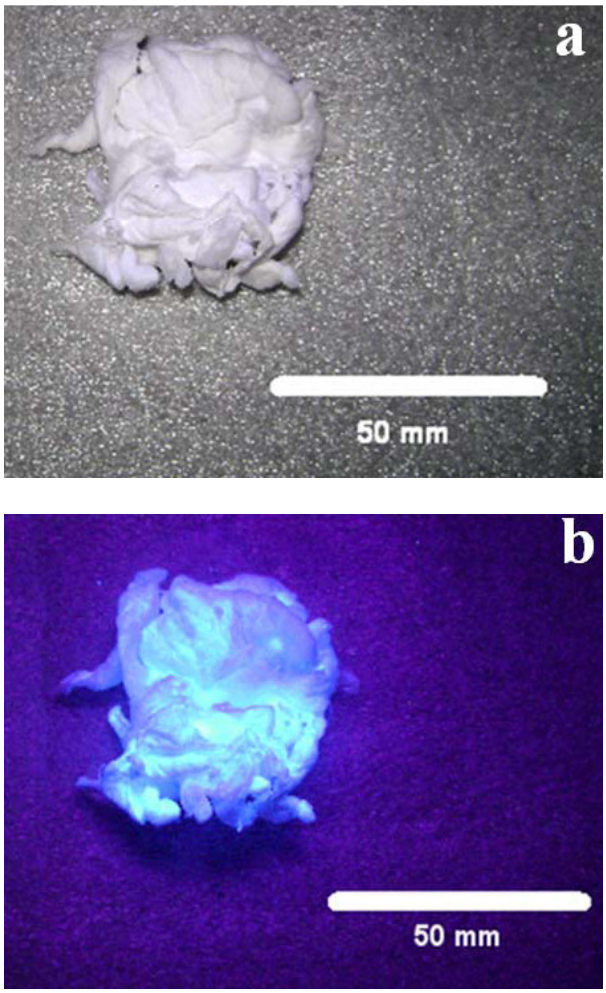

Figure 2.4: (a) Optical image of electrospun ^{6}Li based scintillator and (b) exposure to UV radiation. Note: The fluorescence of the scintillator can be clearly observed in color image.

We selected ^{6}LiSal and ^{6}LiF compounds as candidate neutron capture reagents for electrospun polymeric composite scintillators based on selection criteria previously reported [5].

However, the thermal instability of ^{6}LiSal above 100^{o}C restricted melt processing and annealing techniques. $^{6}LiClO_4$ significantly quenches light output and forms nonhomogeneous blends diffusing to the surface over a period of time by the caking phenomenon. In addition to being nonhygroscopic and nonpyrophoric, ^{6}LiF forms a well defined crystal which is thermally stable with a melting point of 845 ^{o}C. Hence, a composite with ^{6}LiF can be easily melt processed and heat treated at higher temperatures than $^{6}LiClO_4$ and ^{6}LiSal without degradation. ^{6}LiF crystals in a polymer film can significantly reduce the quantum yield of a composite scintillator by scattering light, due to large micron size crystals (crystal size up to 3.2 microns). Prior research has shown that ^{6}LiSal used alone or dispersed in various forms functions not only as a target material for neutron capture, but also as an excellent fluor. ^{6}LiSal is highly soluble and ^{6}LiF is soluble to some extent in common solvents such as tetrahydrofuran (THF), chloroform ($CHCl_3$), and dimethylformamide (DMF) [5].

A boron-10 (^{10}B) based electrospun polymer system, carborane-polyvinyl toluene (PVT), was considered as a candidate for electrospun scintillators. ^{10}B has a large thermal neutron cross-section (3840 barns), and PVT is an industry standard for neutron detection [2]. However, due to the volatility of ^{10}B when

electrospun, the boron quickly rises to the surface and evaporates into the air as the fibers are formed. Subsequently, this polymer system does not detect neutrons due to the absence of boron nuclides inside the electrospun nanofiber mat. Hence, ^{6}Li based electronspun nanofiber mats for neutron detection was chosen.

In order to synthesize and optimize polymeric scintillators, several fundamental questions have to be answered to discern the difference of localized ^{6}Li content in polymer matrix, including the following:

a. Size and dispersion of the ^{6}Li nanophase in polymer matrix.

b. Effect of phase separation of ^{6}Li and solvent evaporation of the fiber as a function of electrospinning parameters such as applied voltage, gap distance, and feed rate.

Synthesis of the electrospun thermal neutron scintillator nanofiber mats using PS and P2VN, a suitable wavelength shifting fluor, and a ^{6}Li compound is herein reported. Optical characterization of electrospun composite samples reporting emission, excitation, light yield and morphological properties are presented. The performance of scintillators subjected to neutron and gamma flux is analyzed and evaluated.

2.3 Experimental Section

Materials. Table 2.2 shows the polymer solutions and the optimized electrospinning conditions used in this research.

Table 2.2: Electrospinning Conditions for ^{6}Li Based Nanofiber Mats [6]

Polymer	PS/P2VN	PS
Solvent	THF/DMF (4:1)	$CHCl_3$/DMF (17:3)
Concentration (w/V)	3 wt % (PS)/2 wt % (P2VN)	3 wt %
^{6}Li compound (wt % in Polymer)	^{6}LiSal (13.5)	^{6}LiF (20)
Fluor (wt % in Polymer)	Anthracene (7)	PPO/POPOP (8)
M_n (g/mol)	$1.0x10^6$ (PS)/$1.2x10^6$ (P2VN)	$1.0x10^6$
Applied Voltage	18 kV	16 kV
Gap distance	18 cm	10 cm
Feed rate (mL h^{-1})	1	0.1
Needle diameter	23 G (0.635 mm)	16 G (1.7 mm)
Average Fiber Diameter	515 nm	505 nm
Sample Net Wt. (mg)	18.5	242
Environment	Air	Air

High molecular weight PS (M_n: 10^6) determined by gel permeation chromography (GPC) and P2VN (M_n: $1.2x10^6$) and three different solvents i.e., anhydrous THF, $CHCl_3$, and DMF were used to prepare polymer solutions. Wavelength shifting fluors, anthracene and (2, 5-diphenyloxazole)/(1,4-bis(5-phenyloxazol-2-yl) (PPO/POPOP), were mixed into the polymer solutions. To prepare solutions, weighted amounts of polymers and solvents were heated up to 75^{o}C for 90 minutes until homogenous solution was obtained.

Electrospinning. Figure 2.5 shows a schematic of the electrospinning setup for collection of the nonwoven fiber mat used in this work. The polymer solutions were electrospun using 3 mL and 5 mL syringes, and 16.5 G (1.7 mm) and 23 G (0.635 mm) needles. In the electrospinning process, a metering pump delivered polymer solution through a syringe and tubing to the tip of a needle. The feed rate used ranged from 0.1 mL h^{-1} to 1.0 mL h^{-1} and a direct current (DC) high voltage power supply (30 kV) was used to apply voltage (16 kV – 18 kV) to the needle, which produced a jet toward the grounded collector [39]. The gap distance used from needle to ground collector ranged from 10 cm to 18 cm. All experiments were performed at room temperature.

Characterization. Fibers were coated with Au using a SPI-Module sputter coater (SPI Supplies, Structure Probe, Inc.) for 20 s. The morphology of electrospun nanofiber mats were examined with a scanning electron microscope (SEM, Hitachi S-4300). The distribution of ^{6}Li phases were examined using energy dispersive X-ray spectroscopy (EDS) performed on LEO 1525 SEM.

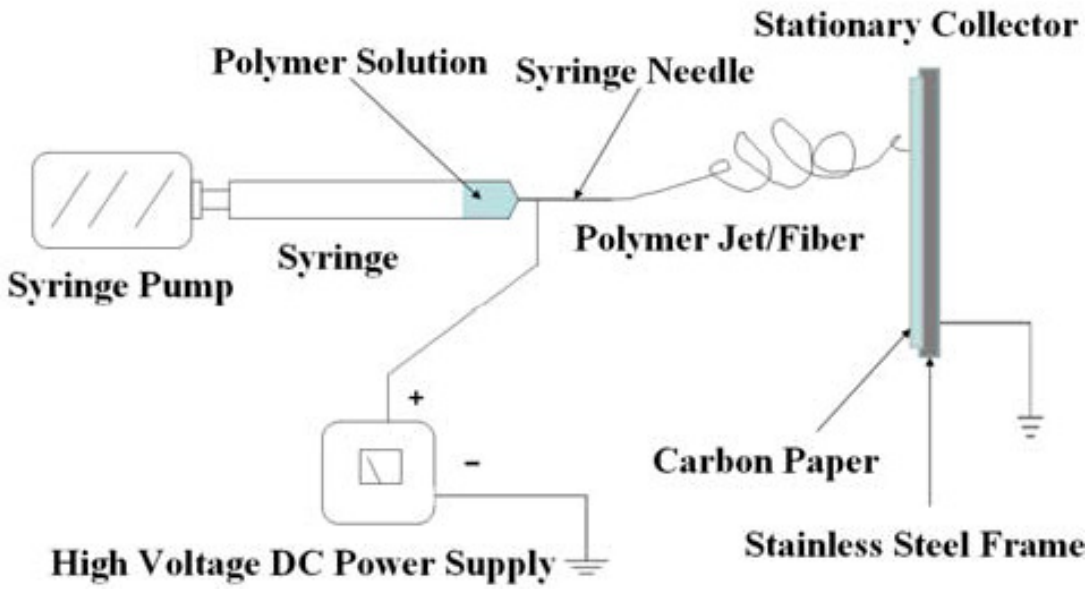

Figure 2.5: Schematic diagram of electrospinning setup.

Image processing and analysis of fiber diameters were performed with image software program IMAGEJ.

2.4 Results and Discussion

Figures 2.6 and 2.7 display SEM micrographs of fibers electrospun from ^{6}LiF/PS and ^{6}LiSal/PS/P2VN compositions and corresponding fiber diameter size distribution. The ^{6}LiF/PS fibers have a collapsed and ribbon-like morphology as shown in Figure 2.6(a). As shown in Figure 2.6(b), the ^{6}LiSal/PS/P2VN fibers have rough surface, which is primarily due to the highly volatile (THF) solvent during the electrospinning process resulting from buckling instabilities [40]. The fibers electrospun from ^{6}LiF/PS and ^{6}LiSal/PS/P2VN (Figure 2.6(a) and Figure 2.6(b)) show occasional spindle-like beads. This can be attributed to the high conductivity and dielectric constant combination from DMF used in the electrospinning process [41,42]. The size distribution of fiber diameter for ^{6}LiF/PS and ^{6}LiSal/PS/P2VN electrospun nanofiber mats is illustrated in the histograms shown in Figure 2.7. As shown in Table 2.2, the average fiber diameter for ^{6}LiSal/PS/P2VN was 515 nm. The ^{6}LiF/PS had a slightly narrower fiber distribution and smaller average fiber diameter (505 nm) than the ^{6}LiSal/PS/P2VN electrospun fiber mat. The narrower fiber size distribution is possibly due to lower polymer concentration of ^{6}LiF/PS (3 wt. %) compared to the polymer blend concentration of ^{6}LiSal/PS/P2VN (3 wt % (PS)/2 wt % (P2VN), where an increase in polymer concentration will increase the average nanofiber diameter.

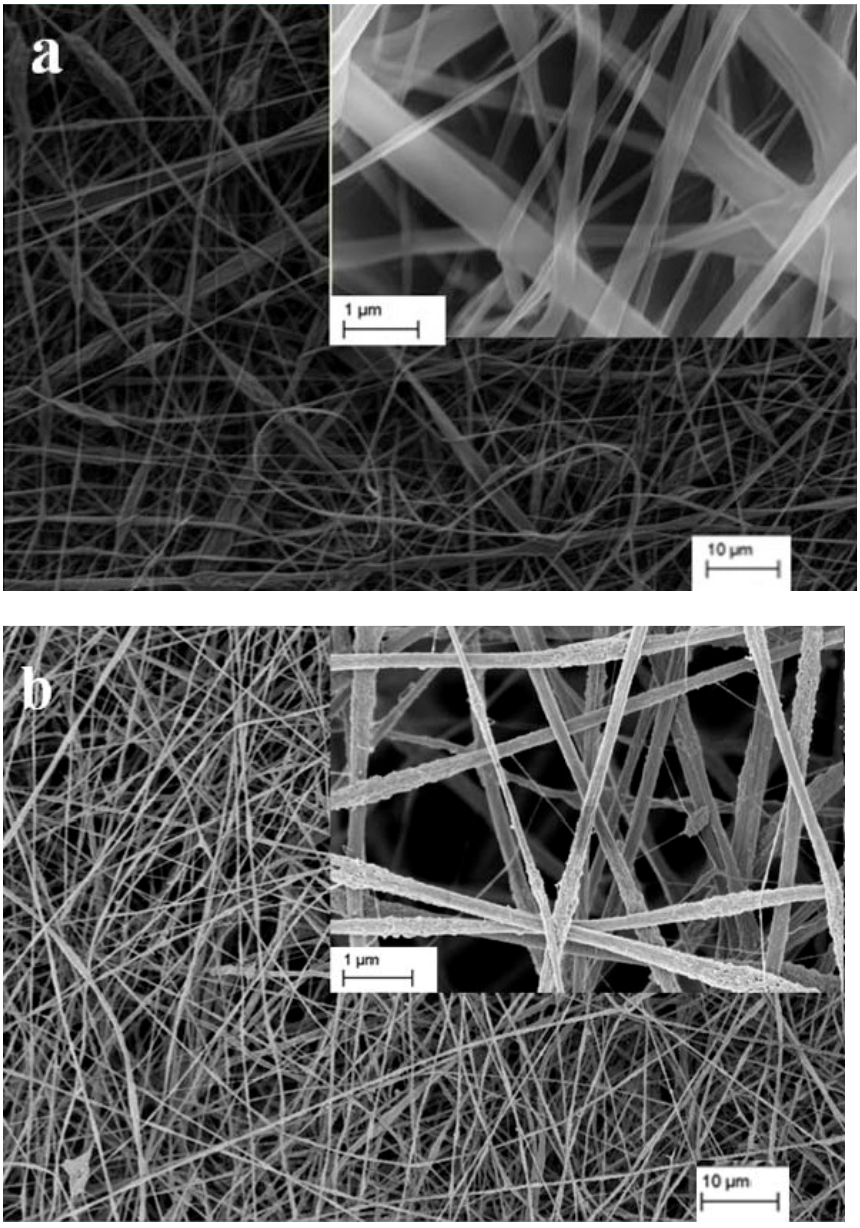

Figure 2.6: SEM micrographs of (a) PS (20 wt %), ^{6}LiF (20 wt % in PS) and PPO/POPOP (8 wt % in PS) electrospun with $CHCl_3$/DMF (17:3) and (b) PS (3 wt %)/P2VN (2 wt %), ^{6}LiSal (13.5 wt % in PS/P2VN), and anthracene (7 wt % in PS/P2VN) electrospun with THF/DMF (4:1) fibers.

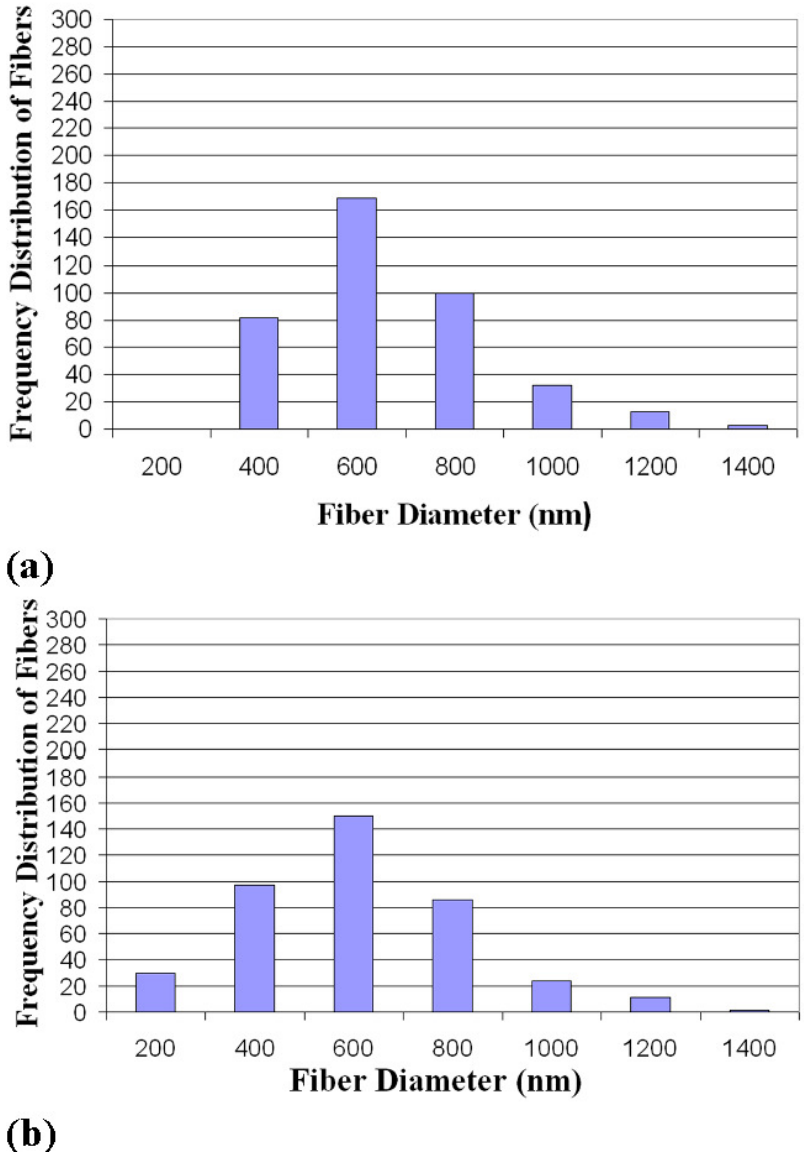

Figure 2.7: Fiber size diameter distribution of (a) PS (20 wt %), ^{6}LiF (20 wt % in PS) and PPO/POPOP (8 wt % in PS) electrospun with CHCl3/DMF (17:3) and (b) PS(3 wt %)/P2VN (2 wt %), ^{6}LiSal (13.5 wt % in PS/P2VN), and anthracene (7 wt % in PS/P2VN) electrospun with THF/DMF (4:1) fibers.

Additionally, dielectric properties and surface tension for the solvents THF and $CHCl_3$ are very different and may influence the phase morphology and resulting fiber diameters [6]. Significant increase in fluorescence has been reported for light emitted polymers with fiber diameters 500 nm and below [43]. The geometry of the waveguide assisted ASE directly affects the spectral properties of the resulting optical amplification [37,44]. Due to the high quantum confinement of the emitted light, each fiber under pulsed optical excitation exhibit sharp emission peaks in the gain region [37]. Both samples average fiber diameter was near the target range of 500 nm fiber diameter, to exploit the aforementioned concept of ASE.

The ^{6}Li nuclide could not be directly detected using EDS, due to its aforementioned low atomic number. As shown in Figure 2.8 and Figure 2.9(a), micron size crystals approximately 3 μm in size were observed in the fiber morphology. Figure 2.9(c) shows the EDS spectrum obtained from the area of the fiber shown in Figure 2.9(b) as well as the area of the electron beam position on the crystal, indicating the presence of fluorine. In addition to this, elemental mapping for the fluorine distribution has provided unambiguous confirmation that the bright spots are fluorine. This is most clearly illustrated in Figure 2.9(b) where there is a high concentration of bright spots corresponding to the ^{6}LiF crystal in Figure 2.9(a). It is interesting to note the molecular distribution of fluorine surrounding the crystal in Figure 2.9(c), where the phases on a nanoscale can be easily observed.

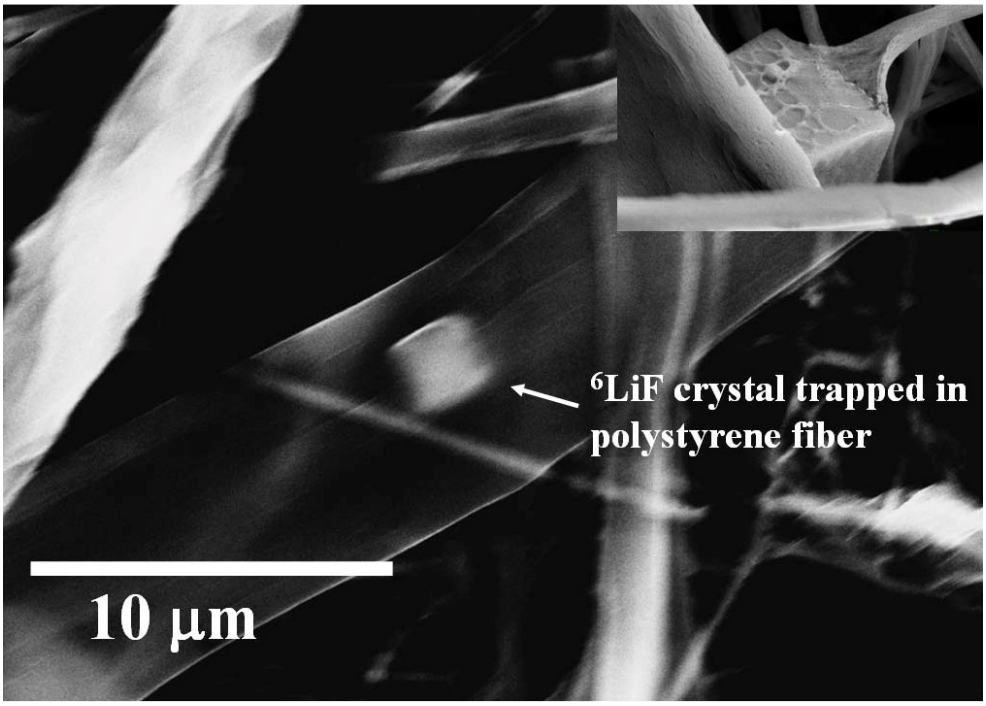

Figure 2.8: SEM micrograph of ^{6}LiF crystals trapped in polystyrene fiber.

Although the discussion for this paper relates to development and optimization of small diameters fibers, an extraneous micron sized fiber shown in Figure 2.9(a) and Figure 2.9(b) clearly demonstrates that ^{6}LiF phases are dispersed within an individual fiber. Thus, we can indirectly detect the local ^{6}Li positions within the fiber. The ^{6}LiSal phase was not expected to be detected, due to its chemical composition.

The ^{6}LiF crystal formation shown in Figure 2.9(a) is primarily due to phase instability in the ^{6}LiF/PS polymer system. The ^{6}LiF/PS polymer solution is homogeneous when heated up to 100^{o}C. However, as the polymer solution approaches room temperature (20^{o}C) during the electrospinning process, PS precipitates and the solution becomes turbid. Subsequently, these conditions make electrospinning the ^{6}LiF/PS nanofibers challenging. The syringe needle gets clogged where the majority of the ^{6}LiF does not transfer as the polymer forms into fibers.

Figure 2.10 shows the excitation-emission response from the ^{6}LiF/PS and ^{6}LiSal/PS/P2VN electrospun nanofiber mat scintillators. As shown in Figure 2.10, for ^{6}LiF/PS the wavelength shifter PPO/POPOP excites at approximately 280 nm and emits at 420 nm. A large spectral overlap of approximately 70 nm between excitation and emission indicates significant re-absorption of emission. It is interesting to note the electrospun nanofiber mats have similar emission peak positions although their excitation peaks are markedly different.

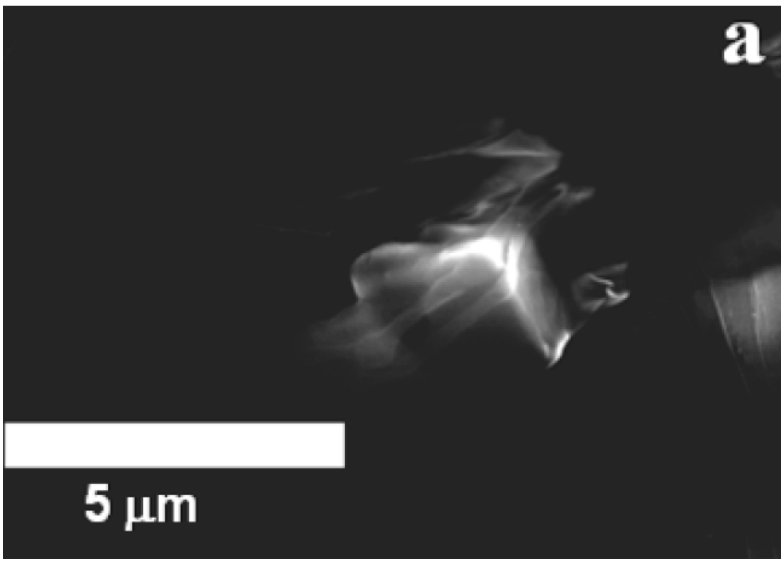

Figure 2.9 : SEM micrograph and of ^{6}LiF crystal showing distribution of fluorine inside electrospun fiber (LiF/PS), (b) elemental mapping of 6LiF crystal showing distribution of fluorine inside electrospun fiber (LiF/PS). EDS spectrum from area shown in (b). The fluorine peak is derived from the micron-size ^{6}LiF crystal and from the nanophase surrounding the crystal, where oxygen and carbon peaks correspond to the polystyrene polymer matrix. The gold peaks come from the sputter coating on nanofibers and copper peak from a copper SEM substrate.

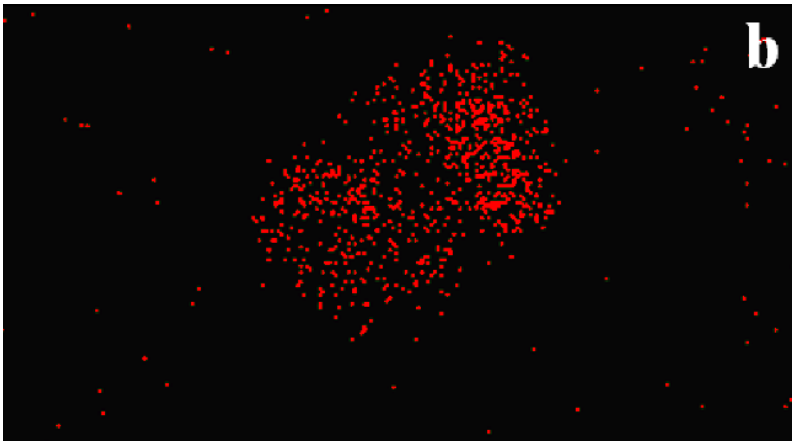

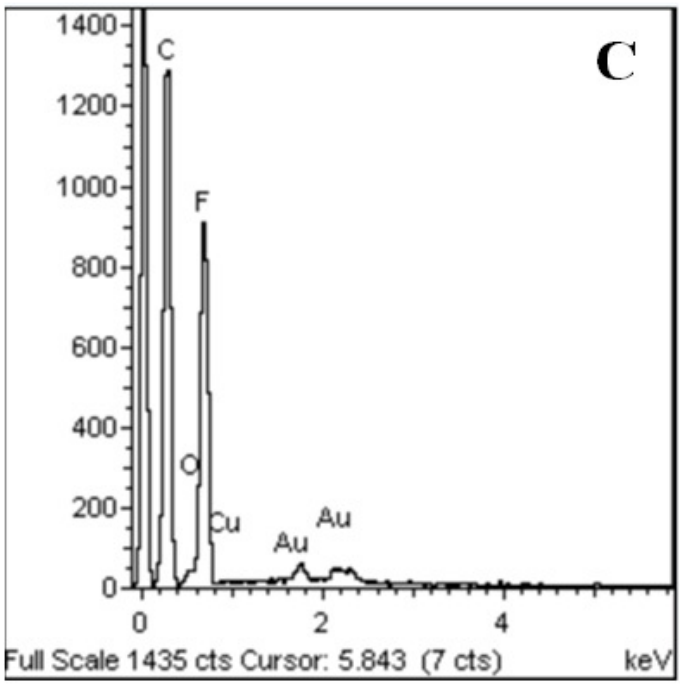

Figure 2.9 continued

The excitation curve for the ^{6}LiSal/PS/P2VN indicates characteristics similar to Forster energy transport from both the matrix (PS/P2VN) and the nuclide (^{6}LiSal) to namely, the fluor molecules [5]. As shown in Figure 2.10, the emission curve of ^{6}LiSal/PS/P2VN has a single peak corresponding to the emission of anthracene, indicating efficient intermolecular energy transport [45]. A possible reason for the above-discussed excitation bandwidth differences is that absorbed photons change the state of the absorbing molecules. Subsequently, these effects could influence its mobility (along benzene rings of the polymer), particularly for unstable absorption centers [2,46]. Additionally, the dispersion of fluorophores within the fibers and random orientation of the fibers may play a role in absorption band differences.

Scintillation Measurements. The samples were tested under irradiation with alpha, beta, and gamma sources to evaluate thermal neutron response and light yield [47]. The electrospun fiber mats (^{6}LiSal/PS/P2VN and ^{6}LiF/PS) were prepared and exposed to radiation flux using a custom neutron irradiator containing arcrylic and cadmium cylinders to obtain net thermal neutron response, as described in detail [5]. In order to determine the net thermal neutron response, neutrons with energies below the cadmium cut-off energy (0.5 eV) of the detector, the cadmium cylinder measurement (response to gamma and fast neutrons) is subtracted from the acrylic cylinder measurement [48]. The subtraction would include the fast neutrons at 250 keV that fall in resonance at ^{6}Li cross-section.

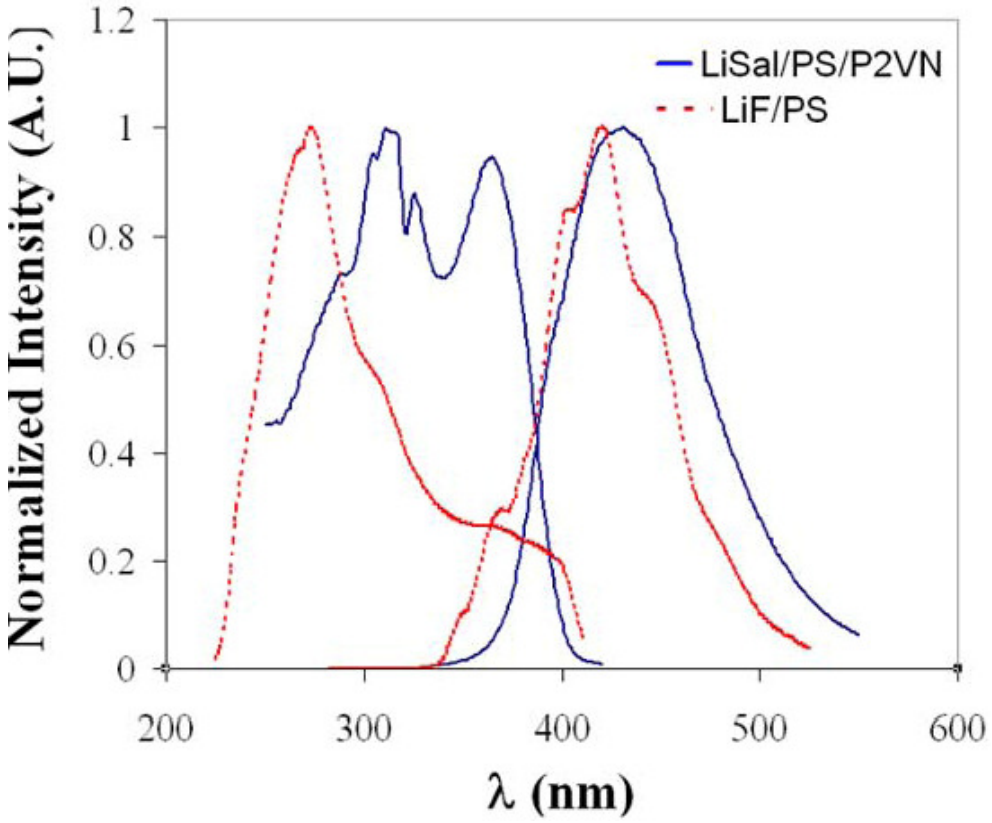

Figure 2.10: ^{6}LiF/PS electrospun nanofiber mat has excitation peak (280 nm) and emission peak (420nm) with Stokes shift (140 nm). ^{6}LiSal/PS/P2VN electrospun nanofiber mat has excitation peak (313 nm) and emission peak (432nm) with Stokes shift (119 nm).

Thermal neutron measurements were performed with ^{252}Cf source. Pulse height spectra were obtained by coupling the scintillator sample to a Canberra 2007P photomultiplier tube (PMT) that included a preamplifier.

Optimal coupling was obtained with minimal optical grease as the quartz disk (bottom surface) adhered perfectly to the PMT glass and Teflon® reflector tape was wrapped around the mounted surface to minimize light losses. The PMT was fed a voltage of 1000V supplied by a high voltage amplifier. The scintillation pulses produced by the PMT were fed into a preamplifier.

The yield was compared with GS20, a commercial glass lithiated scintillator collected in the same experiment [5,47]. A gain of 500 was applied to the electrospun fiber mat samples and gain of 100 was applied to GS20 neutron measurements. The electrospun scintillator had a maximum neutron response around the 4,000 channel number and GS20 had a maximum response at approximately 25,000 channel number as can be observed in Figure 2.11. Additionally, a clear distinction of thermal neutrons is evident for ^{6}LiSal/PS/P2VN electrospun fiber mat and the decay time for this sample was measured to be 3.9 ns. Although the neutron response for the electrospun scintillator is not as large as GS20, this is encouraging given a) that there was only 4 wt. % loading of ^{6}Li in the polymer, b) the fiber mat is hundreds of microns thick, and c) the net weight was 18.5 mg, as shown in Table 2. GS20 by comparison has a significant larger loading of Li, is 2 mm thick and has a net weight of 2460 mg, thus yielding a higher thermal neutron response.

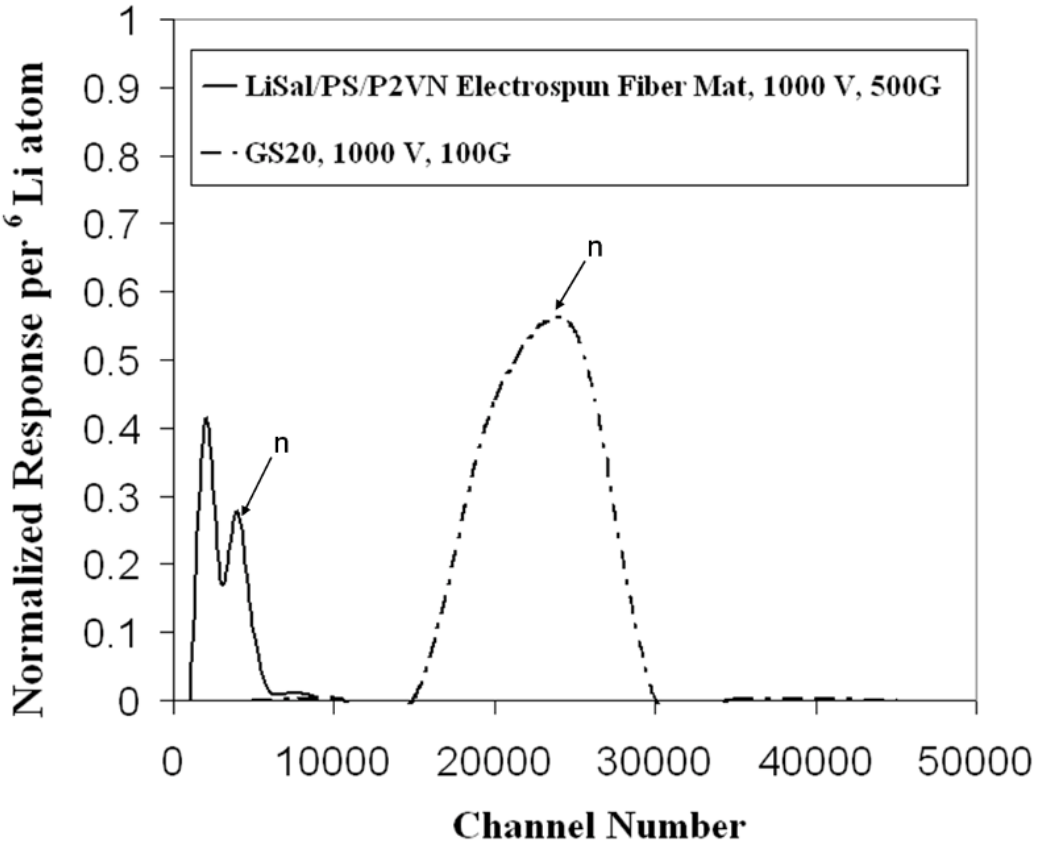

Figure 2.11: ^{6}LiSal/PS/P2VN electrospun scintillation and GS20 net thermal neutron response using ^{252}Cf source. The electrospun scintillator as maximum neutron response around the 4,000 channel number and GS20 has a maximum response at approximately 25,000 channel number.

Neutrons were not detected for ^{6}LiF/PS electronspun fiber mat, due to quenching of light and micron-sized domains scattering light within the samples. As expected for the ^{6}LiSal/PS/P2VN and ^{6}LiF/PS fiber mats, light yield measurements using alpha (^{241}Am), beta (^{36}Cl), and gamma ray (^{137}Cs) did not yield a appreciable light response, due primarily to the small amount of neutron absorbing material in the nanofiber mats.

The novel technique demonstrated in this paper to synthesize nanometer to micron scale functional scintillation fibers shows a lot of promise in moving to the next step of dramatically increasing neutron detection efficiency.

2.5 Conclusions

Lithium-6 based electrospun thermal neutron scintillators were produced using a custom electrospinning setup. ^{6}LiF/PS and ^{6}LiSal/PS/P2VN random oriented nonwoven nanofiber mats were successfully electrospun and evaluated for scintillation yield using alpha, beta, and gamma sources. ^{6}Li nanophases were successfully confirmed in ^{6}LiF/PS electrospun scintillator by the presence of fluorine dispersed throughout the fibers, which were detected using EDS. ^{6}LiSal/PS/P2VN yielded a neutron peak, whereas no neutron response was obtained for ^{6}LiF/PS due to quenching of light yield. Neutron detection was obtained using P2VN based nanofiber mats even at small loading of ^{6}Li. Further research will include using scanning transmission electron microscopy (STEM) to directly detect ^{6}Li phases within fiber and optimize loading of lithium inside fibers to increase thermal neutron response and light yield.

2.6 Acknowledgements

Financial support from the Domestic Nuclear Detection Office (DNDO) through Award No. 003387891 is gratefully acknowledged. Any opinions, findings, and conclusions or recommendations expressed in this material are those of the authors and do not necessarily reflect the views of DNDO. The authors gratefully acknowledge support from Charles L. Melcher from the Scintillation Materials Research group, George Schweitzer and Andrew N. Mabe from the department of Chemistry and Laurence Miller from the department of Nuclear Engineering at the University of Tennessee.

2.7 References

[1] Birowosuto, M. D., 2008, “Li-Based Thermal Neutron Scintillator Research; $Rb_2LiYBr_6 : Ce^{3+}$ and Other Elpasolites,” IEEE Trans. Nucl. Sci., **55**(3), pp. 1152-1155.

[2] Knoll, G. F., 2010, *Radiation Detection and Measurement, 4th ed*. John Wiley and Sons, Hoboken, NJ, pp. 227-522.

[3] van Eijk, C. W. E., de Haas, J. T. M., Dorenbos, P., Krämer, K. W., and Gudel, H. U., 2005, “Development of Elpasolite and Monoclinic Thermal Neutron Scintillators,” Proc. IEEE Nuclear Science Symp. Conf. Rec., pp. 239-243.

[4] Kietze, T., Neher, D., Landfester, K., Montenegro, R., Güntner, R., and Scherf, U., 2003, “Novel Approaches to Polymer Blends Based on Polymer Nanoparticles,” Nature Materials, **2**, pp. 408–412.

[5] Sen, I., Penumadu, D., Williamson, M., Miller, L. F., Green, A. D., and Mabe, A. N., 2011, “Thermal Neutron Scintillator Detectors Based on Poly(2-Vinylnapthalene) Composite Films,” IEEE Trans. Nucl. Sci., **58**(3), pp. 1386-1393.

[6] Andrady, A. L., 2008, *Science and Technology of Polymer Nanofibers*, John Wiley and Sons, Inc., Hoboken, NJ, pp. 81-311.

[7] Kalra, V. et. al., 2008, “Controlling Nanoparticle Location via Confined Assembly in Electrospun Block Copolymer Nanofibers,” Small, **4**(11), pp. 2067-2073.

[8] Song, T., et. al., 2005, “Encapsulation of Self-assembled FePt Magnetic Nanoparticles in PCL nanofibers by Coaxial Electrospinning,” Chemical Physics Letters, **415**(4-6), pp. 317-322.

[9] Ma, M., Krikorian, V., Yu, J. H., Thomas, E. L., and Rutledge, G. C., 2006, “Electrospun Polymer Nanofibers with Internal Periodic Structure Separation of Cylindrically Confined Block Copolymers,” Nano Letters, **6**(12), pp. 2969-2972.

[10] Doshi, J., and Reneker, D. H., 1995, “Electrospinning Process and Applications of Electrospun Fibers,” Journal of Electrostatics, **35**, pp. 151-160.

[11] Dayal, P., and Kyu, T., 2006, “Porous Fiber Formation in Polymer-Solvent System Undergoing Solvent Evaporation,” Journal of Applied Physics, **100**, pp. 043512-043512-6.

[12] Wang, Z. L., 2000, *Characterization of Nanophase Materials, 1st Ed*. Wiley-VCH, Weinheim, DE, pp. 6-7, Chap. 1.

[13] Rotello, V., 2004, *Nanoparticles: Building Blocks for Nanotechnology*, Springer, New York, NY, pp. 38-39, Chap. 2.

[14] Caruta, B. M., 2005, *Nanomaterials: New Research.,* Nova Science Publishers, New York, NY, pp. 3-5, Chap. 1.

[15] Kim, J. K., and Heejon, A., 2008, “Fabrication and Characterization of Polystyrene/Gold Nanoparticle Composite Nanofibers,” Macromolecular Research, **16**(2), pp. 163-168.

[16] Lin, Z., Gilbert B., Liu Q., Ren, G., and Huang F., 2006, "A Thermodynamically Stable Nanophase Material," J. Am. Chem. Soc., **128**(18), pp. 6126-6131.

[17] Yoshimatsu, K., Ye, L., Stenlund, P., and Chronakis, I. S., 2008, "A Simple Method For Preparation of Molecularly Imprinted Nanofiber Materials with Signal Transduction Ability," Chem. Commun., **17**, pp. 2022-2024.

[18] Yoshimatsu, K., Ye, L., Lindberg, J., and Chronakis, I. S., 2008, "Selective Molecular Adsorption Using Electrospun Nanofiber Affinity Membranes," Biosensors and Bioelectronics, **23**, pp. 1208-1215.

[19] Yang, C., Jia, Z., Liu, J., Xu, Z., Guan, Z., and Wang, L., 2009, "Guiding Effect of Surface Electric Field of Collector on Deposited Electrospinning Fibers," IEEE Transactions on Dielectrics and Electrical Insulation, **16**(3), pp. 785–792.

[20] Megelski, S., Stephens, J. S., Chase, D. B., and Rabolt, J. F., 2002, "Micro- and Nanostructured Surface Morphology on Electrospun Polymer Fibers," Macromolecules, **35**(22), pp. 8456-8466.

[21] Dayal, P., 2007, "Dynamics and Morphology Development in Electrospinning of Polymer Solutions", Ph.D. Thesis, The University of Akron, Akron, OH.

[22] Wu, X. F., Salkovskiy, Y., and Dzenis, Y. A., 2011, "Modeling of Solvent Evaporation from Polymer Jets in Electrospinning," Applied Physics Letters, **98**, pp. 223108– 223108-3.

[23] Yeo, L. Y., and Friend, J.R., 2006, “Electrospinning Carbon Nanotube Polymer Composite Nanofibers,” Journal of Experimental Nanoscience, **1**(2), pp. 177-209.

[24] Wang, Y., Wang, B., Wang, G., Yin, T., and Yu, Q., 2009, “A Novel Method for Preparing Electrospun Fibers with Nano-/Micro-scale Porous Structures,” Polym. Bull., **63**, pp. 259-265.

[25] Bognitzki, M., Frese, T., Steinhart, M., Greiner, A., and Wendorff, J. H., 2001, “Preparation of Fibers With Nanoscaled Morphologies: Electrospinning of Polymer Blends,” Polym. Eng. Sci., **41**(6), pp. 982-989.

[26] Dzenis, Y., 2004, “Spinning Continuous Fibers For Nanotechnology,” Science, **304**, pp. 1917-1919.

[27] Dersch, R., Liu, T., Schaper, A.K., Greiner, A., and Wendroff, J. H., 2003, “Electrospun Nanofibers: Internal Structure and Intrinsic Orientation,” Journal of Polymer Science Part A: Polymer Chemistry, **41**, pp. 545-553.

[28] Russo, M. V., 2010, *Advances in Macromolecules: Perspectives and Applications*, Springer, New York, NY, p. 57, Chap. 1.

[29] Semerak, S. N., and Frank, C. W., 1984, "Photophysics of Excimer Formation in Aryl Vinyl Polymers," Advances in Polymer Science, **54**, pp. 31-85.

[30] Wunderlich, B., 2009, “Thermodynamics and Properties of Nanophases,” Thermochimica Acta, **492**, pp. 2–15.

[31] Schiek, M., Balzer, F., Al-Shamery, K., Brewer, J. R., Lutzen, A., and Rubahn, H.G., 2008, "Organic Molecular Nanotechnology," Small, **4**, pp. 176-181.

[32] Xu, C. X., Sun, X. W., Yuen, C., Chen, B. J., Yu, S. F., and Dong, Z. L., 2005, "Ultraviolet Amplified Spontaneous Emission from Self-Organized Network of Zinc Oxide Nanofibers," Applied Physics Letters, **86**, pp. 011118–011118-3.

[33] Lemmer, U., 1998, "Stimulated Emission and Lasing in Conjugated Polymers," Polym. Adv. Technol., **9**, pp. 476-487.

[34] Schnabel, W., 2007, *Polymers and Light: Fundamentals and Technical Applications*, Wiley-VCH, Weinheim, DE, pp. 44-47, Chap. 1.

[35] Yang, P., et al., 2000, "Mirrorless Lasing from Mesostructured Waveguides Patterned by Soft Lithography," Science, **287**, pp. 465-467.

[36] Camposeo, A., Di Benedetto, F., Stabile, R., Neves, A. A. R., Cingolani, R., and Pisignano, D., 2009, "Laser Emission from Electrospun Polymer Nanofibers," Small, **5**(5), pp. 562-566.

[37] Camposeo A., Mele, E., Persano, L., Pisignano, D., and Cingolani, R., 2006, "Role of Doping Concentration on the Competition Between Amplified Spontaneous Emission and Nonradiative Energy Transfer in Blends of Conjugated Polymers," Physical Review B, **73**, pp. 165201-165201-7.

[38] Pang, Y., Li, J., Hu, B., and Karasz, F. E., 1999, "A Highly Luminescent Poly[m-phenylenevinylene)-alt-(p-phenylenevinylene)] with Defined

Conjugation Length and Improved Solubility," Macromolecules, **32**(12), pp. 3946-3950.

[39] Inai, R., Kotaki, M., and Ramakrishna, S., 2005, "Structure and Properties of Electrospun PLLA Single Nanofibers", Nanotechnology, **16**, pp. 208-213.

[40] Bognitzki, M. et al., 2001, "Nanostructured Fibers via Electrospinning," Adv. Mater., **13(**1), pp. 70-72.

[41] Eda, G., Liu, J., and Shivkumar, S., 2007, "Solvent Effects on Jet Evolution During Electrospinning of Semi-Dilute Polystyrene Solutions," European Polymer Journal, **43**, pp. 1154-1167.

[42] Uyar, T., and Besebacher, F., 2008, "Electrospinning of Uniform Polystyrene Fibers: The Effect of Solvent Conductivity," Polymer, **49**, pp. 5336-5343.

[43] Tomczak, N., Gu, S., Han, M., van Hulst, N. F., and Vancso, G. J. 2006, "Single Light Emitters in Electrospun Polymer Nanofibers: Effect of Local Confinement on Radioactive Decay," European Polymer Journal, **42**, pp. 2205-2210.

[44] Sheridan, A. K., Turnbull, G. A., Safonov, A. N., and Samuel, I. D. W. 2000, "Tuneability of Amplified Spontaneous Emission through Control of the Waveguide-Mode Structure in Conjugated Polymer Films," Physical Review B, **62**(18), pp. R11929-R11932.

[45] Ladik, J., 1984, *Quantum Chemistry of Polymers-Solid Aspects*, 1st Ed., D. Reidel, Dordrecht, NL, pp. 259-260.

[46] Wick, K., Hornung, R., and Gosau, T., 2005, “Reduction of the Permanent Radiation Induced Absorption by Illumination of Plastics Scintillators During γ-Irraditation,” Nuclear Instruments and Methods in Physics Research A, **538**, pp. 668-671.

[47] Carturan, S. et. al, 2011, “Novel Polysiloxane-Based Scintillators for Neutron Detection,” Radiation Protection Dosimetry, **143**, pp. 471-476

[48] Carron, N. J., 2007, *An Introduction to the Passage of Energetic Particles through Matter*, Taylor and Francis, NY, pp. 307-308.

3 CHAPTER III
^{6}LI EMBEDDED MELT-SPUN POLYMERIC MICROFIBERS AS THERMAL NEUTRON SCINTILLATORS

3.1 Abstract

Lithium-6 (^{6}Li) loaded polyethylene naphthalate (PEN) microfibers have been melt-spun and tested for thermal neutron detection. The ^{6}Li isotope has a significant thermal neutron cross-section and produces high-energy charged particles upon thermal neutron absorption. In this research study, polymeric scintillation fiber bundles were fabricated using a melt-spinning technique to produce uniaxial microfibers bundles that directly discriminate between neutron and gamma radiation. Fiber bundles response to thermal neutrons, and relative light yield response using alpha, beta, and gamma radiation using a custom neutron irradiator has been reported. Additionally, the fiber bundles were characterized using scanning electron microscopy (SEM) for morphology, differential scanning calorimetry (DSC) for thermal properties, and fluorospectroscopy for optical properties.

3.2 Background

Due to the shortage of ^{3}He, there is a need to develop alternative neutron detection technologies for homeland security applications; effective thermal neutron detectors with prompt and efficient detection of neutrons and good gamma to neutron discrimination that can be economically installed on a large scale in public places are desired [1, 2]. Organic polymeric materials as scintillators can be machined into a wide variety of shapes, including thin films and thin fibers, and have been demonstrated to be effective for thermal neutron

detection due to their high light yield, low Z, and short decay time [3-5]. ^{6}Li and ^{10}B are attractive nuclei for thin detectors due to their large thermal neutron absorption cross-sections, high Q-values, and short range of kinetic energy-charged particles [3, 6]. In this work, we focus on the ^{6}Li isotope, which, upon absorption of a thermal neutron, emits high kinetic energy-charged particles, a α particle (2.05 MeV) and a triton particle (2.73 MeV), and "scintillation light is produced along its ionization track" [2, 7-9]. The ^{6}LiF compound, commonly used for developing neutron detectors, is an attractive neutron capture reagent for polymeric composite scintillators based on previously reported selection criteria [2, 10]. Compared to other salts, ^{6}LiF has a high lithium atomic mass content (24%) and density of 2.46 g/cc, and it is virtually nonhygroscopic, possessing a large optical gap with high transparencies in the near visible and UV spectrum. Furthermore, ^{6}LiF is thermally stable and not easily soluble in common organic solvents [2, 11-13].

There is growing interest in polyethylene naphthalate (PEN) due to its optical and mechanical properties, flexibility, and chemical and heat resistance. PEN, a thermoplastic, due to its melt viscosity, can be melt-processable at elevated temperatures using several processing techniques, including melt-spinning. Such attractive properties make PEN useful for a variety of applications, including scintillators, as it has been reported that PEN emits 10,500 photons/MeV, exceeding the output of conventional plastic scintillators [14-16]. Additionally, PEN is transparent in the visible region of the spectrum, absorbing

light strongly with an emission peak around 430 nm, and it does not easily dissolve in solvents [13, 14, 17, 18]. Mechanical hot-pressed PEN thin films embedded with ^{6}LiF and an organic scintillating fluor have been demonstrated to exhibit high light output for thermal neutron detection [13]. It has been proposed for luminescent solar concentrators (LSC) with similarities to scintillating fibers a cylindrical geometry is more efficient compared to planar geometry of the same luminescence collection volume and area [19, 20]. This result, based on equations derived for scintillation fibers, has triggered further investigations on its applicability using cylindrical geometry [20-23]. The benefit of fibers (micro/nanoscale) is due to its 1-D structure as a waveguide, where light is emitted isotropically and guided along the long axis of the fiber by total internal reflection, exhibiting interesting optical properties such as optical confinement [24,25]. A thin and continuous fiber geometry affords a high surface area to diameter ratio so that luminescence emission occurs close to the surface, as the cylindrical geometry has a larger optical concentration potential than planar geometry [21]. Furthermore, the fibers are lightweight and flexible, and the manufacturing processes can be optimized to produce on a large scale [21, 26]. Plastic scintillator microfibers have been demonstrated to be effective scintillators. For example, polystyrene (PS) based microfibers have been used for scintillation; however, due to their poor fluorescence yield, an aromatic wavelength shifting scintillator is required to be detected by a standard photomultiplier tube (PMT) [27]. However, with the addition of a wavelength

shifting fluor, the competing processes of excitation energy transfer from a monomer unit to scintillating dyes can cause quenching effects and radiation emissions, which can affect the scintillation efficiency [9, 28].

A good plastic scintillator fiber requires a highly transparent fiber with a neutron absorber element uniformly dispersed throughout the polymer matrix. In this paper, our focus on PEN-based fibers is due to the naphthalene repeating units on the backbone of the polyester that are “crystalline in nature,” strongly suggesting that energy migration is favored [29]. These photophysical phenomena are due to the intramolecular energy transfer along the naphthalene units, where the molecules are excited to higher energy levels before the excimeric emission of photons [13, 29]. The fabrication of a two-component system of ^{6}Li-loaded PEN microfibers for thermal neutron detection is proposed and has not been deeply investigated. The hypothesis is that, by incorporating ^{6}Li into a PEN scintillation matrix, the energy from the ^{6}Li neutron capture event will be transferred to naphthalene units for efficient energy transport along the fibers, where photons will be detected on a PMT without the requirement of a wavelength shifter fluor.

A proper initial dispersion of ^{6}LiF in a polymer matrix is critical, as good spatial distribution enhances the scintillation performance of the fibers. The melt-spinning process can influence the arrangement of ^{6}Li phases in the fiber and is a suitable process to make PEN/^{6}LiF without solvent [30]. Forming aligned thermal neutron scintillator melt-spun microfiber bundles embedded with different

concentrations of ^{6}Li-based compounds will allow a better understanding of the scintillation mechanism of the fibers. However, it must be noted that the transparency of the fibers is reduced due to the difference in refractive indices between PEN (1.65~1.9) and LiF (1.4) [13]. In the present study, aligned, melt-spun, ^{6}Li-loaded PEN (PEN/LiF) composite microfibers are evaluated and compared to a commercial cerium-loaded glass, GS20, tested under irradiation with alpha, beta, and gamma sources to evaluate the thermal neutron response and relative light yield [31].

3.3 Experimental Section

Materials. The analytical-grade neat PEN pellets were supplied by the Goodfellow Corporation [13]. Lithium fluoride (^{6}LiF) synthesis was performed according to the methods described by Sarraf-Mamoory et al. [32]. Lithium hydroxide (LiOH) was added to methanol (Fisher) at a concentration of 0.1 g/mL at 20 °C to remove impurities and stirred for 12 hours. The resulting solution was heated to 150 °C to completely evaporate the methanol, leaving only LiOH. The LiOH was dissolved in deionized water (0.1 g/mL), to which 50% hydrofluoric acid (Acros) was added to make the solution acidic. The solution was stirred and heated to 80 °C during the addition of hydrofluoric acid (HF) until reaching a pH value of 2. The ^{6}LiF solution was then immediately added to a 0 °C acetone bath. The resulting ^{6}LiF was collected using vacuum filtration with 1 μm and 450 nm fine-porosity filter paper (Whatman). The ^{6}LiF was then dried for 1 hour at 120 °C.

To prepare the composite mixture, the neat PEN pellets were ground into fine particles using a commercial mechanical grinder. Various loadings of ^{6}LiF was added to the neat PEN and ground until a suitable uniform blend was obtained. The composite mixtures were then dried overnight in an oven set at 72 °C.

Melt-spinning. The PEN-based mixtures were melt-spun into fiber using a single-screw, pressure-controlled extruder (Alex James and Associates, Inc.), where a temperature profile of 240, 270, 280, 280, 283, 285, and 285 °C was used. The ¾" extruder was attached to a metering pump with fiber-exiting die made of two 3 mm diameter holes collecting onto a winder at a take-up speed of 20 m/min. The spinline distance between the die and the winder was approximately 2 meters [15].

Characterization. Fibers were examined using an optical digital microscope (Keyence). Additionally, the fibers were Au-coated using an SPI-module sputter coater (SPI Supplies, Structure Probe, Inc.) for 20 s, and the morphology was examined using a scanning electron microscope (1525 Leo SEM). The fiber diameters were determined using an image software program, IMAGEJ. The thermal properties of PEN-based fibers were investigated using differential scanning calorimetry (Perkins Elmer Diamond DSC) with a scan rate of 10 ^{o}C/min in a nitrogen atmosphere.

Scintillation Measurements. The PEN/^{6}LiF fibers were wrapped around a 22 mm length x 22 mm width x 0.16-0.19 mm thickness microscope glass cover slide. The fibers were then encapsulated using Sylgard 527, a silicone-based

transparent optical dielectric gel with a refractive index of 1.41 [33]. The samples were evaluated for a thermal neutron response using a custom neutron irradiator previously described in detail [2, 13]. The PEN/^{6}LiF-encapsulated fibers were coupled at the center of the photocathode window of the PMT using minimal optical grease and covered with Teflon® reflector tape to minimize light loss [3]. The neutron irradiator consists mainly of a 0.59 μg Californium neutron source with two detector wells equidistant apart in a high-density polyethylene (HDPE) housing. The sample was placed in an acrylic cylinder surrounded by 3.2 mm of lead to obtain the response of neutrons and gamma rays. The sample was then placed in an acrylic cylinder surrounded by 1.6 mm of cadmium. Due to cadmium's large thermal neutron cross-section, the scintillation response measured mostly fast neutrons and gamma response. The net thermal neutron response was obtained by spectrally subtracting the scintillation response between the two wells. A Phillips 2202B PMT mounted on a Canberra 2007P powered by a high-voltage power supply (ORTEC 556) set to 1200 converted the light pulses to electrical pulses. The PMT signal was amplified with a gain setting of 16.6 G and a shaping time of 2 μs with an ORTEC 527A amplifier. The data were recorded using an ORTEC 926 MCD with 8192 channel analog to digital convertor and Maestro 32 software. A ^{60}Co source enclosed in a lead cylinder was used to obtain the gamma response of the sample [9, 13]. Additionally, relative light yield measurements were obtained for the fibers using an alpha

source (^{241}Am), beta (^{36}Cl), and gamma ray (^{137}Cs) source using a Hamamatsu R877 PMT.

3.4 Results and Discussion

Figure 3.1 shows an example SEM micrograph of the resulting ^{6}LiF collected on filter paper. The histograms show the particle size distribution for 450 nm (Figure 3.1(b)) and 1 μm (Figure 3.1(d)) filters, respectively. Despite the use of different filters, the mean particle size and standard deviation was approximately the same as that shown in Table 3.1. Previously, mechanically hot-pressed PEN films loaded with ^{6}LiF and scintillating fluor have been thermally post-processed and shown significant increase in crystallinity and scintillation light output. Cakmak and Kim reported significant increase of crystallinity with increased take-up speed for neat melt-spun PEN fibers [15]. Small diameter melt-spun PEN/LiF fibers with wavelength shifting fluor were fabricated for take-up speeds ranging from 200 m/min to 1200 m/min. As shown in Appendix A (Figure A.1), a significant increase in crystallinity, determined by DSC, can be clearly observed with increase of take-up speed for both neat PEN and PEN/LiF fibers for take-up speeds ranging from 200 m/min to 1200 m/min . The PEN/LiF fibers had a maximum crystallinity of 25% compared to maximum crystallinity of 21 % for neat PEN fibers corresponding to take-up speed of 1200 m/min. The greater crystallinity value for PEN/LiF can be attributed to presence of ^{6}LiF in PEN fiber matrix.

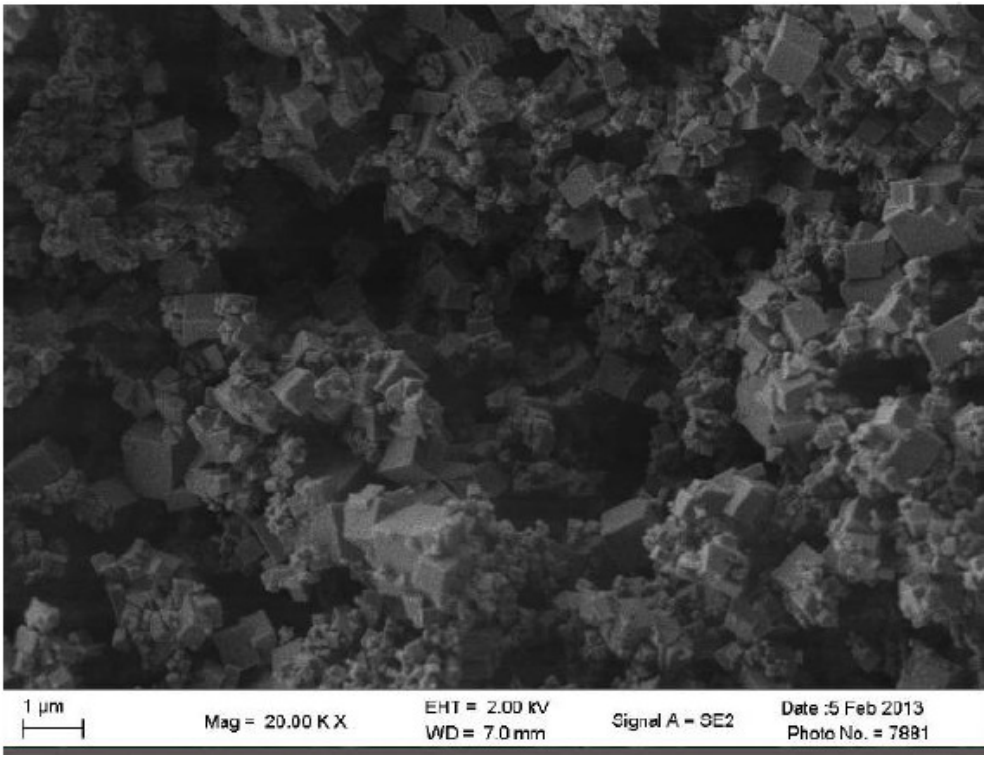

(a)

Figure 3.1: (a)SEM micrograph of ^{6}LiF particles using 450 nm filter, (b) particle size distribution for ^{6}LiF using 450 nm filter, (c) SEM micrograph of 6LiF particles using 1 µm filter, and (d) particle size distribution for 6LiF using 1µm filter.

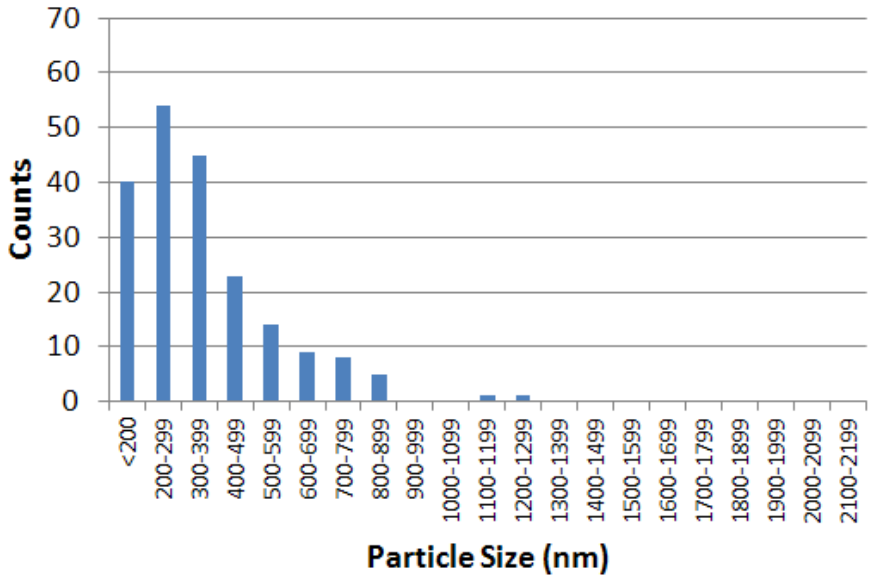

(b)

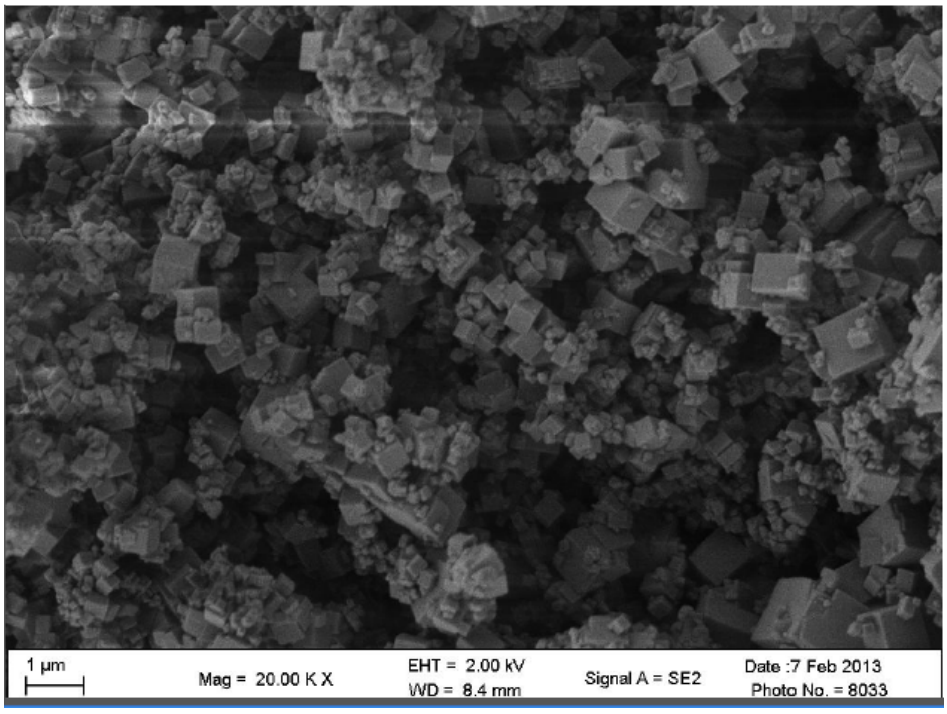

(c)

Figure 3.1 continued

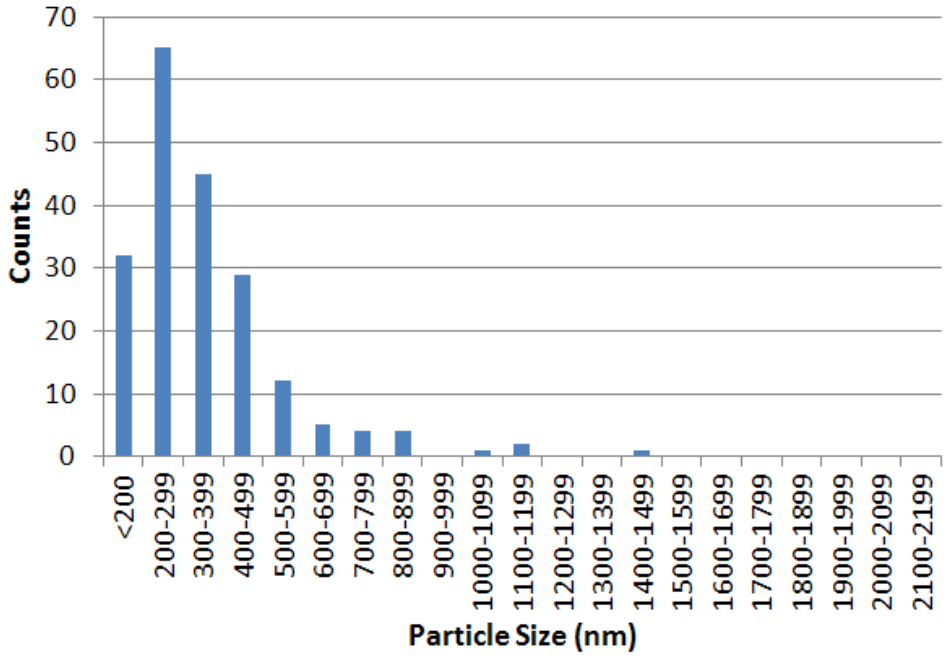

(d)

Figure 3.1 continued

Table 3.1: Mean Size and Standard Deviation of Filtered ^{6}LiF

Filter	Mean (nm)	Standard Deviation (nm)
450 nm	355	197
1 mm	353	198

In this study, neat PEN and PEN/LiF fibers (without wavelength shifting fluor) with ^{6}LiF concentrations of 2.5% wt, 10 % wt, and 25% wt were melt-spun. A thickness of 250 μm for fiber was targeted to compare to the previously reported 66 to 220 μm thick PEN films [13]. However, the PEN/LiF with a concentration of 2.5% wt and 10% wt fibers showed significant degradation, and the fiber diameter varied widely. Thus, this report is based on PEN/LiF fibers with a concentration of 25% wt and average fiber diameter of 238 μm.

Thermal Properties. Figure 3.2 and Table 3.2 show the DSC curves and corresponding thermal properties for the resulting melt-spun neat PEN and PEN/^{6}LiF fibers. As shown in Table 3.2, the melt-spun microfibers had a low degree of crystallinity, as expected for a low take-up speed of 20 m/min for PEN-based fibers. This is due to a lack of orientation of the polyester during spinning [15]. Furthermore, as shown in Figure 3.2 for neat PEN and PEN/LiF fibers, the areas under the melting peak at a temperature range of 250 ^{o}C to 260 ^{o}C and the area under the cold crystallization peak around 190 ^{o}C were approximately the same, indicating low crystallinity in the fibers [15]. It is interesting to note the negative value relating to the degree of crystallinity for the neat PEN fibers as shown in Table 3.2. In theory, a degree of crystallinity value of zero corresponds to a completely amorphous polymer; however, the negative value was most likely due to the accuracy of the DSC [34].

However, an increase in the crystallinity and glass transition temperature (T_g) was observed for PEN/LiF compared to neat PEN, which can be attributed to the

^{6}LiF presence in the fibers such that higher energy is required to move the naphathalene units into the amorphous phase [30].

Furthermore, the cold crystallization peak was lower for PEN/LiF, suggesting that the ^{6}LiF crystals embedded in the fiber causes a reduction of entropy, which is directly related to the preferred orientation in the fibers [15]. Additionally, the mass of ^{6}LiF in fibers was investigated using thermogravametric analysis (TGA Pyris 1). Approximately 8 mg of chopped PEN/LiF fibers were placed in an aluminum pan (Perkins Elmer), crimped, and punctured with a hole. The fibers were heated from 50 ℃ to 500 ℃ at 10 ℃/min and held at 500 ℃ for 2 hours to degrade the PEN matrix thermally, leaving only the ^{6}LiF crystals. As shown in Figure 3.3, it is clear from the TGA curve that a decrease in mass leaves approximately 2 mg of sample, corresponding to the ^{6}LiF mass content in the sample pan. This value equates to approximately 23 % wt ^{6}LiF agrees well with estimated 25% wt loading of ^{6}LiF in PEN fibers.

Optical Microscopy and Measurements. Figure 3.4 and Figure 3.5 shows an example optical and SEM micrographs of neat PEN and PEN/LiF melt-spun microfibers. The resulting neat PEN fibers were visually highly transparent, as the PEN/LiF composite was very opaque in appearance, as shown in Figure 3.4(a) and Figure 3.5(a). Figure 3.4 and Figure 3.5 displays the neat PEN and PEN/LiF excited by UV.

As shown in Figure 3.4(b) and Figure 3.4(c) the neat PEN acts as a waveguide, where the light is completely harvested along the fiber and is emitted on the fiber end. In comparison to the neat PEN fibers, light from the PEN/LiF fibers (Figure 3.5(b) and Figure 3.5(c)) is emitted isotropically along the surface of the fiber, indicating that light is not harvested. This can be attributed to the surface roughness of the fibers and the micron-size ^{6}LiF domain within the fibers, scattering light.

The neat PEN has a relatively smooth surface, as shown in Figure 3.6(a) and Figure 3.6(b), while the PEN/LiF fiber (Figure 3.6(c) and Figure 3.6(d)) has a rough surface due to the ^{6}LiF micron-size crystals, which can be clearly viewed protruding out of the fiber surface. Energy-dispersive X-ray spectroscopy (EDS) was used to evaluate the distribution of ^{6}Li in the fibers. Although ^{6}Li cannot be directly detected using EDS due to its low atomic number, its fluorine distribution can be viewed. Figure 3.7 shows a high magnification of ^{6}LiF on the fiber surface and corresponding elemental mapping of fluorine distribution, where the bright spots are fluorine. The molecular distribution shows high micron-size concentration areas and surrounding smaller nanophases, confirming ^{6}LiF, although some agglomeration is distributed throughout the fiber.

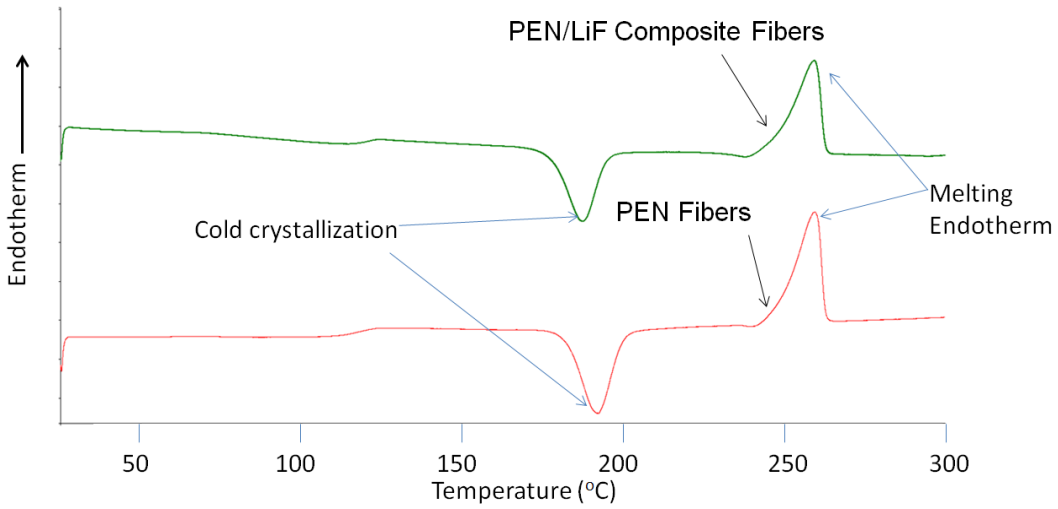

Figure 3.2: DSC spectra for PEN-based meltspun fiber at take-up speed of 20 m/min.

Table 3.2: Thermal Properties of PEN-based fibers

Sample	T_g	T_c	T_m	Enthalpy of Cold crystallization exotherm [ΔH_c (J/g)]	Enthalpy of Melting Endotherm [ΔH_m (J/g)]	H_m-H_c	% Crystallinity [ΔH_m-ΔH_c]/ΔH_{mo}
Neat PEN	118	193	260	39.3	38.5	-0.8	-0.77
PEN/LiF	119	188	260	31.2	34	2.7	2.6

*Heat of Fusion (ΔH_{mo} = 103.7 J/g) [15, 49]

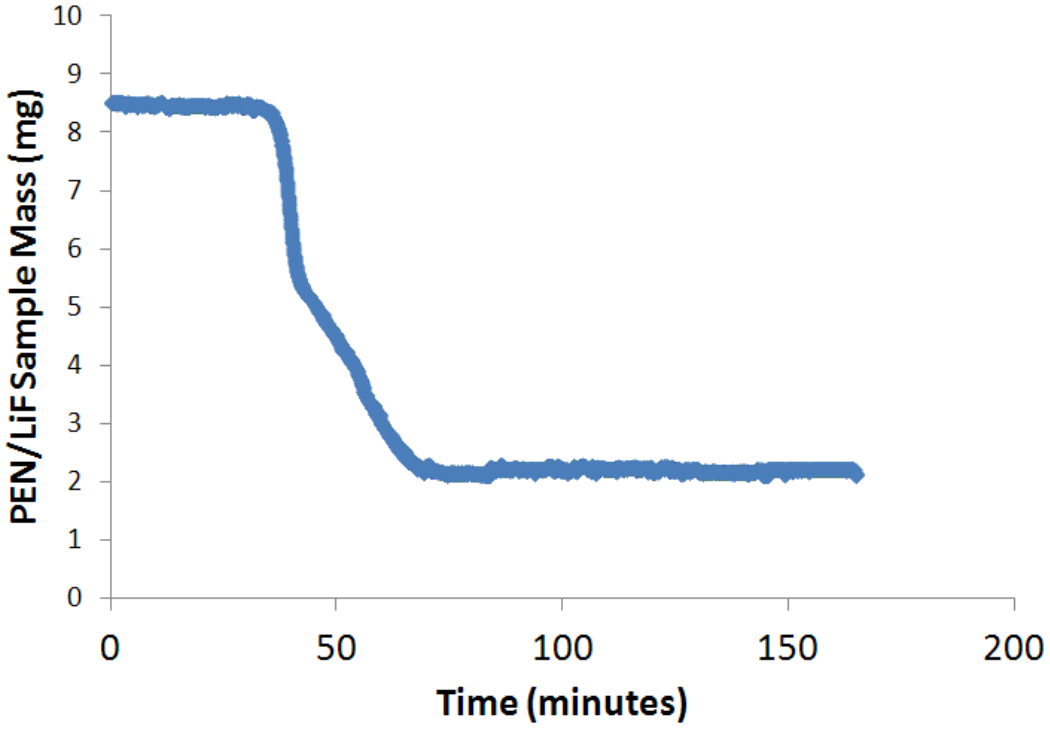

Figure 3.3: Thermal degradation of PEN/LiF melt-spun composite fibers using TGA.

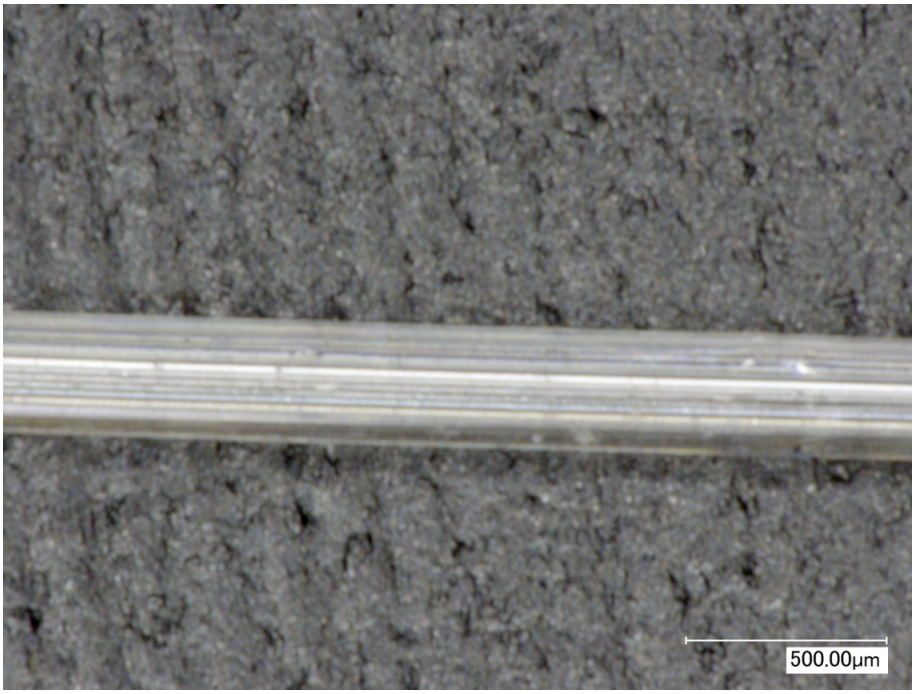

(a)

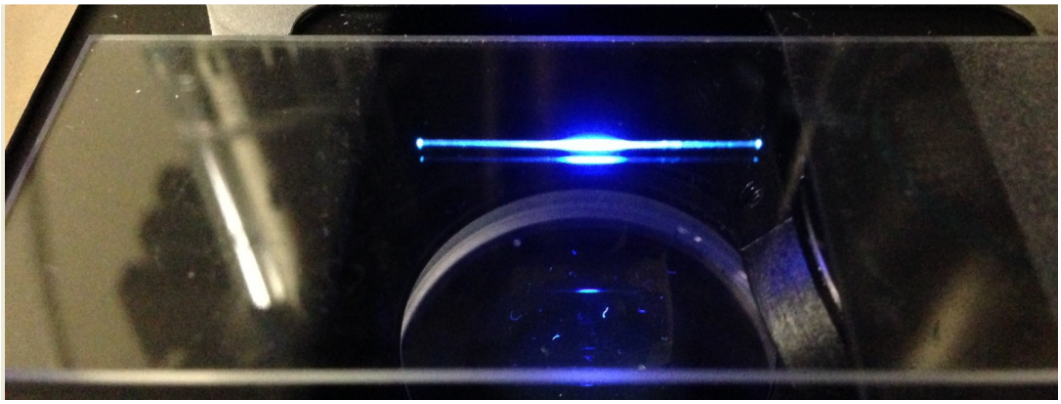

(b)

Figure 3.4: (a) Optical Image of neat PEN melt-spun microfiber, (b) image of neat PEN melt-spun microfiber under UV radiation exhibiting waveguiding behavior, and (c) optical micrograph of neat PEN exhibiting waveguiding behavior.

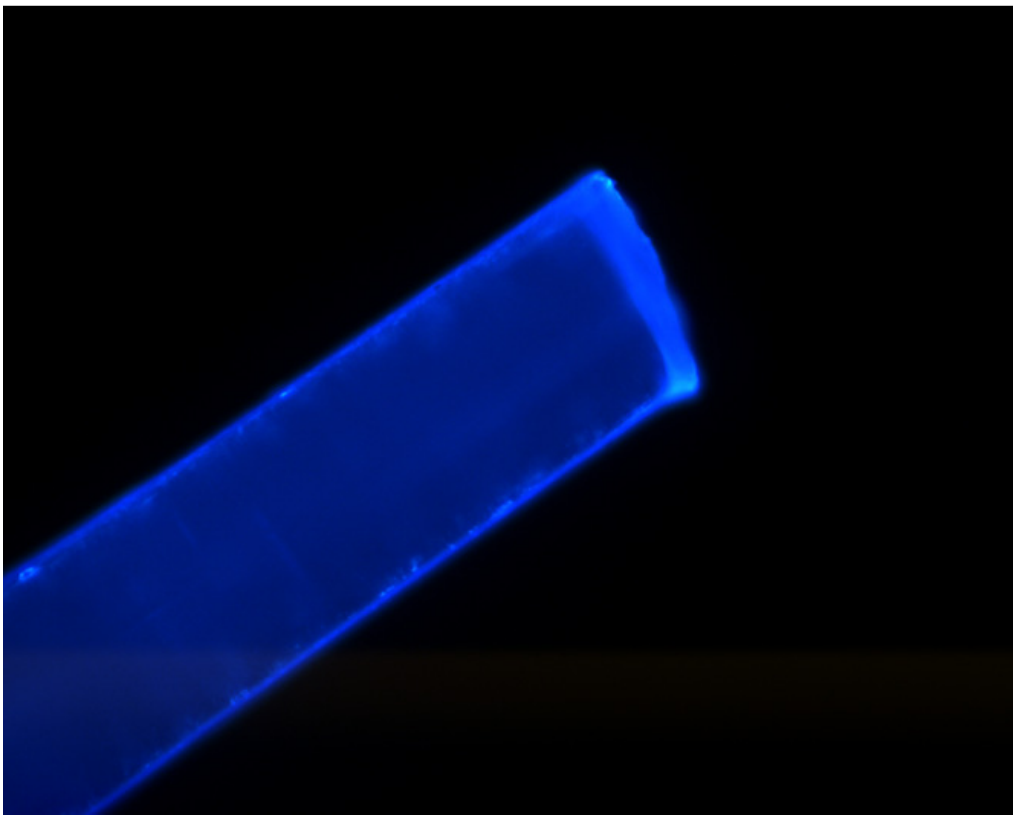

(c)

Figure 3.4 continued

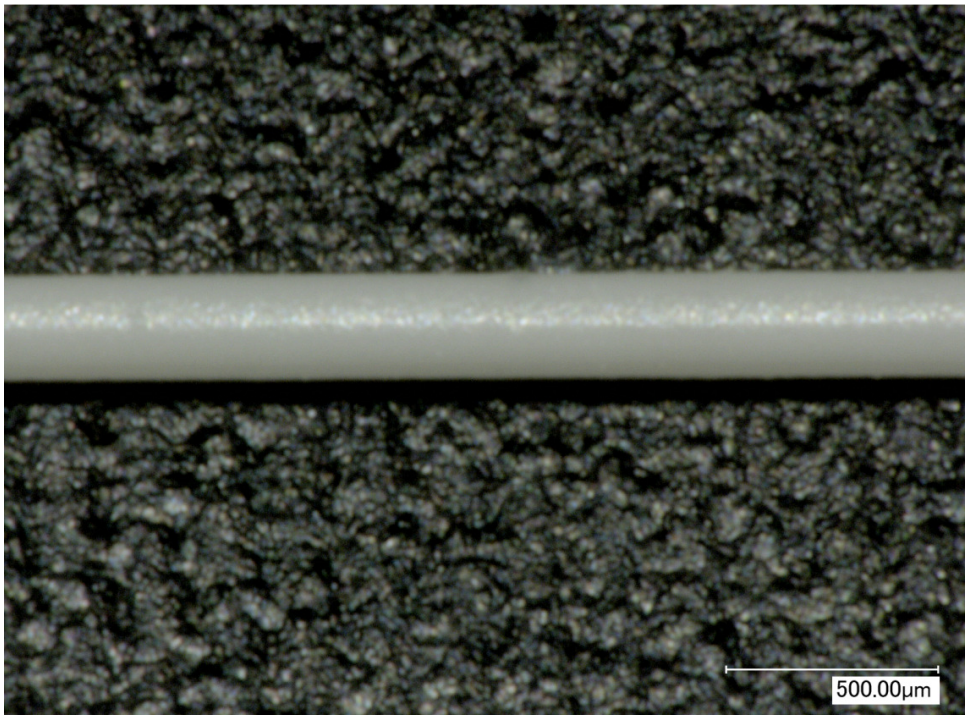

(a)

Figure 3.5: (a) Optical Image of PEN/LiF melt-spun microfiber, (b) image of PEN/LiF composite melt-spun microfiber under UV radiation and (c) optical micrograph of PEN/LiF composite melt-spun microfiber under UV radiation.

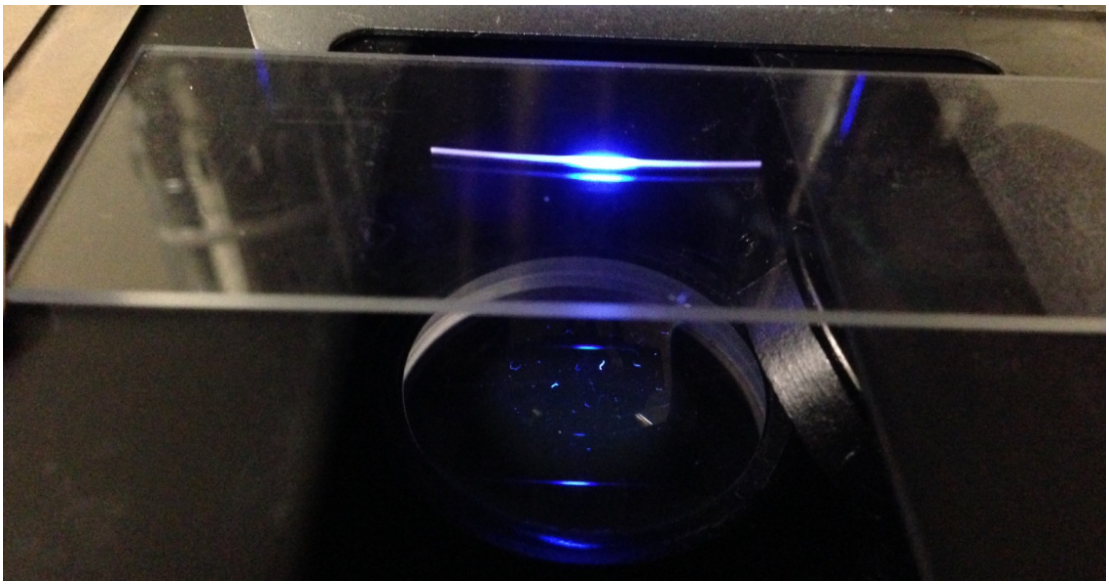

(b)

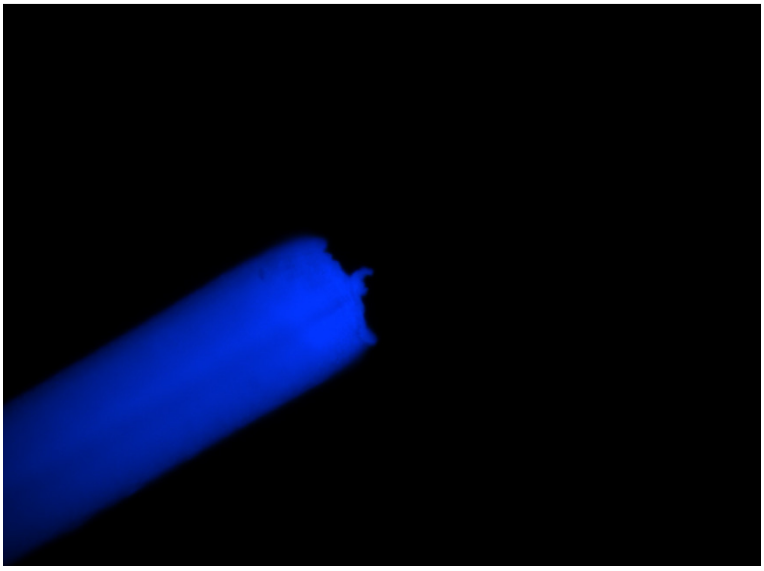

(c)

Figure 3.5 continued

Figure 3.8 shows an example of a 3D fluorescence spectrograph of neat and PEN/LiF fibers. Both samples show broad emission bands around 430 nm, which agrees with values reported in the literature [17]. This indicates intramolecular energy transfer along the naphthalene units, where the molecules are excited to higher energy levels before the excimeric emission of photon [17, 18]. Additionally, Figure 3.9 shows 2D spectra for neat PEN and PEN/LiF fibers. The rising edge of the absorption band for the neat PEN fibers (Figure 3.9) describes the process by which the PEN molecules absorb energy to higher electronic states.

The broad absorption band is due to the highly amorphous semi-crystalline polymer and indicates some energy migration along the napthalate units. This absorption transition is due to the excited state of the naphthalene units, called excimers, due to the naphthalene units located on the backbone of the PEN polymer chain. There are three absorption bands, as shown in Figure 3.9. The excitation peak of 269 nm (1A) and two other bands at 309 nm (2A) and 384 nm (3A) are observed. This indicates that the PEN fibers have multiple excitation states, corresponding to different energy levels. However, it must be noted that, although extensive studies have been reported for PEN excimers, there is very little scientific literature concerning solid PEN.

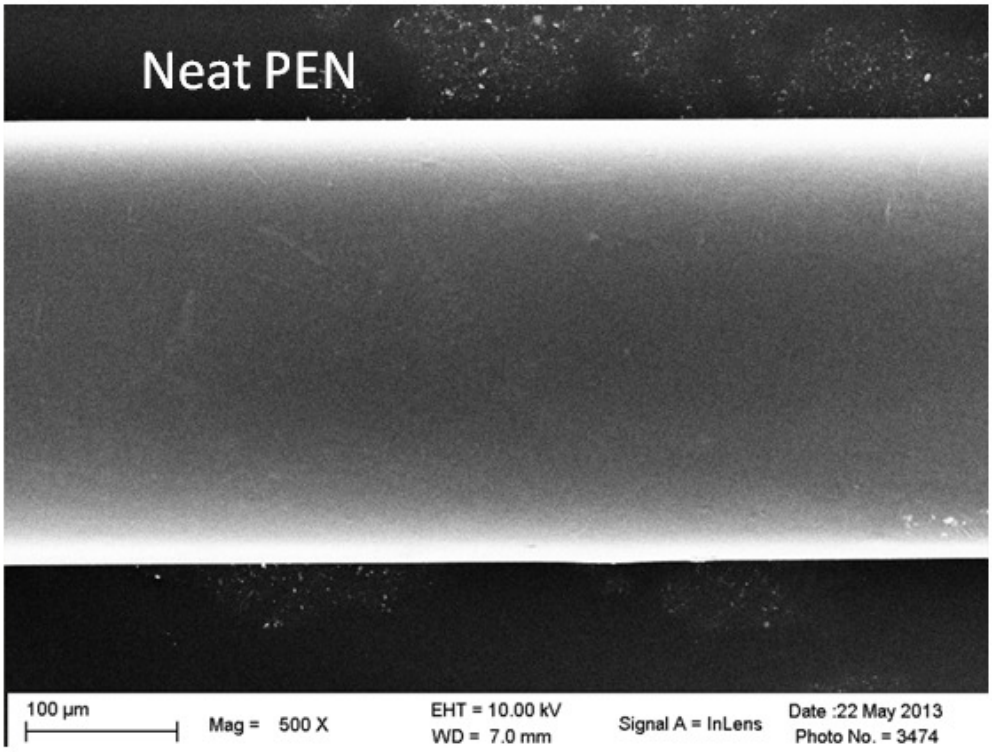

(a)

Figure 3.6: (a) SEM micrograph of neat PEN melt-spun microfiber, (b) SEM micrograph of surface of neat PEN melt-spun microfiber, (c) SEM micrograph of PEN/LiF composite melt-spun microfiber, and (d) SEM micrograph of surface of PEN/LiF composite melt-spun microfiber.

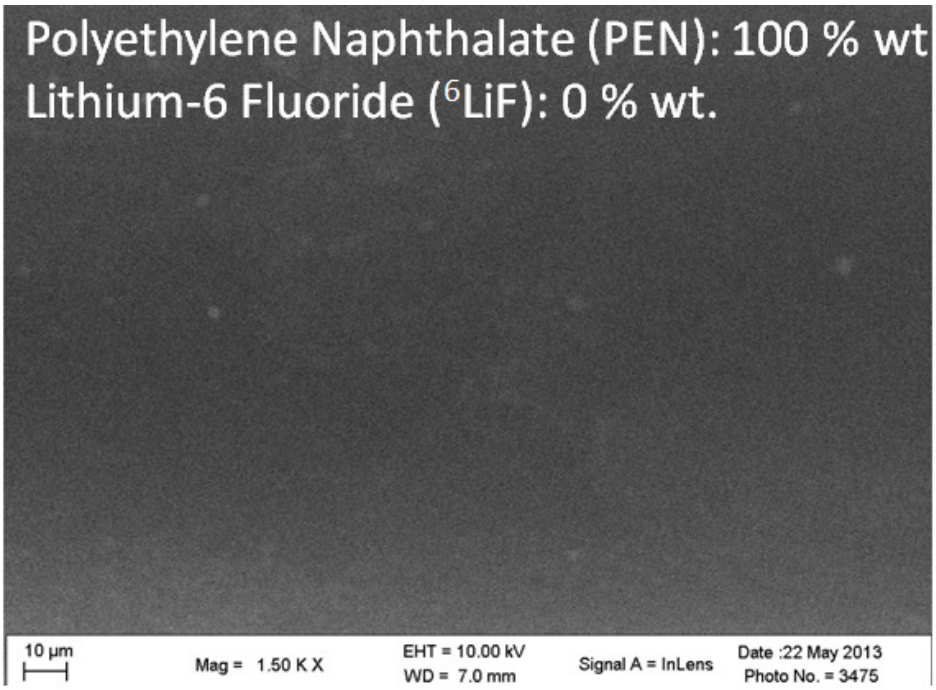

(b)

Figure 3.6 continued

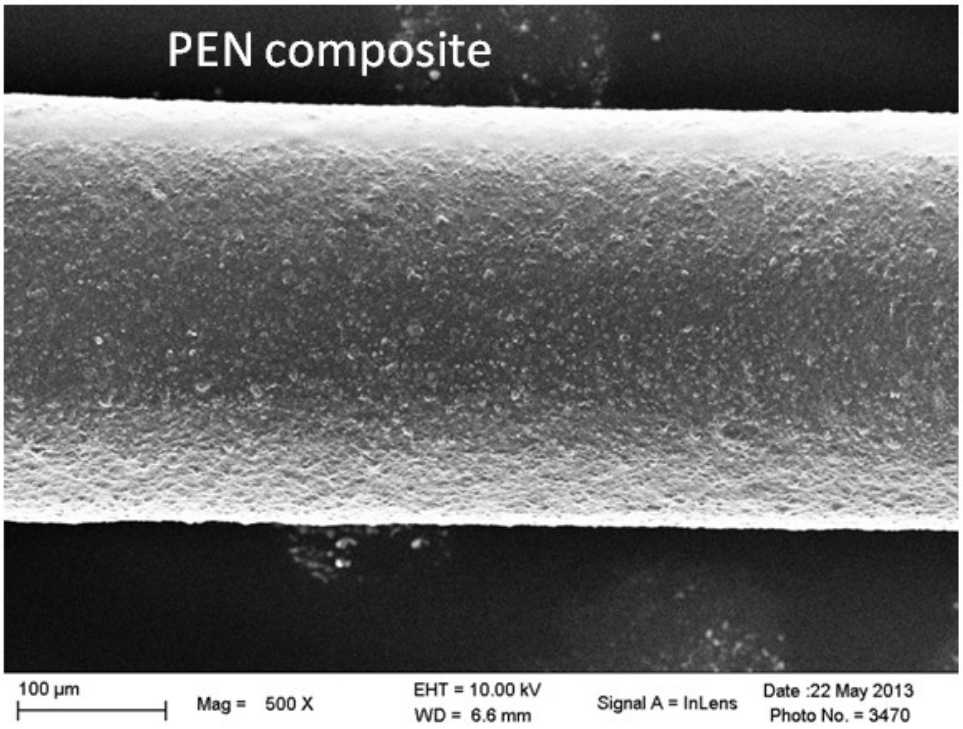

(c)

Figure 3.6 continued

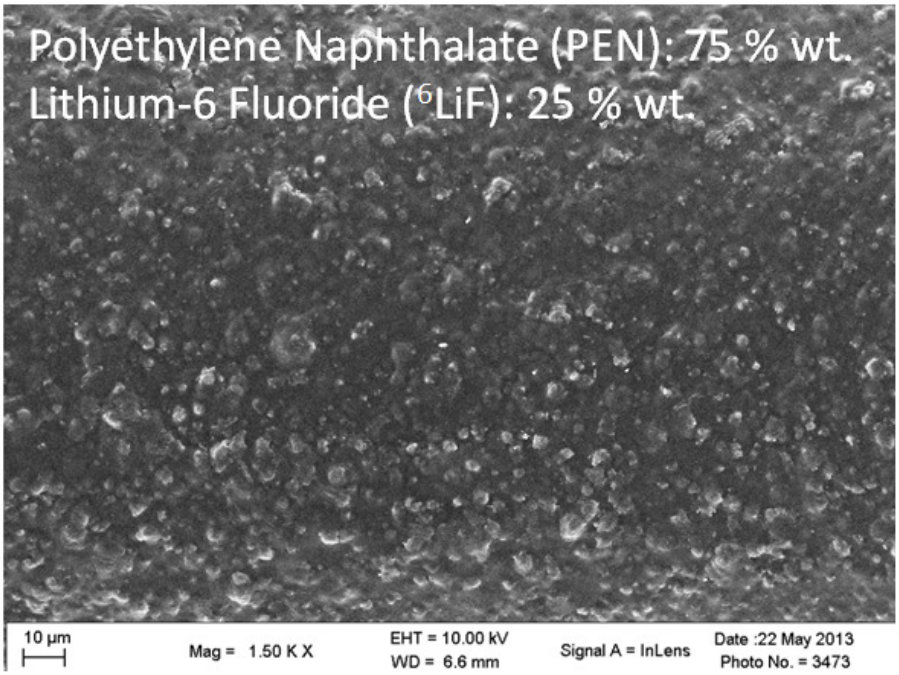

(d)

Figure 3.6 continued

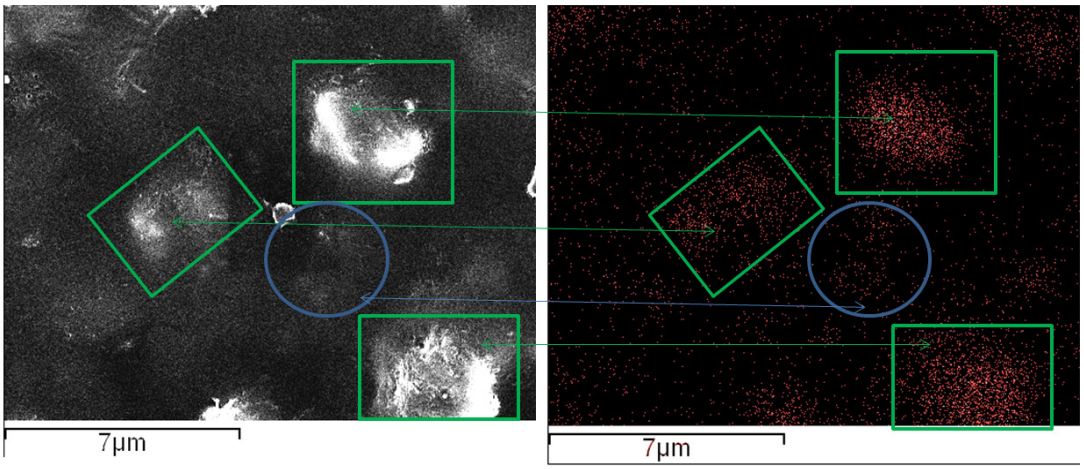

Figure 3.7: SEM micrograph and elemental mapping of fluorine distribution inside PEN/LiF composite microfiber confirming presence of ^{6}Li.

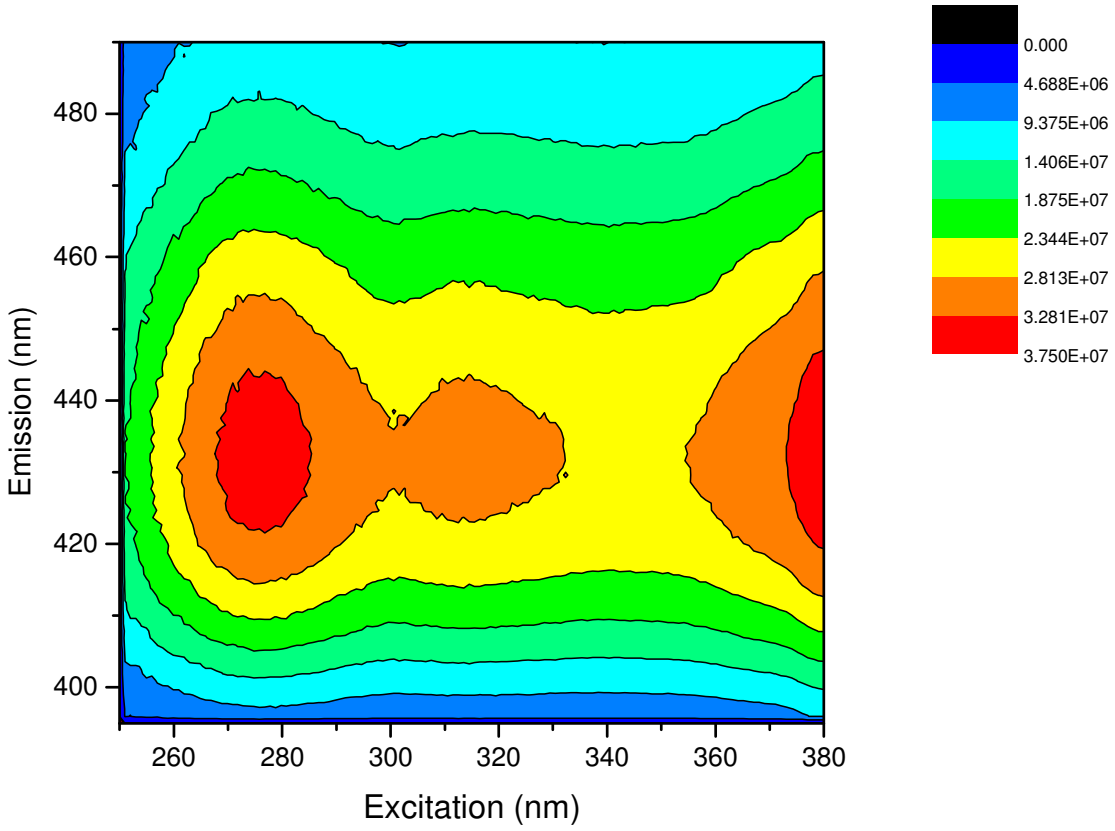

(a)

Figure 3.8: (a) 3D excitation-emission fluorescence spectra of neat PEN and (b) PEN/LiF melt-spun microfibers. Note: Colors can be viewed online.

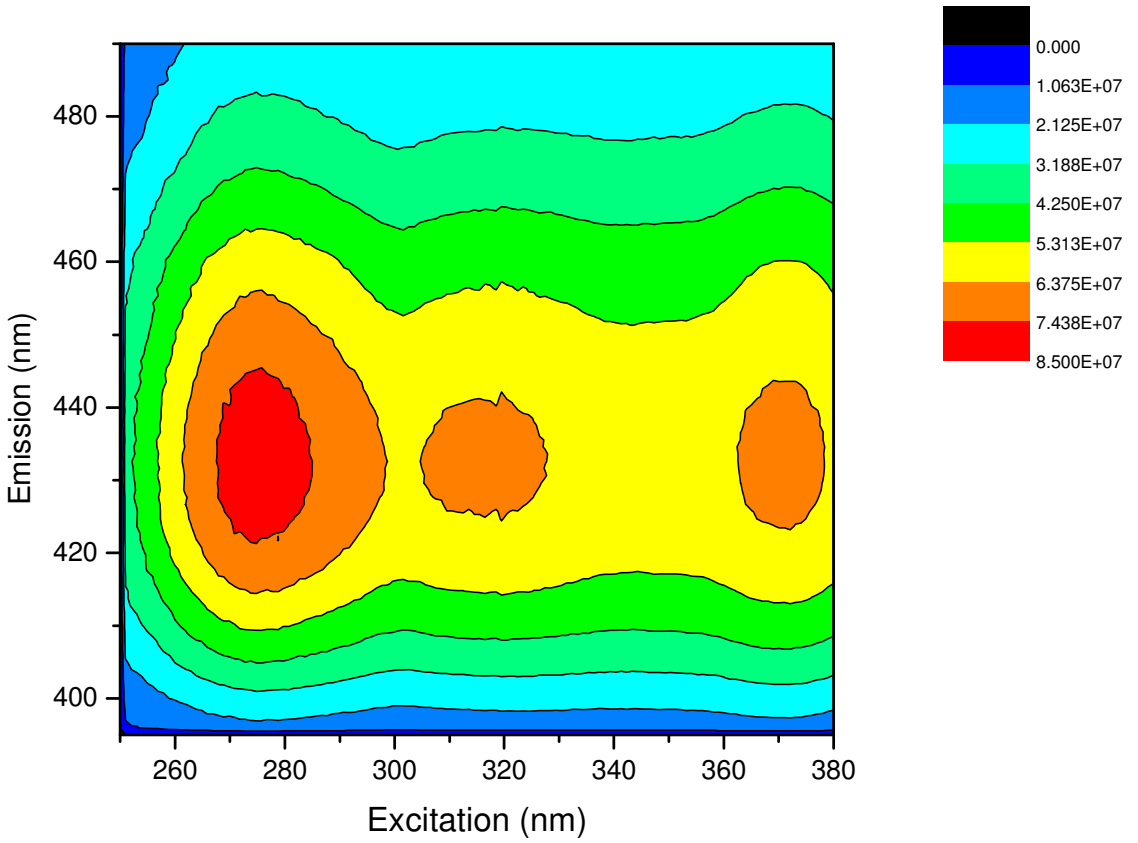

(b)

Figure 3.8 continued

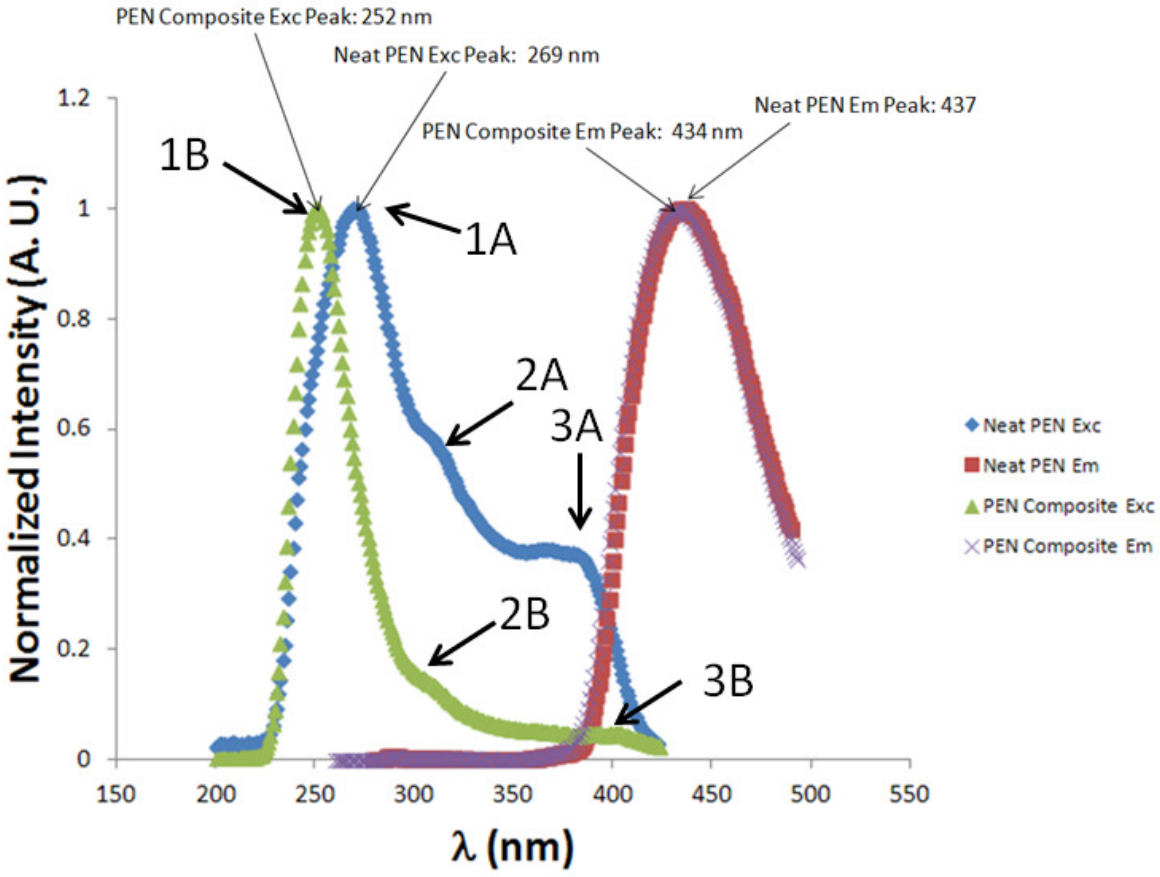

Figure 3.9: Excitation and emission spectra for neat PEN and PEN/LiF composite meltspun microfibers.

Hence, a more theoretical treatment is required to identify the absorption peaks [17, 35-38]. The emission spectrum corresponds to the excimer fluorescence of neat PEN fibers and is very smooth, with a peak of 437 nm. The lack of features in the emission curve is due to the amorphous and crystalline regions of the polymer [17, 39, 40].

The absorption band (Figure 3.9) for the PEN composite fibers is much narrower than that of the neat PEN due to localized ^{6}LiF crystal sites within the fibers. Additionally, the absorption peak is at a lower wavelength (higher energy) than that of neat PEN (a 17 nm difference in excitation peaks). This is thought to be due to the presence of ^{6}LiF crystals, as additional energy is required to excite the naphthalene units to higher vibrational energy levels. Similar to neat PEN, three absorption bands are observed for PEN composite fibers at 252 nm (1B, excitation peak), 303 nm (2B), and around 400 nm (3B), as shown in Figure 3.9. Similar to that of neat PEN fibers, the emission spectrum is very smooth with a peak at 434 nm.

Scintillation measurements. Figure 3.10 shows an example PEN/LiF encapsulated in optical gel and its exposure to UV. The light yield for the PEN/LiF microfibers was determined relative to the commonly used BGO crystal with a reported measured light output of 8200±350 photons per MeV [41, 42]. The samples were mounted onto PMT and covered with Teflon® reflector block with half sphere (dome) machined into surface. A ^{137}Cs source was placed on top of the block to measure gamma response. To obtain alpha (^{241}Am) and beta

(^{36}Cl) response, the sources was placed inside and positioned vertical above the sample by approximately 5 mm. It must be noted the alpha (^{241}Am) particles experience minimal energy lost at this distance [43]. As expected, no peak position was observed for gamma response (Figure 3.11) due to the thin fiber geometry of the scintillator and low gamma interaction from charged particles produced from ^{6}Li neutron capture event. Similarly beta response did not yield a significant response having nearly identical response as gamma. However, a peak position for alpha response was observed, indicating the alpha particle energy deposited in the fibers.

As shown in Table 3.3, an alpha particle with 5.484 MeV (energy corresponding to ^{241}Am source) has a path length of 31 μm, simulated for PEN/LiF with composition of 25% wt ^{6}LIF loading in PEN matrix using Stopping and Range of Ions in Matter (SRIM) software [44, 45]. This indicates that the alpha particles are completely stopped in the fibers. The relative light yield measurements are shown in Table 3.5 for the PEN/LiF fibers compared to GS20. The relative light yield for PEN/LiF and GS20 was determined using the following relationship:

$$\frac{\frac{Sample\ Channel\ Number}{BGO\ Channel\ Number}\times 8200\frac{photons}{MeV}\times\frac{QE_{BGO}}{QE_{Sample}}}{\frac{G_{Sample}}{G_{BGO}}} \quad \text{(Eq. 3.1)}$$

where a) the channel number corresponds to the peak position of response for samples, b) QE is the quantum efficiency of the sample and $\frac{G_{sample}}{G_{BGO}}$ is ratio of gain settings used for light yield measurements. The system was calibrated to BGO having a peak channel number of 100 using a ^{137}Cs source with energy of 662 keV (0.662 MeV) and gain setting of 128 x1.35 (G_{BGO}) at 900 V. A gain setting of 256 x 2.5 (G_{sample}) was used for PEN/LiF and GS20. Energy value of aforementioned 5.484 MeV was used for ^{241}Am.

The quantum efficiency values were approximated for the aforementioned using Hamamatsu R877 PMT using manufacturer's guidelines for relationship between QE and wavelength as shown in Table [46]. An example calculation is shown below for light yield of PEN/LiF irradiation using ^{241}Am corresponding to values in Table 3.4 and Table 3.5:

$$\frac{\frac{38}{100}\times 8200\times\frac{0.17}{0.23}}{\frac{265\times 2.5}{128\times 1.35}} = 622\ photons/\alpha \qquad \text{(Eq. 3.2)}$$

This value indicates PEN/LiF emits 622 photons per alpha event. Additionally, dividing this value by 5.484 MeV yields 113 photons/MeV. Similar calculations were performed for GS20 and are shown in Table 3.5. A photopeak could not be identified for the beta and gamma response therefore light yield measurements were not calculated. Figure 3.12 shows the neutron responses for PEN/LiF samples compared to GS20 as a reference to calibrate scintillation response.

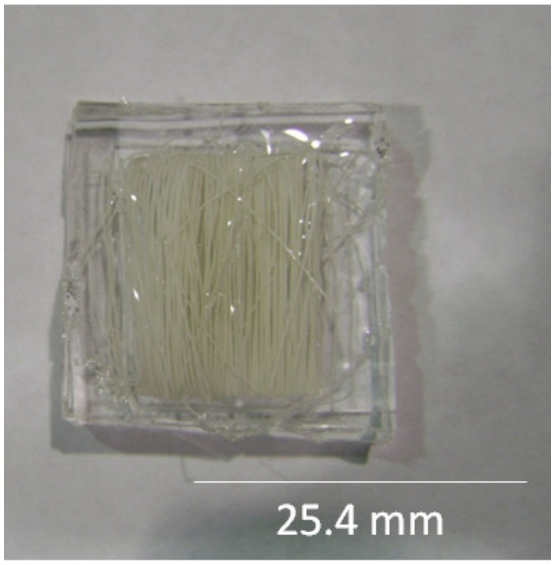

(a)

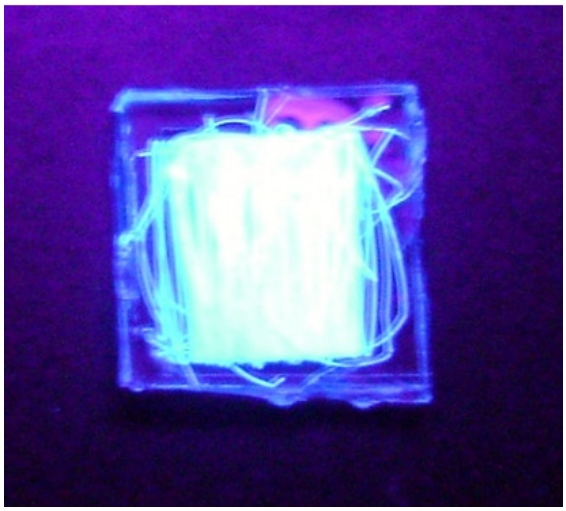

(b)

Figure 3.10: (a) Image of PEN/LiF composite meltspun microfibers wrapped around thin microscope glass cover encapsulated in optical gel and (b) exposure to UV radiation.

Table 3.3: Ranges of Ions in PEN Composite

Material	$\alpha 2+$ (5.484 MeV)	$\alpha 2+$ (2.05 MeV)	t+ (2.73 MeV)
PEN	33.9 μm	9.20 μm	54 μm
PEN + 25 % ^{6}LiF	31 μm	8.59 μm	49.1 μm

*These values are the results from simulating 5000 incident ions.

Table 3.4: Parameters for Determination of Relative Light Yield

Sample	Emission Wavelength (nm)	QE	Alpha(^{241}Am) Channel Number
PEN/LiF	430	0.23	38
GS20	395	0.24	254
BGO	480	0.17	-

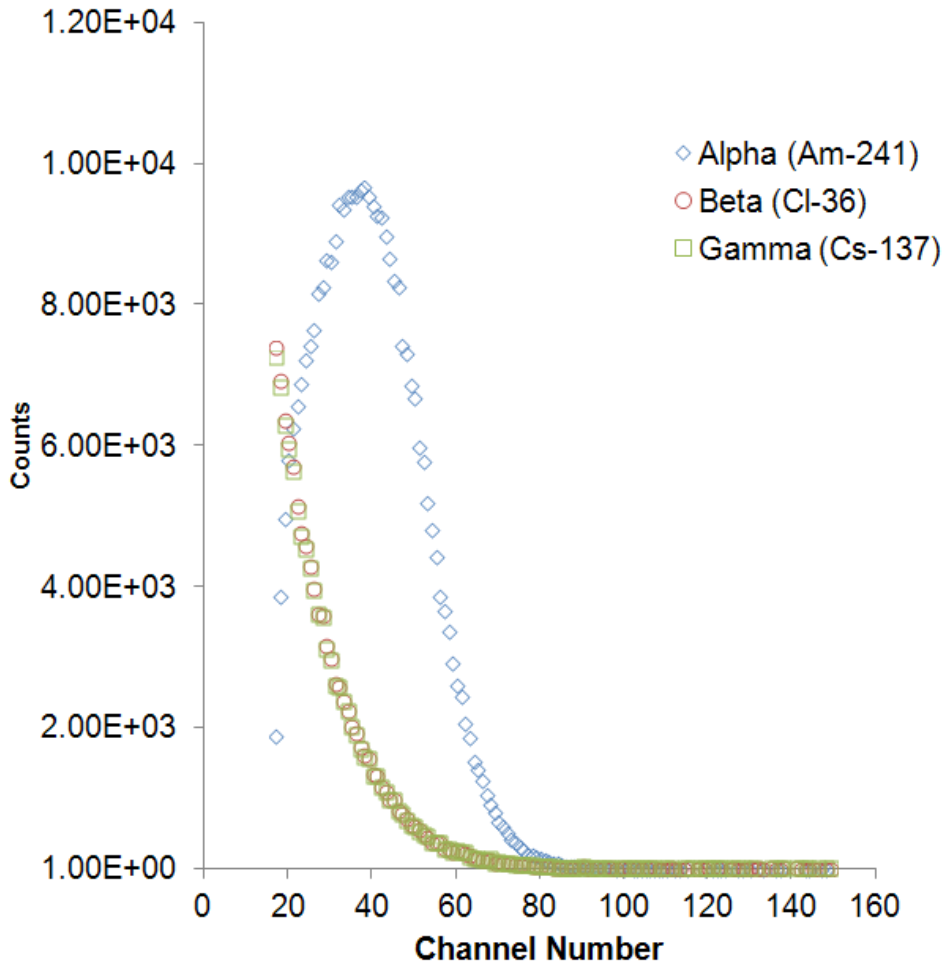

Figure 3.11: Alpha, beta and gamma response for PEN/LiF composite meltspun microfibers.

Table 3.5: Relative Light Yield Measurements for PEN/LiF and GS20

	Alpha(^{241}Am) (Photons/α)	Alpha(^{241}Am) (Photons/MeV)
PEN/LiF	622	113
GS20	3983	727

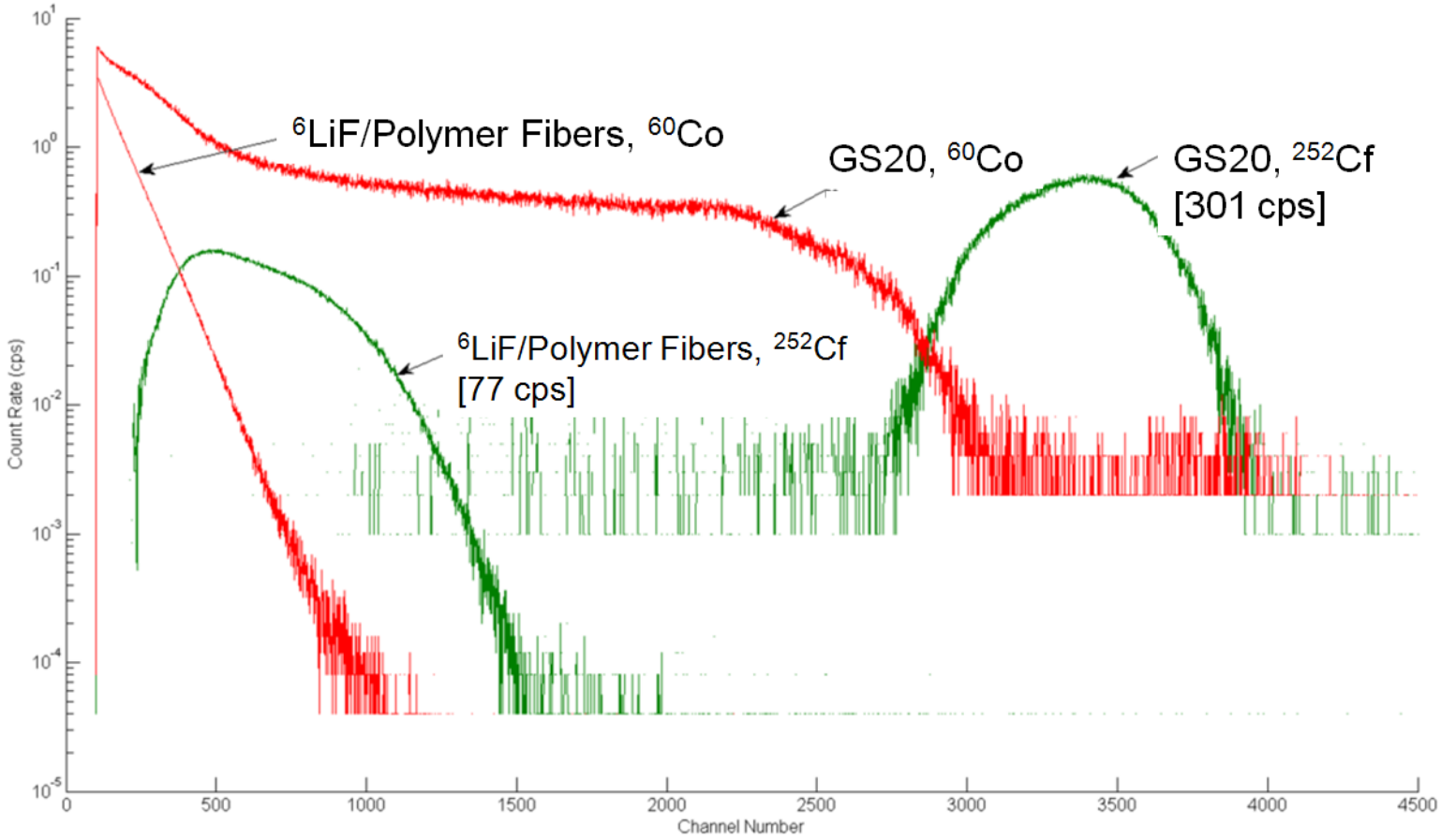

Figure 3.12: Neutron response for PEN/LiF melt-spun microfibers encapsulated in optical gel compared to GS20.

The PEN/LiF had a count rate of 77 cps, with a maximum neutron response of around channel 600 and an endpoint around channel 1500 compared to GS20 maximum response at approximately channel 3400. Additionally, a clear distinction of thermal neutrons is evident for PEN/LiF microfibers. The neutron count rate for GS20 was 301 cps. GS20 has been reported to emit 6250 photons for each neutron capture event [9].

Estimated photons per neutron for PEN/LiF were determined using the following relationship:

$$6250\,\frac{photons}{neutron} \times \left(\frac{\frac{PEN}{LiF} neutron\ spectra\ average\ channel\ number}{GS20\ neutron\ spectra\ average\ channel\ number} \right) \qquad \text{(Eq. 3.3)}$$

As shown in Table 3.6, the PEN/LiF was estimated to emit an average of 1166 photons per neutron capture event. It is thought that the lower neutron response than that of GS20 is due to the charged particle path length of the secondary electrons, alpha and triton in the fiber. As shown in Table 3.3, light approximately 58 μm below the fiber surface is detected by PMT. Thus, there is increased self-absorption and scattering probability due to the greater distance that must be traveled through the fiber to be detected by PMT [45].

Table 3.6: Photons per Neutron Capture Event for PEN/LiF and GS20

Sample	Neutron Average Spectra	Photons/Neutron
GS20	3356	6250
PEN/LiF	626	1166

However, the results are encouraging given that the fibers were simply wrapped around thin glass disk where light collection geometry was not optimized, weighed only 283 mg and had approximately 17 mg of ^{6}Li.

GS20, by comparison, is a flat, circular disk with a high loading of Li, is 2 mm thick, and has a net weight of 2460 mg, yielding a higher thermal neutron response. It is interesting to note the cross sections for both neat PEN and PEN/LiF melt-spun fibers as shown in Appendix A (Figure A.2, Figure A.3). The fibers have significant voids and are typical artifacts for melt spun fibers. These voids mainly result from extended residence time in extruder and possible air traps. Additionally, void formation could be attributed to either moisture in polymer or insufficient pressure during extrusion [47, 48]. Future research will include investigating melt-spun processing conditions, minimizing the voids, and effect of scintillation efficiency from void formation.

3.5 Conclusions

Composite microfibers were fabricated using a two-component system consisting of PEN and ^{6}LiF. The PEN/LiF fibers were successfully melt-spun and evaluated for thermal neutron and gamma discrimination. The distribution of ^{6}Li was successfully confirmed to be distributed throughout the fiber by the confirmation of fluorine using EDS. PEN/LiF yielded a neutron peak and relative light yield alpha peak. Future research will include optimizing the light collection geometry of fibers and investigating the scintillation properties of fibers for various loadings of ^{6}LiF.

3.6 References

[1] Kouzes, R. T., 2009, "The ^{3}He Supply Problem," Pacific Northwest National Laboratory Technical Report, PNNL-18388.

[2] Sen, I., Penumadu, D., Williamson, M., Miller, L. F., Green, A. D., and Mabe, A. N., 2011, "Thermal Neutron Scintillator Detectors Based on Poly(2-Vinylnapthalene) Composite Films", IEEE Trans. Nucl. Sci., **59**(3), pp. 1386-1393.

[3] Breukers, R. D., Bartle, C. M., and Edgar, A., 2013, "Transparent Lithium Loaded Plastic Scintillators for Thermal Neutron Detection," Nuclear Instruments and Methods in Physics Research A, **701**, pp. 58-61.

[4] Kulkarni, P. V., et al., 1997, "Plastic Scintillating Materials in Nuclear Medical Imaging," Polymer-Plastics Technology and Engineering, **36(1)**, pp. 1-51.

[5] Tsoulfanidis, N. and Landsberger S., 2011, *Measurement and Detection of Radiation,* Taylor and Francis Group, Boca Raton, FL, p. 178.

[6] Fisher, B. M., et al., 2011, "Fast Neutron Detection with 6Li-loaded Liquid Scintillator," Nuclear Instruments and Methods in Physics Research A, **646**, pp. 126-134.

[7] Knoll, G. F., 2000, *Radiation Detection and Measurement, 3rd ed*. John Wiley and Sons, Hoboken, NJ, pp. 227-522.

[8] Birowosuto, M. D. , 2008, "Li-Based Thermal Neutron Scintillator Research; $Rb_2LiYBr_6 : Ce^{3+}$ and Other Elpasolites," IEEE Transactions On Nuclear Science, **55**(3), pp. 1152-1155.

[9] Mabe, A. N., Auxier II, J. D., Urffer, M. J., Penumadu, D., Schweitzer, G. K., and Miller, L. F., 2013, "Transparent Lithiated Polymer Films For Thermal Neutron Detection," Nuclear Instruments and Methods in Physics Research A, **772**, pp. 29-33.

[10] Ianakiev, K. D., Swinhoe, M. T., Favalli, A., Chung, K., and MacArthur, D. W., 2011, "^{6}Li Foil Scintillation Sandwich Thermal Neutron Detector," Nuclear Instruments and Methods in Physics Research A, **652**, pp. 417-420.

[11] Fox, M., 2001, *Optical Properties of Solids,* Oxford University Press, New York, NY, pp. 87.

[12] Baldacchini, G. I., Bonfigli, F., Menchini, F., and Montereali, R. M., 2002, "High Concentrations of Aggregrate Colour Centres in Heavily Irradiated LiF Crystals," Physics Research Section B, **191**(1-4), pp. 216-220.

[13] Sen, I., Urffer, M., Penumadu, D., Young S. A., Miller, L. F., and Mabe, A. N., 2012, "Polyester Composite Thermal Scintillation Films," IEEE Trans. Nucl. Sci., **59**(4), pp. 1781-1786.

[14] Nakamura., H., *et al,* 2011, "Evidence of Deep-Blue Photon Emission at High Efficiency by Common Plastic," EPL (Europhysics Letters), 95(2), pp. 22001 –p1 – 22001-p3.

[15] Cakmak, M., and Kim, J. C., 1997, "Structure Development in High-Speed Spinning of Polyethylene Naphthalate (PEN) Fibers ," Journal of Applied Polymer Science, **64(4)**, pp. 729-747.

[16] Galay, J., and Cakmak, M., 2001, “Online Monitoring of Birefringence Development in Heat-Setting Polymer Films with a Fast Dual-Wavelength Optical Technique. I. Uniaxial Oriented Poly(ethylene naphthalate),” Journal of Polymer Science: Part B: Polymer Physics, 39, pp. 1107 – 1121.

[17] Ouchi, I., Nakai, I., Ono, M., and Kimura, S., 2007, “Features of Fluorescence Spectra of Polyethylene 2,6-Naphthalate Films,” Journal of Applied Polymer Science, 105, pp. 114 – 121.

[18] Ouchi, I., Miyamura, R., Sakaguchi, M., Hosaka, S., and Kitagawa, M., 1999, “Excitation and Emission Spectra of Polyethylene Terephthalate and Polyethylene 2,6-Naphthalate Films,” Polym. Adv. Technol., 10, pp. 195 – 198.

[19] McIntosh, K., Yamada, N., and Richards, B. S., 2007, “Theoretical Comparison of Cylindrical and Square-Planar Luminescent Solar Concentrators,” Appl. Phys. B, **88(2)**, pp. 285-290.

[20] Leutz, H., 1995, “Scintillating Fibres,” Nuclear Instruments and Methods in Physics Research A, **364**, pp. 422-448.

[21] Edelenbosch, O. Y., Fisher, M., Patrignani, L., van Sark, W. G. J. H. M., and Chatten, A. J., “Luminescent Solar Concentrators with Fiber Geometry,” Optical Express, **21(S3)**, pp.A 503-A514.

[22] Colantuono, G., Buckley, A., and Erdelyi R., 2013, “Ray-Optics Modelling of Rectangular and Cylindrical 2-Layer Solar Concentrators,” J. Lightwave Technol., **31(7)**, pp. 1033-1044.

[23] Inman, R. H., Scherbatyuk, G., Medvedko, D., Gopinathan, A., and Ghosh, S., 2011, "Cylindrical Luminescent Solar Concentrators with Near-Infrared Quantum Dots," Opt. Express., **19(24)**, pp. 24308-24313.

[24] Fery-Forgues, S., and Fournier-Noël, C., 2010, "Organic Fluorescent Nanofibers and Sub-Micrometer Rods, Nanofibers," Kumar, A. (Ed.), ISBN: 978-953-7619-86-2, InTech, DOI: 10.5772/8164. Available from: http://www.intechopen.com/books/nanofibers/organic-fluorescent-nanofibers-and-sub-micrometer-rods.

[25] Li, L., Yang, X., and Yuan, L., 2012, "One-dimensional Optical Materials of Microfibers by Electrospinning," Materials Letters, 1, pp. 292-295.

[26] Kirkby, J., 1987, "Today and Tomorrow for Scintillating Fibre (SCIFI) Detectors," European Organization For Nuclear Research, CERN-EP/87-60.

[27] Blumenfeld, H., Bourdinaud, M., Rebourgeard, P., and Thevenin, J. C., 1989, "Production and Test of Coherent Bundles of Plastic Scintillating Microfibers," Nuclear Instruments and Methods in Physics Research A, **364**, pp. 619-621.

[28] Leibowitz, M., and Weinreb, A., 1967, "Effects of Fluorescence and Energy Transfer in Polystyrene Under Excitation in the Vaccuum Ultraviolet," J. Chem. Phys., **46**, pp. 4652-4659.

[29] Cheung, P. S. R., Roberts C. W., and Wagener, K. B., 1979, "Synthesis, Photodegradation, and Energy Transfer in a Series of Poly(ethylene

Terephthalate-co-2,6-Naphthalenedicarboxylate) Copolymers," Journal of Applied Polymer Science, **24**, pp. 1809-1830.

[30] Solarski, S., Ferreira M., and Devaux, E., 2005, "Characterization of the Thermal Properties of PLA Fibers by Modulated Differential Scanning Calorimetry," Polymer Communication, **46**, pp. 11187-11192.

[31] Carturan, S. et. al, 2011, "Novel Polysiloxane-Based Scintillators for Neutron Detection," Radiation Protection Dosimetry, **143**, pp. 471-476

[32] Sarraf-Mamoory, R. Nadery, S., and Riahi-Noori, N., 2007, "The Effect of Precipitation Parameters on Preparation of Lithium Fluoride (LiF) Nanopowder," Chem. Eng. Comm., **194**, pp. 1022-1028.

[33] Iwanowska, J., et al., 2011, "Neutron/Gamma Discrimination Properties of Composite Scintillation Detectors," JINST, **6**, pp. 1-10.

[34] Zhou, W. Y., Duan, B., Wang, M., and Cheung, W. L., 2009, "Crystallization Kinetics of Poly(L-Lactide)/Carbonated Hydroxyapatite Nanocomposite Microspheres," Journal of Applied Polymer Science, **113**, pp. 4100-4115.

[35] Mendicuti, F., Patel, B., and Mattice, W. L., 1990, "Intramolecular Excimer Formation in Model Compounds for Polyesters Prepared from 2,6-Naphthalene Dicarboxylic-Acid and 8 Different Glycols," Polymer, **31(3)**, pp. 453-457.

[36] Mendicuti, F., Saiz, E., and Mattice, W. L., 1992, "Intramolecular Energy Migration in Polyesters from 2,6-Naphthalene Dicarboxylic-Acid – Polarization

of Fluorescence in the Polymers and in Bichromophoric Model Compounds," Polymer, **33(23)**, pp. 4908-4912.

[37] Bravo, J., Mendicuti, F., and Mattice, W. L., 1992, "Intramolecular Formation of Excimers in Model Compounds for Polyesters Obtained from 2,6-Naphthalene Dicarboxylic-Acid and Cyclohexanediols," Journal of Polymer Science Part B –Polymer Physics, **32(8)**, pp. 1511-1519.

[38] Martin, O., Mendicuti, F., Saiz, E., and Mattice, W. L., 1992, "Intramolecular Excited State Complexes in Trichromophoric Model Compounds for Polyesters Derived from 2,6-Naphthalenedicarboxylic Acid and Aliphatic Glycols: Experiment, Rotational Isomeric State Model, and Molecular Dynamics," Journal of Polymer Science Part B –Polymer Physics, **37**, pp. 253-266.

[39] Phillips, D. H., and Schug, J.C., 1969, "Luminescence from Aromatic Polymers, Monomers, and Dimers under High Energy Electron Excitation," J. Chem. Phys., **50**, pp. 3297-3306.

[40] Mary, D., Albertini, M., and Laurent, C., 1997, "Understanding Optical Emissions from Electrically Stressed Insulated Polymers: Poly(ethylene terephalate) and Poly(ethylene 2,6 –naphthalate) Films," J. Phys. D: Appl. Phys., **30**, pp. 171-184.

[41] Moszynski, M., Kapusta, M., Mayhugh M., Wolski, D., and Flyckt, S. O., 1997, "Absolute Light Output of Scintillators," IEEE Transactions on Nuclear Science, **44(3)**, pp. 1052-1061.

[42] Holl, I., Lorenz, E., M., and Mageras, G., 1988, “A Measurement of the Light Yield of Common Inorganic Scintillators,” IEEE Transactions on Nuclear Science, **35(1)**, pp. 105-109.

[43] Orchard, G. M., Isham, U., M., and Walker, A. J., 1988, “Design and Initial Testing of an Electron Attachment Spectrometer,” IEEE Toronto Section 2nd International Workshop on Real-Time Measurement, Instrumentation and Control 2-3, June, 2001.

[44] Ziegler, J. F., Ziegler, D., M., and Biersack, J. P., 2010, “SRIM-The Stopping and Range of Ions in Matter,” Nuclear Instruments and Methods in Physics Research B, **268(11-12)**, pp. 1818-1823.

[45] Mabe, A. N., II Auxier, J. D., Urffer, M. J., Young, S. A., Penumadu, D., Schweitzer, G. K., and Miller, L. F., 2013, “Thin Film Polymer Composite Scintillators for Thermal Neutron Detection,” Journal of Composites, **Volume 2013(2013)**, Article ID 539060, pp. 1-8.

[46] Hamamatsu Catalog, <http://www.hamamatsu.com/jp/en/R877.html >(accessed 07.25.2013)

[47] Wiley, 2011, *Processing and Finishing of Polymeric Materials Volume 2,* John Wiley and Sons, Inc., Hoboken, NJ, p. 1264.

[48] Rauwendaal, C, 2011, *Polymer Extrusion Revised 4th Ed.,* Hanser Gardner Publications, Inc., Cincinnati, OH, p. 692.

[49] Cheng SZD, and Wunderlich, B., 1988, “Glass-Transition and Melt Behavior of Poly(Ethylene-2,6-Naphthalenedicarboxylate,” Macromolecules, **21(3)**, pp. 789-797

4 CHAPTER IV
INTEGRATION OF NEUTRON SCINTILLATOR FIBERS INTO MULTI-FUNCTIONAL COMPOSITES FOR STRUCTURAL APPLICATIONS

4.1 Abstract

^{6}Li-loaded polyethylene naphthalate (PEN) melt-spun scintillation microfibers were developed and tested for thermal neutron detection. The ^{6}Li isotope has a large thermal neutron cross-section, producing high-energy charged particles upon thermal neutron absorption. In this research study, polymeric composite laminates were fabricated using traditional adhesion techniques to produce scintillator detectors that directly discriminate between neutron and gamma radiation. PEN-based fibers were integrated with a composite laminate structure consisting of a carbon fiber/vinyl ester-reinforced backing. The composite laminate scintillator was characterized for response to thermal neutrons and gamma radiation using a custom neutron irradiator. Laminate scintillators were evaluated to study the mechanical properties and the effect of scintillation performance. Important microstructural information using a digital optical microscope and mechanical behavior, including the modulus, is reported.

4.2 Introduction

Non-intrusive neutron-based inspection of mobile units such as cargo and marine containers carrying hazardous materials and chemical agents are of great interest for homeland security applications [1]. Thermal neutrons, with energy of 0.025 eV, are particularly advantageous due to their attenuation of low atomic number materials [2]. The inspection is based on neutrons' ability, due to their uncharged nature, to deeply penetrate a detector medium without directly ionizing. Their detection, such as with thermal neutrons, proceeds by neutron-

induced reactions, creating secondary ionizing particles of sufficient energy [3-5]. The supply of ^{3}He, commonly used in gas proportional counters for neutron detection, has “dwindled” due to the current demand for ^{3}He [6]. Thus, there is a need to develop thermal neutron detectors as replacement technologies that can effectively discriminate between gamma and neutrons [6-8]. Organic plastic scintillators are attractive alternatives due to their low atomic number, high light yield, and fast response time. Organic polymer materials can be formed into complex shapes at comparatively low cost [3, 9]. Furthermore, they can be blended with neutron absorber elements and wavelength shifters to improve the light output [10-12].

Polyethylene naphthalate (PEN) based scintillators have been demonstrated to be effective neutron scintillators with emissions of 10,500 photons/MeV [13]. It is transparent in the visible region, with a strong emission peak of 430 nm that can be detected on a standard photomultiplier tube (PMT). Additionally, PEN is non-volatile, is chemically resistant, and can be melt-processed to form solid plastic films and fibers [14, 15]. Sen et al. investigated PEN-based films loaded with ^{6}LiF and organic scintillating fluor [8]. The films were mechanically hot-pressed for various thicknesses ranging from 66 to 220 μm. Although organic fluor was not necessary, it was added to increase the brightness of the films. The films showed successful neutron-gamma discrimination; however, the films were not transparent due to large micron ^{6}LiF crystals scattering light and differences in the refractive indices between ^{6}LiF and PEN [8]. Furthermore, melt-spun PEN-

based microfibers loaded with ^{6}LiF were investigated for thermal neutron detection as described in detail in the previous chapter. The fibers, with average diameter of 238 μm, were encapsulated in transparent optical gel medium and irradiated with a ^{252}Cf source. The initial results, although not as bright as films, were encouraging given that good neutron-gamma discrimination could be clearly observed.

The focus on PEN is due to its repeated naphathalene units on the backbone of the polyester, which is "crystalline in nature," and energy migration is favored [8, 16]. When the naphthalene units are excited to higher energy levels, energy is transported along the polymer chains, leading to photon emission [8, 16-18]. Carbon fiber composites are well known for their high stiffness, high strength, low weight and resistance to environmental degradation [19]. Carbon fiber with vinyl ester resin (CFVE) is an attractive composite for aerospace and marine applications due to its mechanical properties and the relatively low cost of fabrication using the vacuum-assisted resin transfer molding (VARTM) technique. Shivakumar investigated the mechanical properties of the carbon fiber composite and found CFVE modulus and strength exceed that of marine steel [20].

In this paper, the integration of PEN embedded with ^{6}LiF (PEN/LiF) melt-spun microfibers and carbon fiber with vinyl ester (CFVE) is investigated as a multifunctional laminate composite for thermal neutron detection. The aim of the development of scintillation neutron detector laminate is two-fold. The first is to manufacture thin fibers with a high ^{6}Li concentration that directly discriminates

between neutron and γ radiation. The second is to obtain a thin, lightweight composite structural material with high stiffness and high strength with in which scintillating fibers can be integrated. Melt-spun PEN-based microfibers loaded with ^{6}LiF encapsulated in silicone-based optical dielectric gel are adhered to a carbon fiber/vinyl ester resin composite to form a laminate is proposed as shown in Figure 4.1. ^{6}LiF was chosen due to its large atomic mass density of ^{6}Li, thermal stability, and transparency in the near-visible region. The hypothesis is that, by attaching a thermal neutron PEN/LiF fiber scintillators to CFVE, the fibers will be able to effectively detect thermal neutrons with gamma discrimination for various mechanical design loads. The laminate was tested for response to neutron and gamma radiation. Additionally, the relationship between mechanical behavior and scintillation performance of the composite laminate is reported.

4.3 Materials and Experimental Section

Analytical-grade neat PEN pellets were supplied by the Goodfellow Corporation. Lithium fluoride (^{6}LiF) synthesis was performed according to methods described by Sarraf-Mamoory et al. as described in previous chapter [21]. Lithium hydroxide (LiOH) was added to methanol (Fisher) at a concentration of 0.1 g/mL at 20 ℃ to remove impurities and stirred for 12 hours. The resulting solution was heated to 150 ℃ to completely evaporate the methanol, leaving only LiOH. The LiOH was dissolved in deionized water (0.1 g/mL), where 50% hydrofluoric acid (Acros) was added to make the solution acidic. The solution was stirred and heated to 80 ℃ during the addition of hydrofluoric acid (HF) until reaching a pH

value of 2. The ^{6}LiF solution was then immediately added to a 0 °C acetone bath. The resulting ^{6}LiF was collected using vacuum filtration with 1 mm and 450 nm fine porosity filter paper (Whatman). The ^{6}LiF was then dried for 1 hour at 120 °C.

To prepare the composite mixture, the neat PEN pellets were ground into fine particles using a commercial mechanical grinder. ^{6}LiF was added to neat PEN and ground until a suitable uniform blend was obtained. The composite mixtures were then dried overnight in an oven set at 72 °C.

Melt-spinning. The PEN-based mixtures were melt-spun into fiber using a single-screw, pressure-controlled extruder (Alex James and Associates, Inc.), where a temperature profile of 240, 270, 280, 280, 283, 285, and 285 °C was used. The ¾" extruder was attached to a metering pump with fiber exiting die made of two 3 mm diameter holes collecting onto a winder at a take-up speed of 20 m/min. The spinline distance between the die and the winder was approximately 2 meters [14].

Composite Laminate Preparation. The CFVE composite properties and manufacturing has been described in detail [20, 22]. A specimen made of carbon stitch bonded fabric (LT650-C10-R2VE) was supplied by the Devold AMT AS, Sweden. This was an "equibiaxial fabric produced using Toray's Toraya T700 12K carbon fiber tow with vinyl ester compatible sizing" [20]. The manufacturer reported for T700 fiber a tensile strength of 4.9 GPa, a tensile modulus of 230 GPa, and elongation of 2.1%.

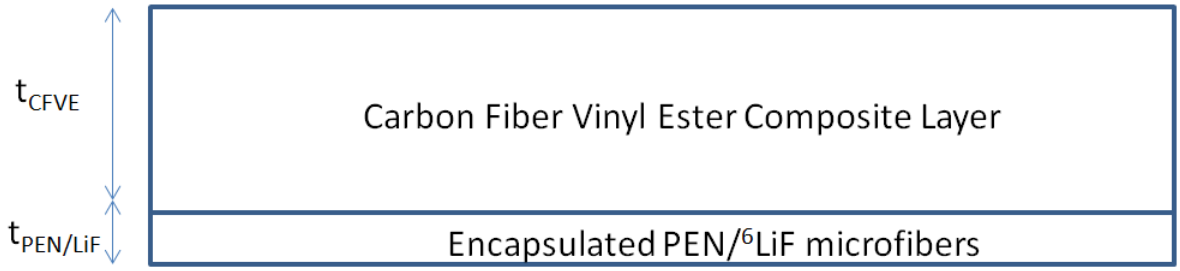

Figure 4.1: Schematic of gage area of proposed laminate structure for carbon fiber/vinyl ester (CFVE) and polyethylene naphthalate (PEN) composite microfibers encapsulated in transparent optical gel.

Dow Chemical DERAKANE 510A-40, a brominated vinyl ester resin, was used as the matrix, and the composite material was fabricated using the VARTM process. The fiber volume fraction was determined to be “58% by the area density method and includes 2.2% weight of polyester stitch” [20, 22]. The CFVE was cut using a band saw from a 60 cm x 60 cm panel with an average thickness of 2.8 mm. The coupon samples were then cut from the 45^{o} oriented CFVE material and machined to form the sample in accordance with ASTM standard D3039, as shown in Figure 4.2 [22, 23].

The PEN/^{6}LiF fibers were wrapped around a 22 mm length x 22 mm width x 0.16-0.19 mm thick microscope glass cover slide. The fibers were then encapsulated using Sylgard 527, a silicone-based transparent optica dielectric gel with a refractive index of 1.41 [24]. In order to compare the effects of mechanical behavior on scintillation performance of composite laminates, two samples were fabricated. The encapsulated fibers were then attached to a 25.4 mm x 42 mm CFVE sample designated as Sample A and a 25.4 mm x 200 mm CFVE sample (Sample B) using Loctite plastic bonding adhesive. This technique resulted in good adhesion of encapsulated PEN fibers to CFVE to form the laminate structure shown in Figure 4.3 and Figure 4.4. Sample A was fabricated mounted on a 50.4 mm window of PMT for scintillation testing. Furthermore, Sample A was designated as the “not mechanically tested” composite laminate sample that was fabricated to compare to the mechanically tested sample (Sample B) for scintillation response.

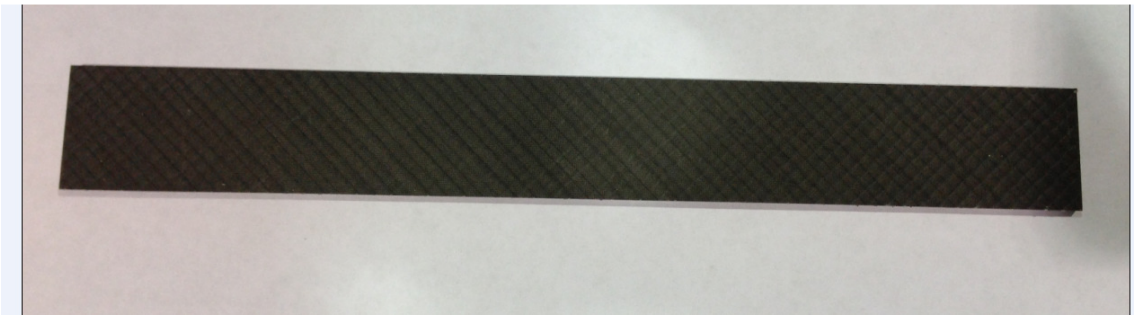

Figure 4.2: Image of 25.4 mm length x 200 mm width x 2.8 mm thick [±45, 2s] carbon fiber with vinyl ester resin (CFVE) tensile sample.

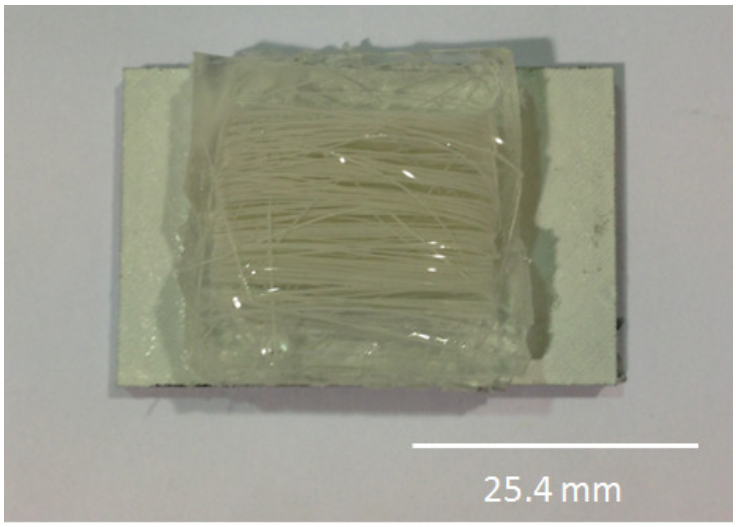

(a)

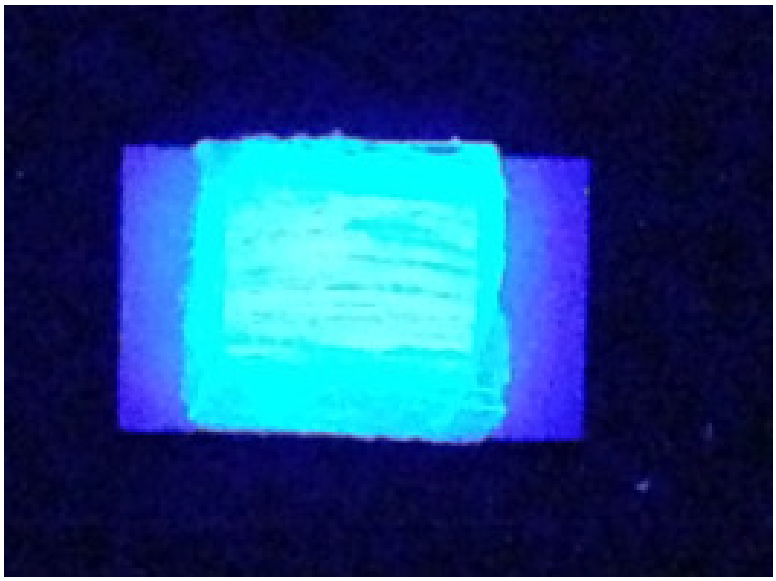

(b)

Figure 4.3: (a) Image of PEN/LiF composite (not mechanically tested) meltspun microfibers wrapped around thin microscope glass cover encapsulated in optical gel integrated with CFVE and (b) exposure to UV radiation. Note: Fluorescence can be viewed in color online.

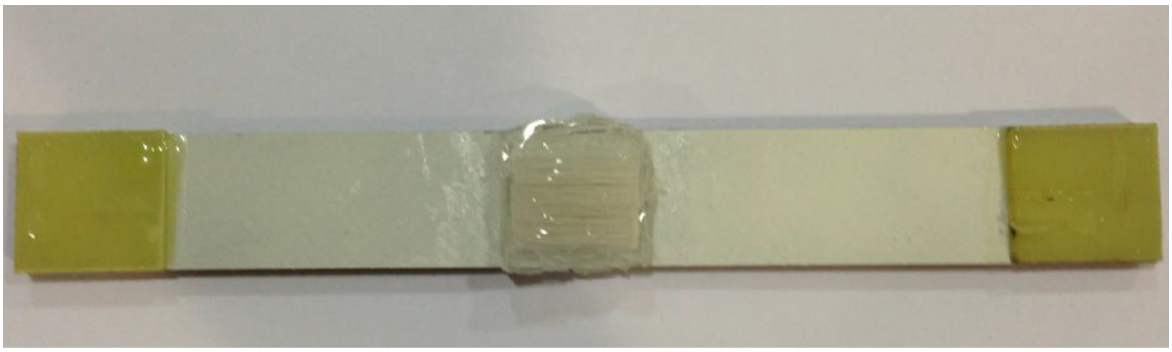

(a)

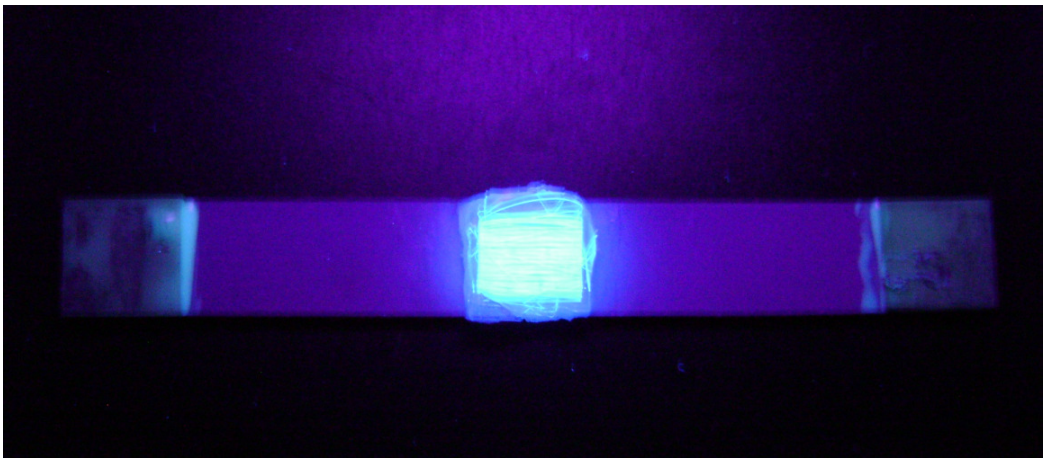

(b)

Figure 4.4: (a) Image of PEN/LiF/CFVE composite meltspun microfibers wrapped around thin microscope glass cover encapsulated in optical gel integrated with CFVE (200 mm x 25.4 mm x 2.8 mm) prior to tensile test and (b) exposure to UV radiation. Note: Fluorescence can be viewed in color online.

Following testing Sample B was cut approximately to the same dimensions as Sample A for testing of scintillation response. As shown in Figure 4.3 and Figure 4.4, CFVE were painted white on the side attached to the PEN/^{6}LiF to reflect light toward the PMT during scintillation measurement.

Scintillation measurements. The samples were evaluated for thermal neutron response using a custom neutron irradiator previously described in detail [7, 8, 25]. Samples A and B were coupled at the center of the photocathode window of the PMT using minimal optical grease and covered with Teflon® reflector tape to minimize light loss [10]. The neutron irradiator mainly consists of a 0.59 μg Californium neutron source with two detector wells equidistant apart in a high-density polyethylene (HDPE) housing. The sample was placed in an acrylic cylinder surrounded by 3.2 mm of lead to obtain the response of neutrons and gamma rays. The sample was then placed in an acrylic cylinder surrounded by 1.6 mm of cadmium. Due to cadmium's large thermal neutron cross-section, the scintillation response measured mostly fast neutrons and gamma response. The net thermal neutron response was obtained by spectrally subtracting the scintillation response between the two wells. A Phillips 2202B PMT mounted on a Canberra 2007P powered by a high-voltage power supply (ORTEC 556) set to 1200 converted the light pulses to electrical pulses. The PMT signal was amplified with a gain setting of 16.6 G and a shaping time of 2 μs with an ORTEC 527A amplifier. The data was recorded using an ORTEC 926 MCD with 8192 channel analog to digital convertor and Maestro 32 software. A ^{60}Co source

enclosed in a lead cylinder was used to obtain the gamma response of the sample.

4.4 Results and Discussion

Mechanical Testing. Figures 4.3 and 4.4 show images of a laminate of encapsulated melt-spun microfibers integrated with a CFVE composite and exposure to UV. Sample B was mounted with plastic tabs to prevent local failure stress concentrations at the grips, as shown in Figure 4.4(a). The PEN/LiF/CFVE laminate sample was then mounted onto an MTS 858 Table Top System for tensile testing as shown in Figure 5.5. A 25.4 mm extensometer (MTS 634.12E-24) was attached to the center of the CFVE composite to record strain data. Loading was introduced by means of the MTS system under displacement control, where loads were monotonically increased until 75% of CFVE failure (120 MPa) [22]. Digital images were captured in an attempt to observe any deformation behavior in the gage length section of the sample under tensile loading using the VIC-3D software. The load, displacement, and strain data were continuously recorded, where the modulus was determined from the linear part of the stress-strain curve. The resulting modulus and strain was 12.5 GPa with a strain of approximately 0.2% prior to nonelastic region as indicated by red line on stress-strain curve shown in Figure 4.6. Figure 4.7 show the PEN/LiF/CFVE sample after tensile loading where there was no evidence of delamination. Figure 4.8 and Figure 4.9 show optical micrographs of the side view of the thickness of Sample A and Sample B.

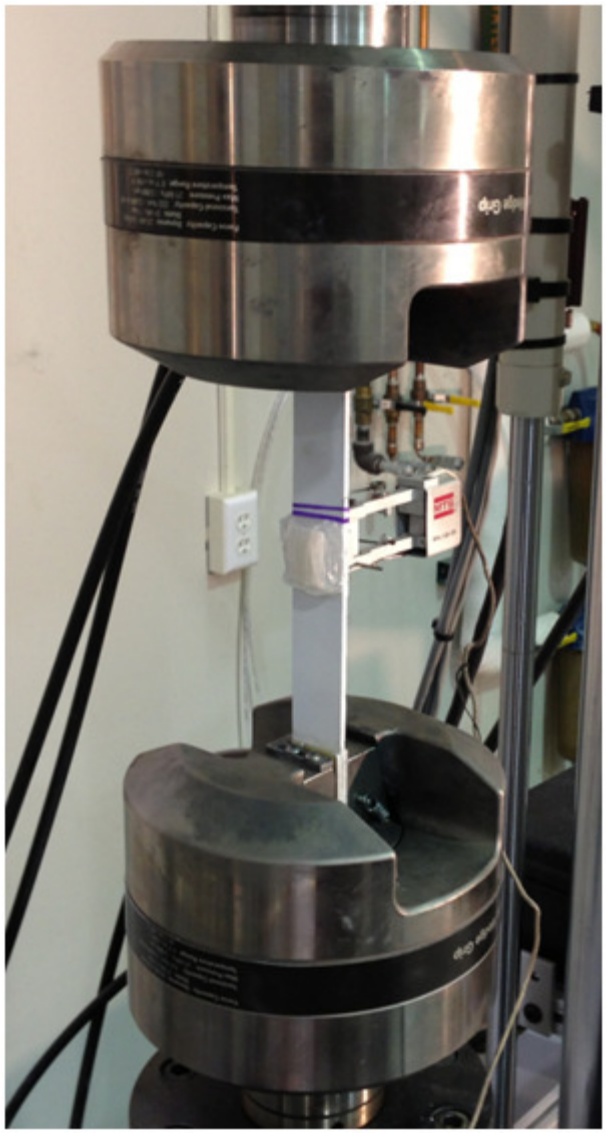

Figure 4.5 Tensile test experimental setup.

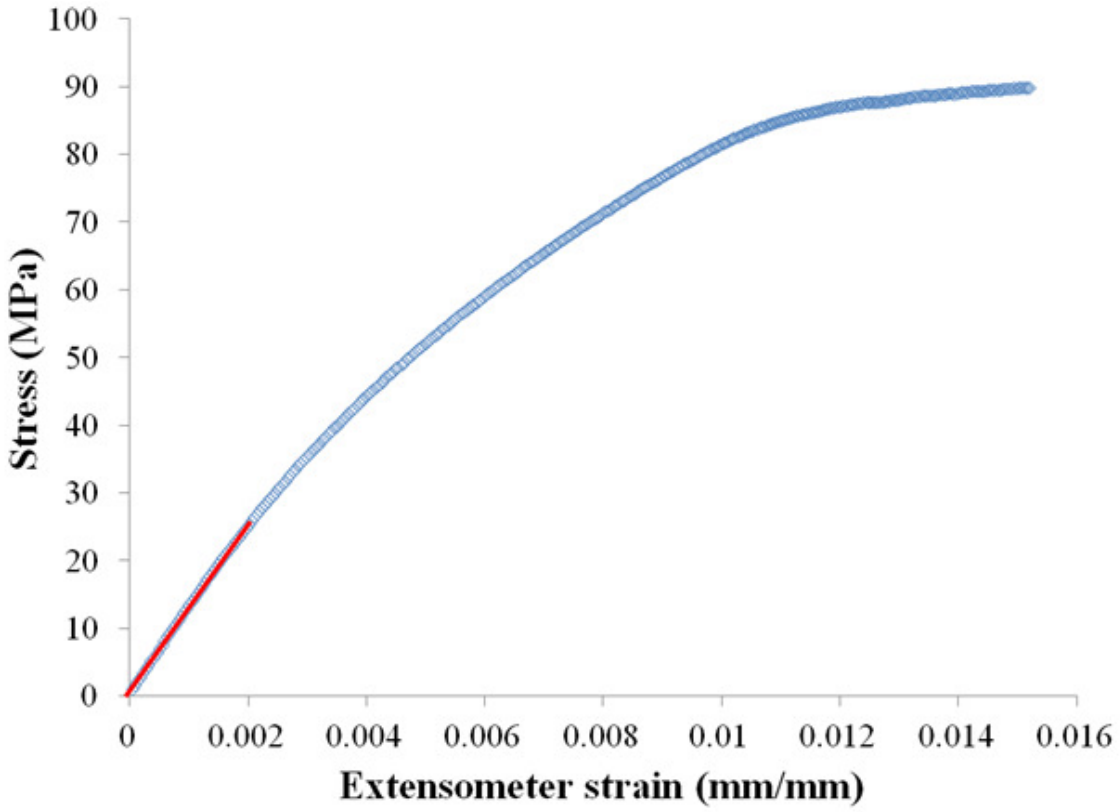

Figure 4.6: Stress-strain data corresponding to PEN/LiF/CFVE composite.

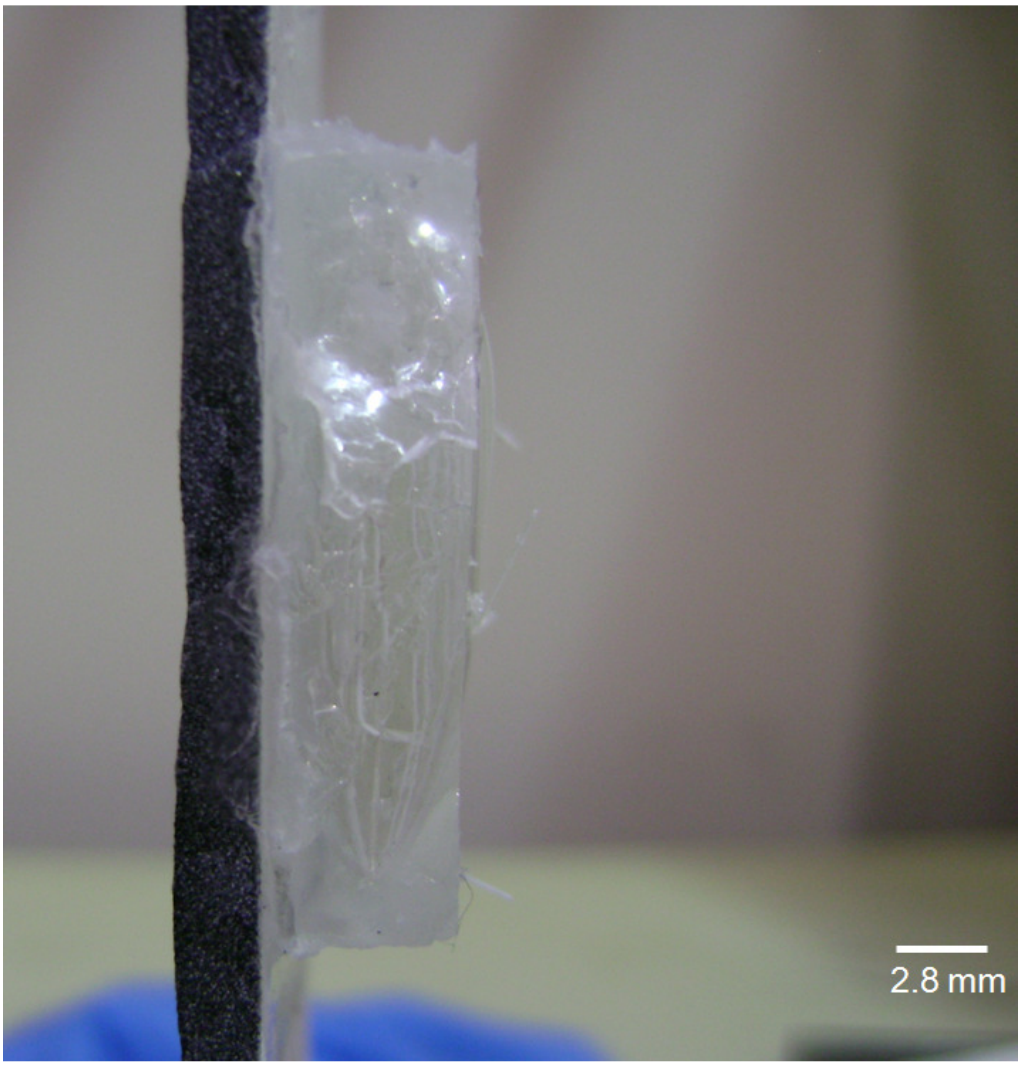

Figure 4.7: Image of PEN/LiF/CFVE laminate after tensile test.

.

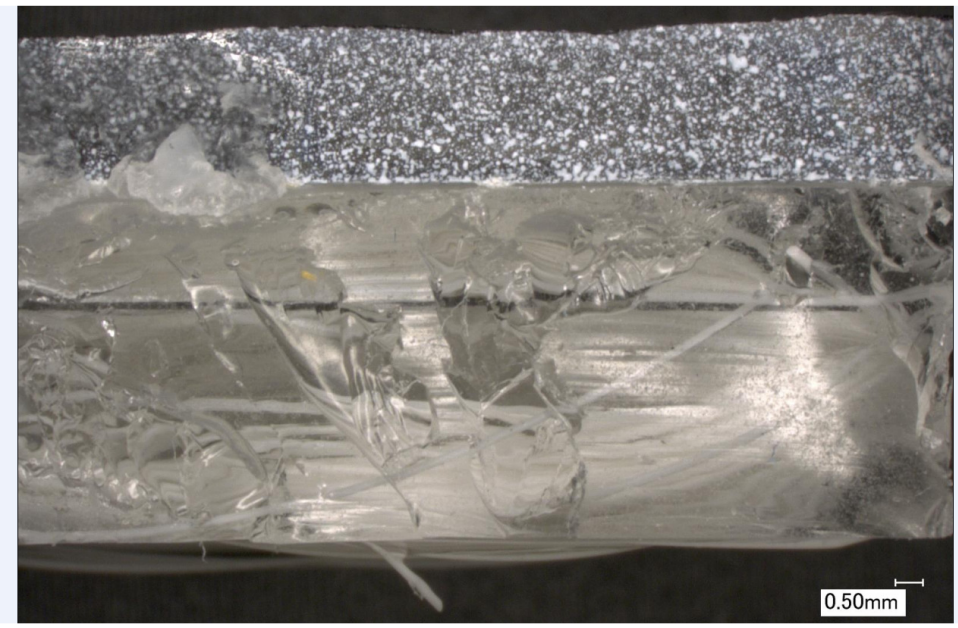

(a)

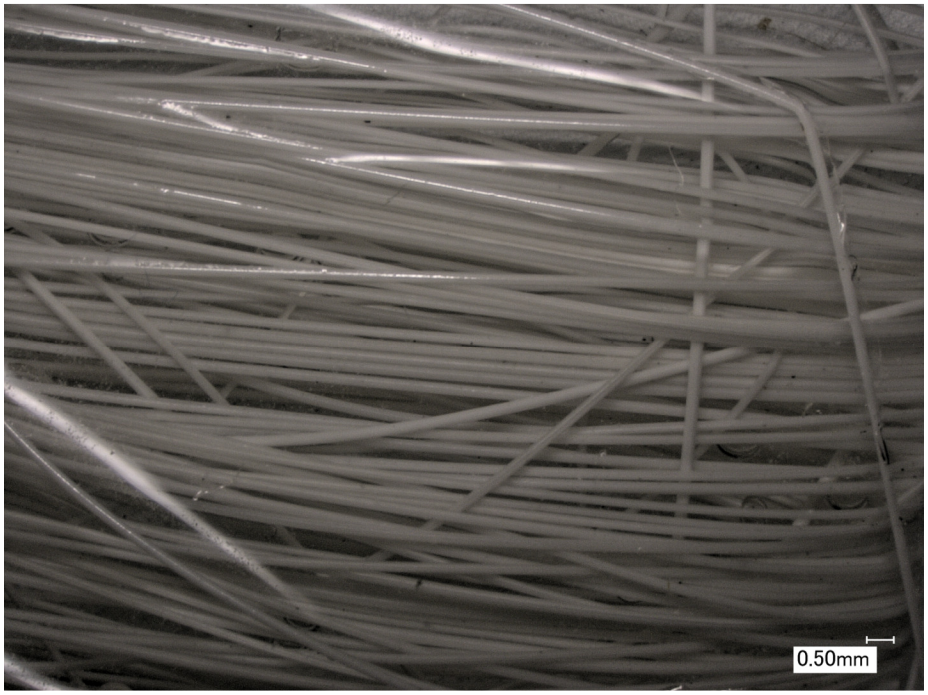

(b)

Figure 4.8: (a) Optical micrograph of side view and (b) front view of PEN/LiF/CFVE gage area (not mechanically tested).

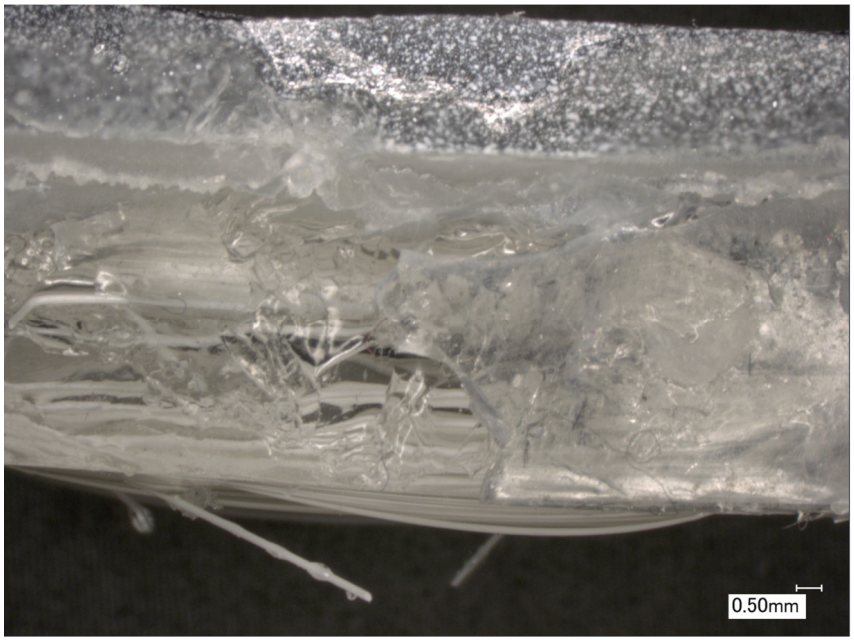

(a)

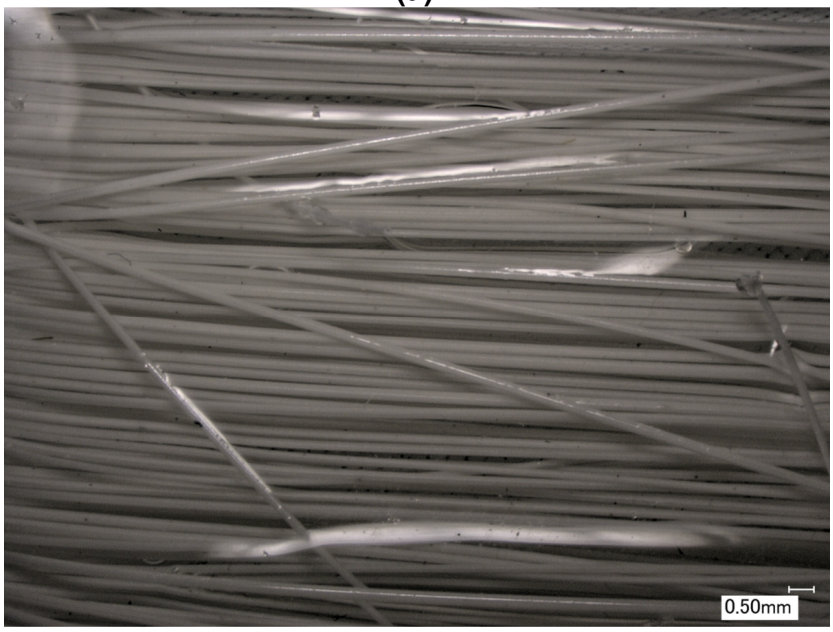

(b)

Figure 4.9: (a) Optical micrograph of side view and (b) front view of PEN/LiF/CFVE (mechanically tested) gage area.

No obvious delamination was observed for Sample B on both sides of the sample. Additionally, no tears were observed in the optical gel, nor was fiber fracture. It must be noted that few fibers can be viewed protruding out of the optical gel (Figure 4.9a) , however these stray fibers became unwrapped from around glass cover glass prior to mechanical testing.

Scintillation Measurements. Samples A and B were tested under irradiation with alpha and gamma sources to evaluate thermal neutron response [26]. After mounting the PEN/LiF/CFVE samples on PMT, as shown in Figure 4.10, Teflon tape was wrapped carefully to cover the optical gel/composite faces to minimize light loss. Figure 4.11 shows the neutron response for the two laminate samples compared to GS20.

The mechanically tested PEN/LiF/CFVE laminate (Sample B) had a count rate of 54 cps compared to 49 cps for Sample A resulting in approximately 10 percent increase for Sample B. The neutron count rate for GS20 was 312 cps. Both samples had a maximum neutron response of around 430 channel number compared to GS20 maximum neutron response at approximately 3400 channel number. Both samples showed a clear distinction of thermal neutrons. GS20 has been reported to emit 6250 photons for each neutron capture event [25].

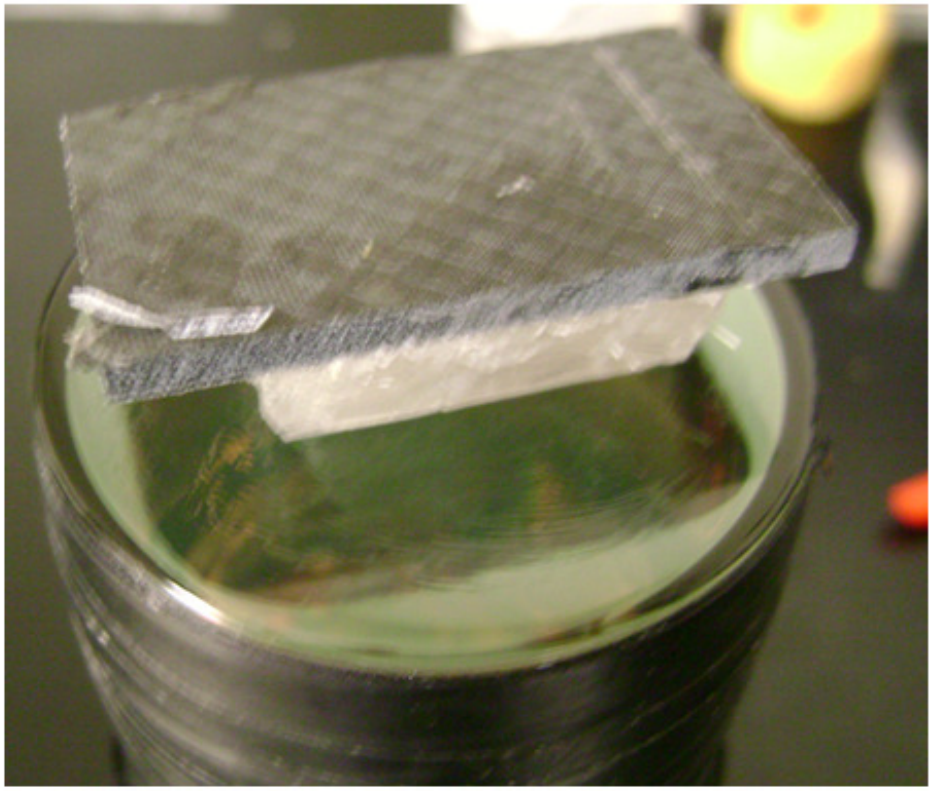

Figure 4.10: Image of front view of PEN/LiF/CFVE gage area mounted on photomultiplier tube after tensile test (mechanically tested).

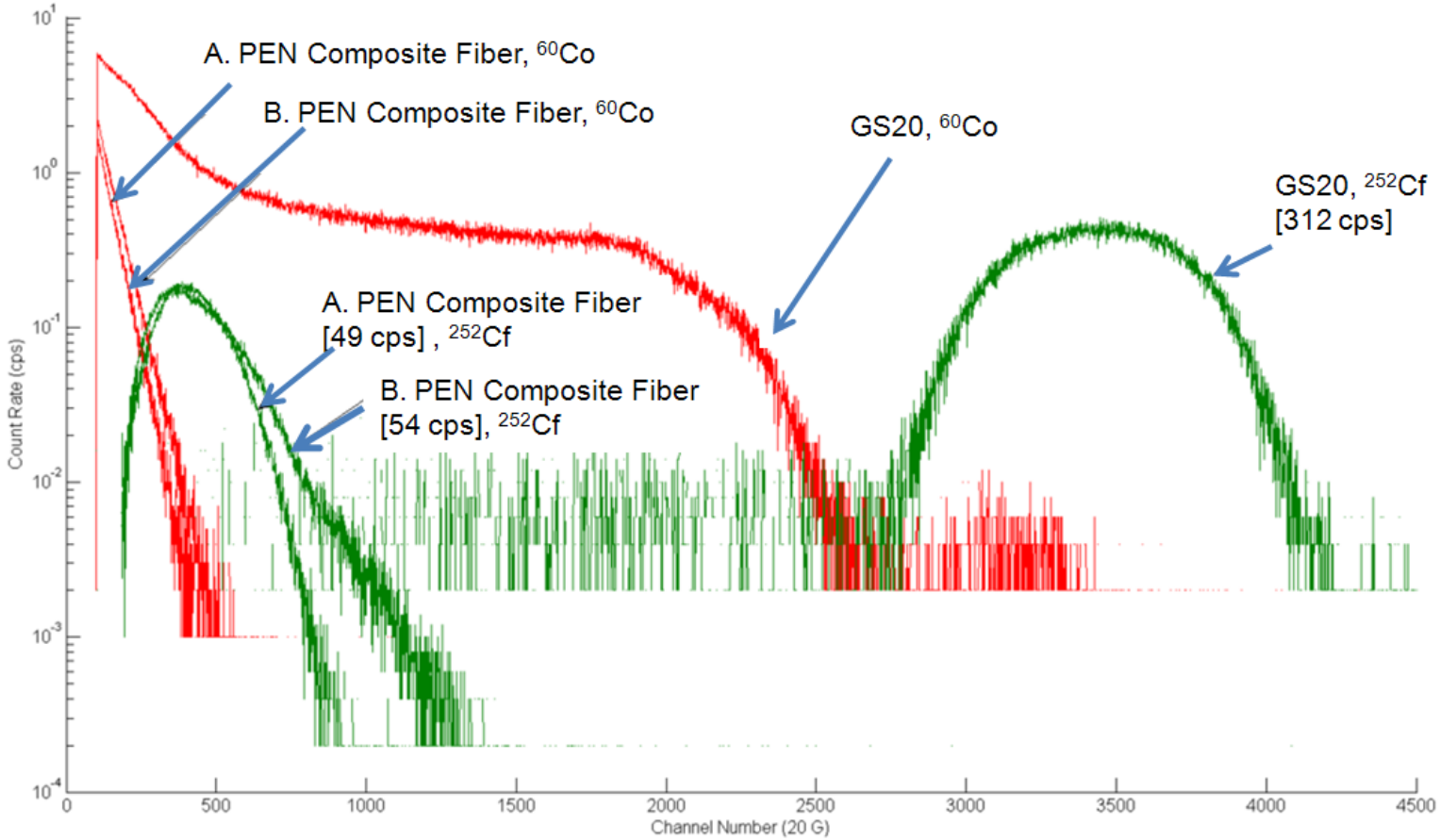

Figure 4.11: Neutron response for PEN/LiF melt-spun microfibers encapsulated in optical gel compared to GS20, where A is not mechanically tested sample and B mechanically tested sample.

As shown in Table 4.1 estimated photons per neutron for PEN/LiF were determined using the following relationship:

$$6250\,\frac{photons}{neutron} \times \left(\frac{\frac{PEN}{LiF} neutron\ spectra\ average\ channel\ number}{GS20\ neutron\ spectra\ average\ channel\ number} \right) \qquad \text{(Eq. 4.1)}$$

Sample B was significantly brighter with a neutron endpoint of 1316 channel number compared to Sample A neutron endpoint (924 channel number). Furthermore, the Sample B emits 816 photons per neutron capture event compared to Sample A of 778 photons/neutron, resulting in 4.9% increase of photons/neutron. It is thought that the fibers were partially stretched while tensile test further orienting fibers for better light collection. However, the difference in scintillation response is most likely due to the fibers having slightly different geometry and weight between the two samples. This indicates that the scintillation properties are essentially the sample when subjected to mechanical stretching. Thus, the laminate composite will stay integral for design loads of the structure with dual functionally robust structural material and scintillation detection.

Table 4.1: Neutron Response for Composite Laminates and GS20

Sample	Neutron Average Spectra	Photons/Neutron
GS20	3417	6250
Sample A	425	777
Sample B	446	816

4.5 Conclusions

A composite laminate consisting of ^{6}LiF-loaded PEN melt-spun microfibers encapsulated in transparent optical dielectric gel was integrated with CFVE backing. Two laminates were tested for thermal response to compared scintillation effects for mechanical testing. The laminate was pulled to 75% of tensile failure, and the encapsulate fiber scintillation stayed intact without delamination. The deformed laminate yielded a brighter yield; however, this was most likely due to a slight difference in the geometry and weight between the two samples.

4.6 References

[1] Gozani, T., and Strellis, D., 2007, "Advances in Neutron Based Bulk Explosive Detection," Nuclear Instruments and Methods in Physics Research Section B: Beam Interactions with Materials and Atoms, **261**(1-2), pp. 311-315.

[2] Berger, H., 1976, *Practical Applications of Neutron Radiography and Gaging,* ASTM, Hoboken, NJ, p 1.

[3] Knoll, G. F., 2000, *Radiation Detection and Measurement, 3rd ed*. John Wiley and Sons, Hoboken, NJ, pp. 227-522.

[4] Squires G. L., 1978, *Introduction to theTheory of Thermal Neutron Scattering,* Dover Publications, Mineola, NY, p. 1.

[5] Pawelczak, I. A., 2011, "NSTAR –A Capture Gated Plastic Neutron Detector," Nuclear Instruments and Methods in Physics Research A, **629**, pp. 230-238.

[6] Kouzes, R. T., 2009, "The ^{3}He Supply Problem," Pacific Northwest National Laboratory Technical Report, PNNL-18388.

[7] Sen, I., Penumadu, D., Williamson, M., Miller, L. F., Green, A. D., and Mabe, A. N., 2011, "Thermal Neutron Scintillator Detectors Based on Poly(2-Vinylnapthalene) Composite Films," IEEE Trans. Nucl. Sci., **59**(3), pp. 1386-1393.

[8] Sen, I., Urffer, M., Penumadu, D., Young S. A., Miller, L. F., and Mabe, A. N., 2011, "Polyester Composite Thermal Scintillation Films," IEEE Trans. Nucl. Sci., **59**(4), pp. 1781-1786.

[9] Tsoulfanidis, N., and Landsberger S., 2011, *Measurement and Detection of Radiation,* Taylor and Francis Group, Boca Raton, FL, p. 178.

[10] Breukers, R. D., Bartle, C. M., and Edgar, A., 2013, "Transparent Lithium Loaded Plastic Scintillators for Thermal Neutron Detection," Nuclear Instruments and Methods in Physics Research A, **701**, pp. 58-61.

[11] Kulkarni, P. V., et al., 1997, "Plastic Scintillating Materials in Nuclear Medical Imaging," Polymer-Plastics Technology and Engineering, **36(1)**, pp. 1-51.

[12] Moser, S. W., Harder, W. F., Hurlbut, C. R., and Kusner, M. R., 1993, "Principles and Practice of Plastic Scintillator Design," Radiat. Phys. Chem., **41(1/2)**, pp. 31-36.

[13] Nakamura, H., et al., 2011, "Evidence of Deep-Blue Photon Emission at High Efficiency by Common Plastic," EPL (Europhysics Letters), 95(2), pp. 22001 –p1 – 22001-p3.

[14] Cakmak. M., and Kim, J. C., 1997, "Structure Development in High-Speed Spinning of Polyethylene Naphthalate (PEN) Fibers," Journal of Applied Polymer Science, **64(4)**, pp. 729-747.

[15] Galay, J., and Cakmak, M., 2001, "Online Monitoring of Birefringence Development in Heat-Setting Polymer Films with a Fast Dual-Wavelength Optical Technique. I. Uniaxial Oriented Poly(ethylene naphthalate)," Journal of Polymer Science: Part B: Polymer Physics, 39, pp. 1107 – 1121.

[16] Cheung, P. S. R., Roberts C. W., and Wagener, K. B., 1979, "Synthesis, Photodegradation, and Energy Transfer in a Series of Poly(ethylene Terephthalate-co-2,6-Naphthalenedicarboxylate) Copolymers," Journal of Applied Polymer Science, **24**, pp. 1809-1830.

[17] Ouchi, I., Nakai, I., Ono, M., and Kimura, S., 2007, "Features of Fluorescence Spectra of Polyethylene 2,6-Naphthalate Films," Journal of Applied Polymer Science, 105, pp. 114 – 121.

[18] Ouchi, I., Miyamura, R., Sakaguchi, M., Hosaka, S., and Kitagawa, M., 1999, "Excitation and Emission Spectra of Polyethylene Terephthalate and Polyethylene 2,6-Naphthalate Films," Polym. Adv. Technol., 10, pp. 195 – 198.

[19] Chung, D. D. L., 1994, *Carbon Fiber Composites,* Butterworth-Heinemann, Newton, MA, p. ix.

[20] Shivakumar KN., 2006, "Carbon/Vinyl Ester Composites for Enhanced Performance in Marine Applications", J. Reinf Plast Comp., 25(10): pp. 1101-1116.

[21] Sarraf-Mamoory, R. Nadery, S., and Riahi-Noori, N., 2007, "The Effect of Precipitation Parameters on Preparation of Lithium Fluoride (LiF) Nanopowder," Chem. Eng. Comm., **194**, pp. 1022-1028.

[22] Siriruk, A., Penumadu, D., and Weitsman, J. Y., 2009, "Effect of Sea Environment on Interfacial Delamination Behavior of Polymeric Sandwich Structures," Composites Science and Technology, 69: pp.821-828.

[23] ASTM D3039, Standard Test Method for Tensile Properties of Polymer Matrix Composite Materials

[24] Iwanowska, J., et al., 2011, “Neutron/Gamma Discrimination Properties of Composite Scintillation Detectors,” JINST, **6**, pp. 1-10.

[25] Mabe, A. N., Auxier II, J. D., Urffer, M. J., Penumadu, D., Schweitzer, G. K., and Miller, L. F., 2013, “Transparent Lithiated Polymer Films For Thermal Neutron Detection,” Nuclear Instruments and Methods in Physics Research A, **772**, pp. 29-33.

[26] Carturan, S. et. al, 2011, “Novel Polysiloxane-Based Scintillators for Neutron Detection,” Radiation Protection Dosimetry, **143**, pp. 471-476.

CONCLUSIONS AND FUTURE WORK

^{6}Li-based electrospun thermal neutron scintillators were developed using a custom electrospinning setup in which the nanofiber mats had an average fiber diameter size of 515 nm. The fiber matrix was made out of an aryl vinyl polymer and a wavelength-shifting fluor with efficient resonant energy transfer characteristics. The fibers successfully demonstrated detection of thermal neutrons and nanophases. The dispersion of ^{6}Li in individual nanofibers was also verified.

^{6}Li-loaded polyethylene (PEN) microfibers were fabricated for thermal neutron detection using a melt-spinning method. The PEN/LiF fibers were successfully melt-spun and evaluated for thermal neutron and gamma discrimination. The distribution of ^{6}Li throughout the fiber was successfully confirmed.

A composite laminate was developed consisting of ^{6}LiF-loaded PEN melt-spun microfibers encapsulated in transparent optical dielectric gel integrated with carbon fiber vinyl-ester resin (CFVE) backing for thermal neutron detection. Two laminates were tested for scintillation response to investigate the relationship between mechanical testing and scintillation response. The laminate was pulled to 75% of tensile failure, and the encapsulated fiber scintillation remained intact without delamination. The deformed laminate yielded a brighter yield; however, this was most likely due to a slight difference in the geometry and weight of the two samples.

The following recommendations may lead to more efficient light collection and enhanced scintillation properties for future research:

- Both the electrospun and melt-spun methods should be modeled to determine the design parameters in order to enhance light collection. The parameters should include the optimal fiber diameter, concentration of neutron absorber, and organic fluor. Additionally, optimal fiber geometry should be investigated to mount onto a photomultiplier tube (PMT).
- Melt-electrospinning and electrospinning techniques should be used to align nanofibers to produce uniaxial nanofibers that directly discriminate between neutron and gamma radiations.
- The development of PEN-based composite microfibers with high crystallinity and appropriate cladding material using fiber drawing techniques to mount onto a PMT for optimal light collection should be investigated.
- Dual function composite laminate should be further tested for repeatability. Additionally, optimal fiber geometry should be investigated in order to integrate with the CFVE backing.

A. APPENDIX

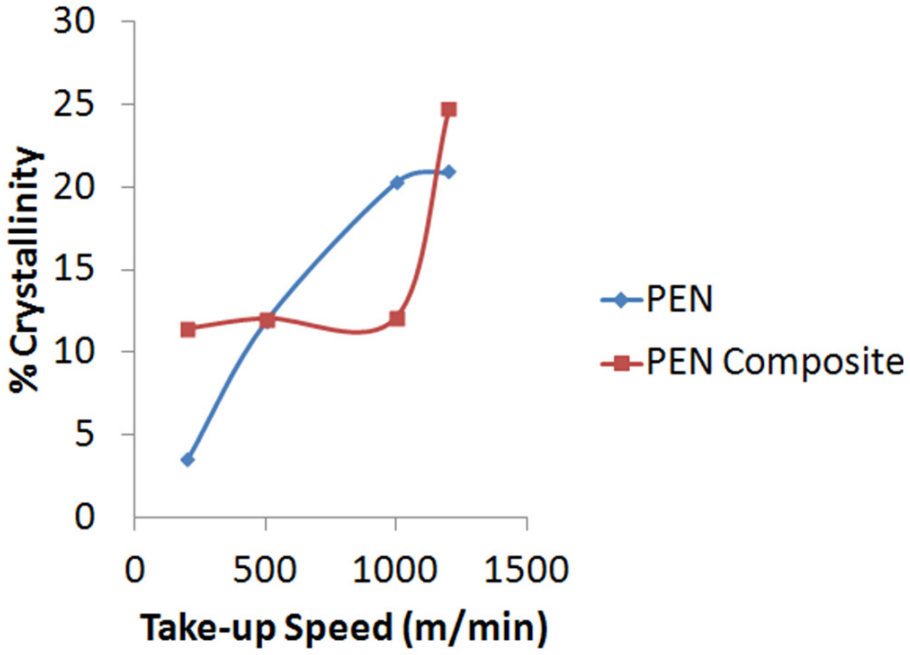

Figure A.1: Crystallinity of melt-spun neat PEN and PEN/LiF fibers versus take-up speed.

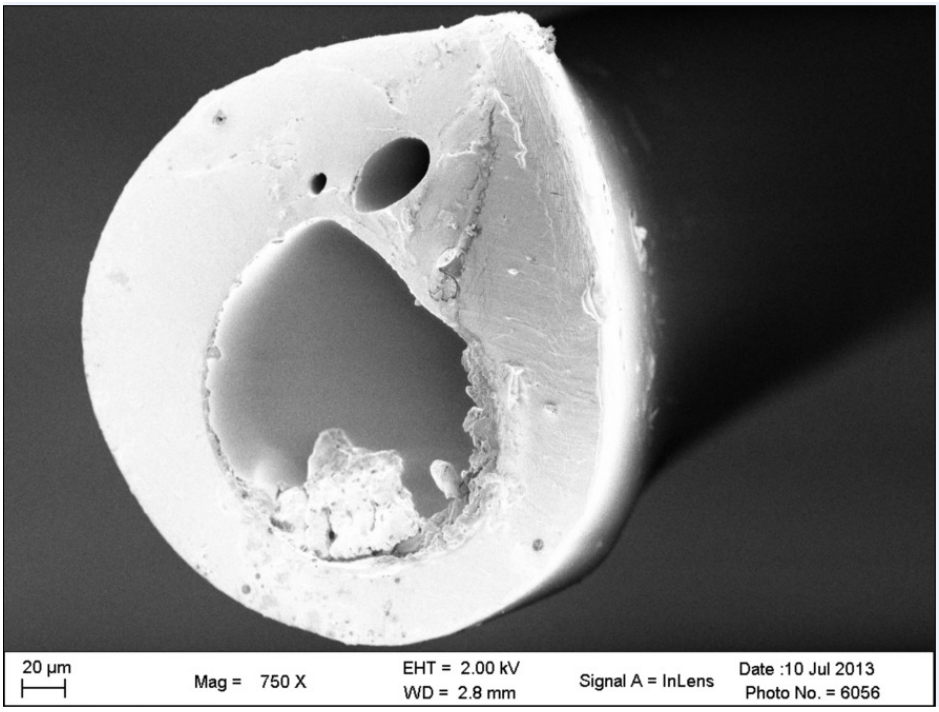

Figure A.2: SEM micrograph of neat PEN melt-spun fiber.

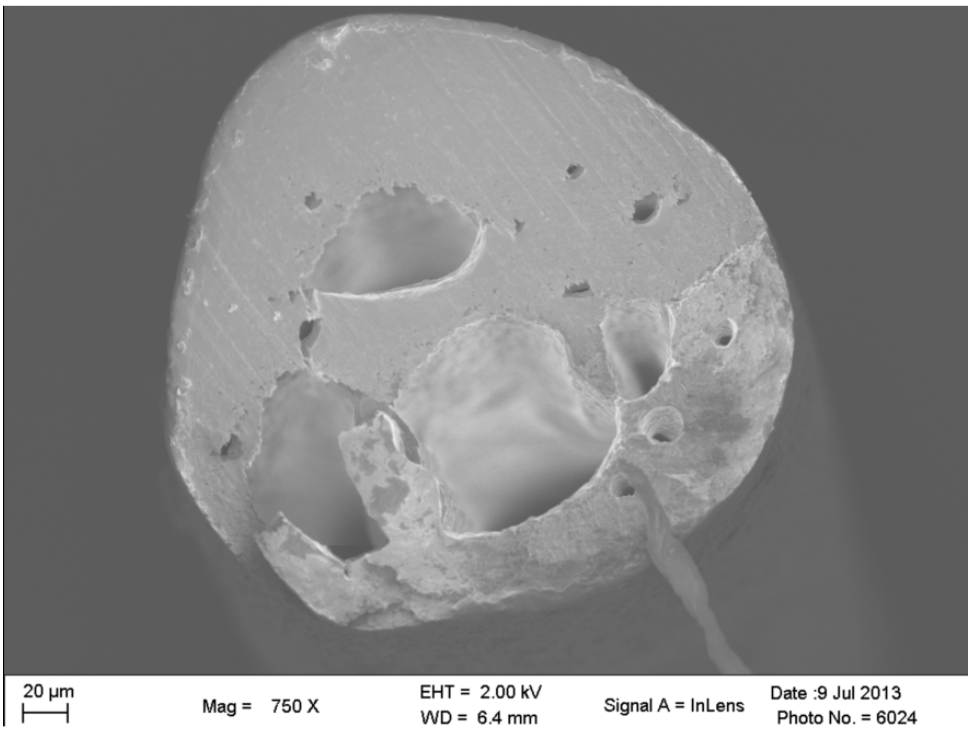

Figure A.3: SEM micrograph of PEN/LiF melt-spun fiber.

VITA

Stephen Andrew Young was born September 19, 1981, in Atlanta, Georgia to John and Sonja Young. Stephen has two brothers, John and Paul. He attended and is a graduate of Southwest DeKalb High School. Stephen holds a Bachelor of Science in Mechanical Engineering (May 2005), a Master of Science in Engineering Science and Mechanics (August 2009), and Doctor of Philosophy in Engineering Science and Mechanics (August 2013) from The University of Tennessee, Knoxville.